

2. ...
N.A. 44 2194. Rev. 2

02 Copy 74
RM SL56H27

UNCLASSIFIED

NACA

RESEARCH MEMORANDUM

for the
U. S. Air Force

LONGITUDINAL AND LATERAL STABILITY,
CONTROL CHARACTERISTICS, AND VERTICAL-TAIL-LOAD
MEASUREMENTS FOR 0.03-SCALE MODEL OF THE AVRO
CF-105 AIRPLANE AT MACH NUMBER 1.41

By M. Leroy Spearman, Ross B. Robinson,
and Cornelius Driver

Langley Aeronautical Laboratory
Langley Field, Va.

UNCLASSIFIED
CONFIDENTIAL
4-17-55
3/15

CLASSIFICATION CHANGED

To: [Redacted]
By authority of: [Redacted] Date: 7/11/55

CLASSIFIED DOCUMENT

This material contains information affecting the National Defense of the United States within the meaning of the espionage laws, Title 18, U.S.C., Secs. 793 and 794, the transmission or revelation of which in any manner to an unauthorized person is prohibited by law.

NATIONAL ADVISORY COMMITTEE
FOR AERONAUTICS
WASHINGTON

44-60-1955
[Redacted]

SEP 7 1955
[Redacted]



NATIONAL ADVISORY COMMITTEE FOR AERONAUTICS

RESEARCH MEMORANDUM

for the

U. S. Air Force

LONGITUDINAL AND LATERAL STABILITY,
CONTROL CHARACTERISTICS, AND VERTICAL-TAIL-LOAD
MEASUREMENTS FOR 0.03-SCALE MODEL OF THE AVRO
CF-105 AIRPLANE AT MACH NUMBER 1.41

By M. Leroy Spearman, Ross B. Robinson,
and Cornelius Driver

SUMMARY

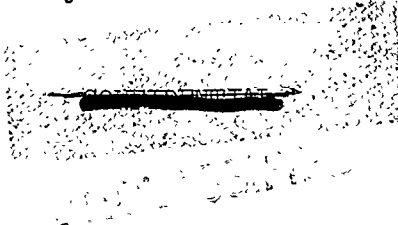
An investigation has been made in the Langley 4- by 4-foot supersonic pressure tunnel at a Mach number of 1.41 to determine the aerodynamic characteristics of an 0.03-scale model of the Avro CF-105 airplane. The investigation included the determination of the static longitudinal and lateral stability, the control and the hinge-moment characteristics of the elevator, the aileron, and the rudder, as well as the vertical-tail-load characteristics.

The results indicated a minimum drag coefficient of about 0.0270, and a maximum trimmed lift-drag ratio of about 4.25 which occurs at a lift coefficient of 0.16.

The directional stability decreased with increasing angle of attack until a region of static instability occurred above an angle of attack of about 9° .

INTRODUCTION

At the request of the U. S. Air Force, an investigation of the aerodynamic characteristics of the Avro CF-105 airplane has been undertaken by the National Advisory Committee for Aeronautics.



This airplane is a twin-jet-propelled tailless fighter design having a cambered 61.4° delta wing with a thickness ratio of 3.5 percent. The inner wing leading edge is drooped 8° , the outer wing leading edge is extended 10 percent of the wing chord and drooped 4° , and a leading-edge notch is located at about the midsemispan of the wing. Twin inlets are located on the sides of the fuselage forward of the wing leading-edge juncture. A swept vertical tail is used to provide the directional stability. Directional control is provided by a conventional rudder, whereas the longitudinal control and lateral control are provided by separate elevators and ailerons on the wing trailing edge.

The purpose of the present paper is to present the results of an investigation of an 0.03-scale model of the Avro CF-105 conducted in the Langley 4- by 4-foot supersonic pressure tunnel at a Mach number of 1.41. In addition to six-component results for the model, three-component results were obtained for the vertical tail, and hinge-moment results were obtained for the elevator, the rudder, and the aileron.

COEFFICIENTS AND SYMBOLS

All the results for the model are referred to the body axis system except the lift and drag coefficients which are referred to the stability axis system. The moment reference point is at a longitudinal station corresponding to the 28-percent point of the wing mean geometric chord. The measurements of the vertical-tail load are referred to an axis system which is parallel to the body axis system which has its origin at the leading edge of the tail theoretical root chord. The axis systems involved are shown in figure 1.

The coefficients and symbols are defined as follows:

C_L lift coefficient, $\frac{L}{qS}$

C_D' drag coefficient (approximate), equivalent to true drag at $\beta = 0^\circ$, $\frac{D'}{qS}$

C_m pitching-moment coefficient, $\frac{M_y}{qSc}$

C_n yawing-moment coefficient, $\frac{M_z}{qSb}$

C_l	rolling-moment coefficient, $\frac{M_x}{qSb}$
C_Y	side-force coefficient, $\frac{Y}{qS}$
C_{h_e}	elevator hinge-moment coefficient, $\frac{H_e}{qS_e \bar{c}_e}$
C_{h_r}	rudder hinge-moment coefficient, $\frac{H_r}{qS_r \bar{c}_r}$
C_{h_a}	aileron hinge-moment coefficient, $\frac{H_a}{qS_a \bar{c}_a}$
$C_{Y_{v,w}}$	side-force coefficient of vertical tail, based on wing area, $\frac{Y_v}{qS}$
C_{B_v}	root-bending-moment coefficient of vertical tail about the theoretical vertical-tail root (0.96 in. above fuselage reference line), $\frac{B_v}{qS_v b_v}$
C_{n_v}	yawing-moment coefficient of vertical tail about a vertical axis through the leading-edge point of the theoretical vertical-tail root, $\frac{n_v}{qS_v \bar{c}_v}$
q	free-stream dynamic pressure
S	wing area, including body intercept
S_e	elevator area (one)
S_r	rudder area
S_a	aileron area (one)
S_v	vertical-tail area to station 0.96 inch above the fuselage line
\bar{c}	wing mean geometric chord

\bar{c}_e	elevator mean geometric chord in stream direction
\bar{c}_r	rudder mean geometric chord in stream direction
\bar{c}_a	aileron mean geometric chord in stream direction
\bar{c}_v	mean geometric chord of vertical tail
b	wing span
b_v	vertical-tail span from theoretical root
α	angle of attack, deg
β	angle of sideslip, deg
δ_e	elevator deflection perpendicular to the hinge line, deg
δ_r	rudder deflection perpendicular to the hinge line, deg
δ_a	aileron deflection perpendicular to the hinge line, deg
L/D	lift-drag ratio, C_L/C_D
$C_{n\beta}$	directional-stability parameter ($\beta \approx 0^\circ$), $\frac{\partial C_n}{\partial \beta}$
$C_{l\beta}$	effective-dihedral parameter ($\beta \approx 0^\circ$), $\frac{\partial C_l}{\partial \beta}$
$C_{Y\beta}$	side-force parameter ($\beta \approx 0^\circ$), $\frac{\partial C_Y}{\partial \beta}$
ΔC_D	drag increment from minimum drag
$C_{l\delta_a}$	aileron effectiveness, $\frac{\partial C_l}{\partial \delta_a}$
$C_{n\delta_r}$	rudder effectiveness, $\frac{\partial C_n}{\partial \delta_r}$

$C_{h\delta a}$ aileron hinge-moment parameter, $\frac{\partial C_{h_a}}{\partial \delta_a}$

$C_{h\delta r}$ rudder hinge-moment parameter, $\frac{\partial C_{h_r}}{\partial \delta_r}$

MODEL AND APPARATUS

Details of the model are shown in figure 2 and its geometric characteristics are given in table I. A photograph of the model is presented in figure 3.

The model had a modified delta wing with a leading-edge sweep of 61.4° , an aspect ratio of 2, a taper ratio of 0.089, and was composed of 3.5-percent-thick cambered sections. The outer wing leading edge was extended 10 percent of the chord and drooped 4° . The inner wing leading edge was drooped 8° . A leading-edge notch was located between the inner and outer portions of the wing at about the midsemispan point.

The model was equipped with twin side inlets that were ducted to a single exit around the sting at the base of the model. For most of the investigation the inlets were open to permit air flow through the model. In addition, for one test, faired plugs (outlined in fig. 2(a)) were used to close the inlets so that some results might be obtained without flow through the ducts. The internal flow characteristics for the configurations having open inlets were not determined since the internal lines of the model were such that an accurate determination of the characteristics could not be made. A schlieren photograph of the flow characteristics at the open inlet is shown in figure 4.

One test was made with transition fixed on the model. The transition strips, which consisted of one-quarter inch wide strips of No. 60 carborundum particles adhered to the surface with shellac, were located about 1 inch rearward of the fuselage nose and along the 10-percent-chord lines on both surfaces of the wing and vertical tail.

The basic model had a nose cone included angle of 50° . One test was made with a slightly longer nose having a cone angle of 30° . (See fig. 2(a).)

The external lines of the model fuselage were altered slightly from those of the airplane in that a portion of the afterbody on the underside of the fuselage was enlarged to accommodate the sting support.

A rudder, two elevators, and a single aileron on the right wing only were provided. These controls were manually adjustable and were equipped with strain-gage beams. The vertical tail was equipped with a three-component strain-gage balance designed for the purpose of determining the side force on the tail, the root bending moment of the tail, and the tail yawing or twisting moment. Forces and moments for the model proper were measured by means of a six-component internal strain-gage balance. The model was mounted on a remotely controlled rotary sting in order to facilitate testing at combined angles of attack and sideslip.

TESTS

Test Conditions

The tests were conducted at a Mach number of 1.41, a stagnation pressure of 10 pounds per square inch, and a stagnation temperature of 100° F. The dewpoint was maintained at -25° F or less to prevent adverse condensation effects.

The Reynolds number based on the wing mean geometric chord was 2.69×10^4 . The dynamic pressure for the test was about 620 pounds per square foot.

Tests were made through an angle-of-attack range of about 4° to 15° at $\beta \approx 0^\circ$ and through a $\pm 12^\circ$ sideslip range at nominal angles of attack of 0°, 4.3°, 8.7°, 13°, and 15.2°. The results, except where noted, are for the open inlet configuration.

Corrections and Accuracy

The angles of attack and sideslip and the control surface angles have been corrected for the deflection under load. No corrections for internal flow effects or base conditions have been applied to the drag measurements. It is estimated, however, on the basis of results for similar arrangements, that the drag corrections would result in an increase in the minimum drag coefficient of about 0.004 for the open inlet configuration and in a decrease in the minimum drag coefficient of about 0.002 for the faired inlet configuration.

The estimated errors in the individual measured quantities are as follows:

C_L	±0.0090
C_D'	±0.0007

C_m	±0.0005
C_n	±0.0005
C_l	±0.0002
C_Y	±0.0057
C_{h_e}	±0.0070
C_{h_r}	±0.0025
C_{h_a}	±0.0064
$C_{Y_{V,W}}$	±0.0010
C_{B_V}	±0.0013
C_{n_V}	±0.0016
α , deg	±0.2
β , deg	±0.2
δ_e , deg	±0.3
δ_r , deg	±0.3
δ_a , deg	±0.4

RESULTS

The results are presented in the following manner:

	Figure
Effects of elevator deflection on longitudinal characteristics; complete model, $\delta_a = \delta_r = 0^\circ$, $\beta = 0^\circ$	5
Effects of fuselage nose and inlet fairings on longitudinal characteristics; $\delta_a = \delta_e = \delta_r = 0^\circ$, $\beta = 0^\circ$	6
Effects of fixed transition on aerodynamic characteristics of complete model in pitch and sideslip; $\delta_e = \delta_a = \delta_r = 0^\circ$	7
Effects of inlet fairings on aerodynamic characteristics in sideslip of complete model and the wing-fuselage combination; $\delta_a = \delta_e = \delta_r = 0^\circ$	8
Effects of fuselage nose shape on aerodynamic characteristics in sideslip at various angles of attack; complete model, $\delta_a = \delta_e = \delta_r = 0^\circ$	9
Effects of rudder deflection on aerodynamic characteristics in pitch; complete model, $\delta_a = \delta_e = 0^\circ$, $\beta = 0^\circ$	10
Aerodynamic characteristics in sideslip at several angles of attack of complete model with various rudder deflections and of wing-fuselage combination; $\delta_a = \delta_e = 0^\circ$	11

	Figure
Rudder hinge-moment characteristics in sideslip at several angles of attack; $\delta_e = \delta_a = 0^\circ$	12
Effects of aileron deflection on aerodynamic characteristics in pitch; complete model, $\delta_e = \delta_r = 0^\circ$, $\beta = 0^\circ$	13
Effect of aileron deflection on aerodynamic characteristics in sideslip for various angles of attack; $\delta_e = \delta_r = 0^\circ$	14
Aileron hinge-moment characteristics in sideslip; complete model, $\delta_e = \delta_r = 0^\circ$	15
Effect of angle of attack on variation of side-force coefficient of vertical tail based on wing area with angle of sideslip; $\delta_e = \delta_a = \delta_r = 0^\circ$	16
Effect of rudder deflection on variation of side-force coefficient of vertical tail based on wing area with angle of sideslip for various angles of attack	17
Effect of angle of attack on the variation of root-bending-moment coefficient of vertical tail with angle of sideslip; $\delta_e = \delta_a = \delta_r = 0^\circ$	18
Effect of rudder deflection on variation of root-bending-moment coefficient of vertical tail with angle of sideslip for various angles of attack	19
Effect of angle of attack on yawing-moment coefficient of vertical tail with angle of sideslip; $\delta_e = \delta_a = \delta_r = 0^\circ$	20
Effect of rudder deflection on variation of yawing-moment coefficient of vertical tail with angle of sideslip for various angles of attack	21
Trim longitudinal characteristics; complete model, open inlets (uncorrected drag)	22
Variation of elevator hinge-moment coefficient with elevator deflection; $\beta = 0^\circ$	23
Characteristics of drag due to lift; complete model, open inlets, $\delta_e = \delta_a = \delta_r = 0^\circ$, (uncorrected drag)	24
Variation of lateral and directional stability characteristics for open and faired inlets for complete model and wing-fuselage combination. $\delta_a = \delta_e = \delta_r = 0^\circ$	25
Variation of rudder control characteristics with rudder deflection; $\alpha = 0^\circ$	26
Variation of aileron control characteristics with aileron deflection; $\alpha = 0^\circ$	27
Effects of angle of attack on aileron and rudder control characteristics; $\beta = 0^\circ$	28

•••
•••
•••
•••

A limited analysis of the results has been made and some points of general interest have been noted. The uncorrected minimum drag values are about 0.0230 with the inlets open and about 0.0290 with the inlets faired (fig. 6). It is estimated, on the basis of investigations of similar configurations, that the corrected minimum drag coefficient would be about 0.0270.

A maximum trimmed lift-drag (L/D) ratio of about 4.25 was obtained at a lift coefficient of 0.16 (fig. 22). For an assumed wing loading of 40 pounds per square foot this would correspond to an altitude of about 57,000 feet. A lift coefficient of 0.32 was obtained with the maximum elevator deflection of -30° (fig. 22). Hence, if sufficient power is assumed to be available, a normal acceleration of 2g's could be attained from an initial trim position corresponding to the maximum L/D ($C_L = 0.16$).

The directional stability results (fig. 25) indicate that about 63 percent of the total tail contribution to $C_{n\beta}$ is required to overcome the unstable moment of the wing-fuselage combination at $\alpha = 0^\circ$. This, of course, is caused primarily by the far rearward center of gravity (moment reference point) which results in a large unstable fuselage moment and a short tail moment arm. The directional stability $C_{n\beta}$ decreases with increasing angle of attack until a region of static instability occurs above $\alpha \approx 9^\circ$. This reduction in $C_{n\beta}$ results primarily from a loss in the vertical-tail contribution and, to some extent, to an increase in the instability of the wing-fuselage combination. The loss in tail contribution probably results primarily from sidewash changes induced at the tail by vortices emanating from the rather square upper corners of the fuselage. The directional stability for the prototype airplane may be further aggravated by the additional losses in tail contribution to be expected from aeroelastic effects and, with increasing Mach number, by the decrease in tail lift-curve slope.

Fairing the inlets had little effect on the tail contribution to $C_{n\beta}$ (fig. 25) but did provide small positive increments of $C_{n\beta}$ for both the tail-on and tail-off configurations.

~~CONFIDENTIAL~~

The control characteristics of the elevator, the rudder, and the aileron indicated positive control effectiveness that was reasonably linear with control deflection and decreased slightly with increasing angle of attack.

Langley Aeronautical Laboratory,
National Advisory Committee for Aeronautics,
Langley Field, Va., August 13, 1956.

M. Leroy Spearman

M. Leroy Spearman
Aeronautical Research Scientist

Ross B. Robinson

Ross B. Robinson
Aeronautical Research Scientist

Cornelius Driver

Cornelius Driver
Aeronautical Research Scientist

Approved:

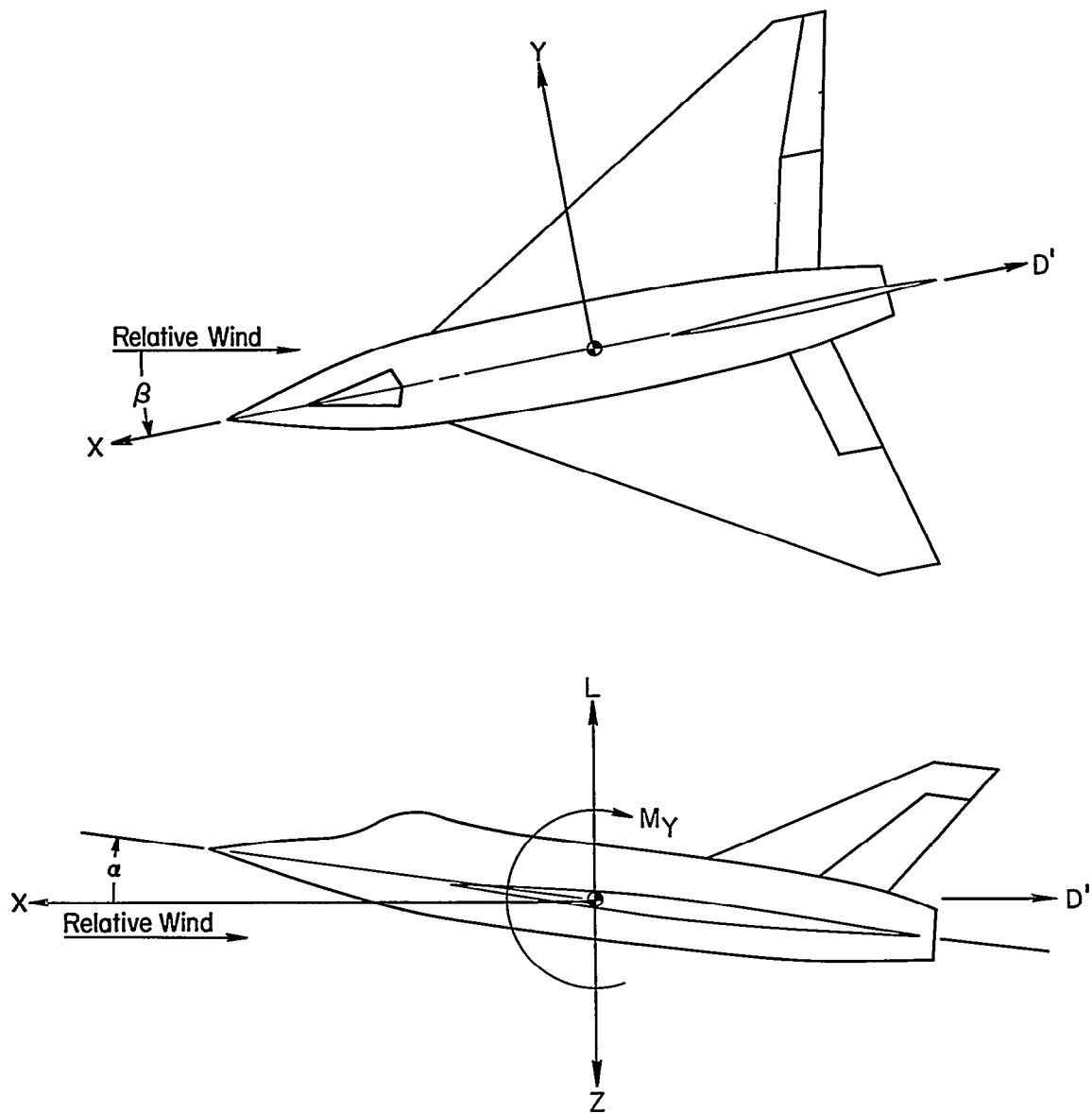
John V. Becker

John V. Becker
Chief of Compressibility Research Division

pf

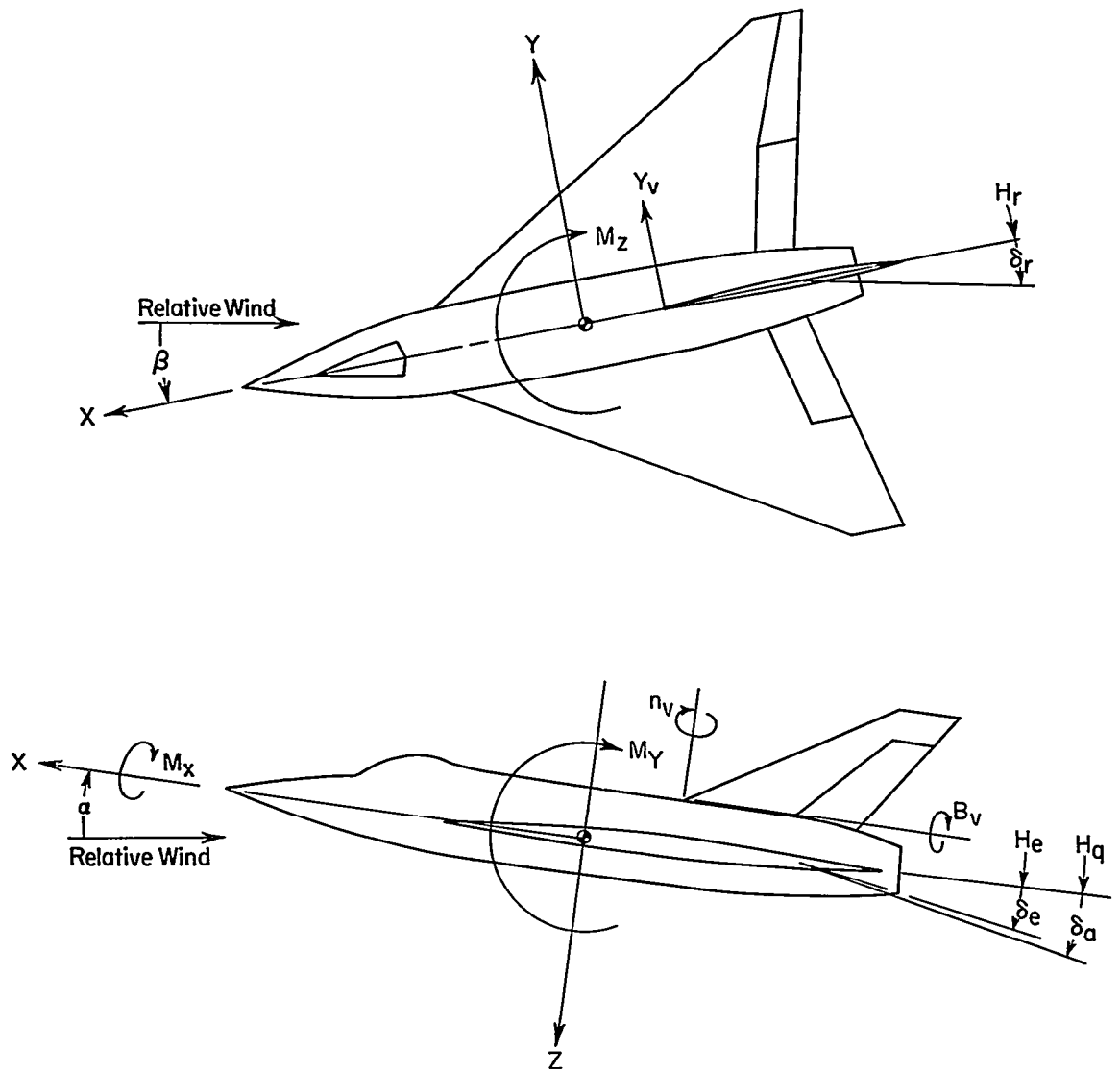
TABLE I.- GEOMETRIC CHARACTERISTICS OF MODEL

Wing:	
Area, sq ft	1.1025
Span (projected), in.	18.000
Mean geometric chord, in.	10.878
Sweep of quarter-chord line, deg	55
Sweep of leading edge, deg	61.4
Aspect ratio	2.04
Taper ratio	0.089
Dihedral, deg	-4
Incidence, deg	0
Thickness ratio, percent	3.5
Vertical tail (theoretical, with root station 0.96 inch above fuselage reference line):	
Area, sq ft	0.143
Span, in.	4.635
Mean geometric chord, in.	4.872
Sweep of leading edge, deg	59.3
Aspect ratio (panel)	1.04
Taper ratio	0.298
Elevator:	
Area, sq ft	0.048
Span, in.	3.665
Mean geometric chord, in.	1.89
Rudder:	
Area, sq ft	0.0343
Span, in.	3.615
Mean geometric chord, in.	1.422
Aileron:	
Area, sq ft	0.030
Span, in.	3.605
Mean geometric chord, in.	1.261



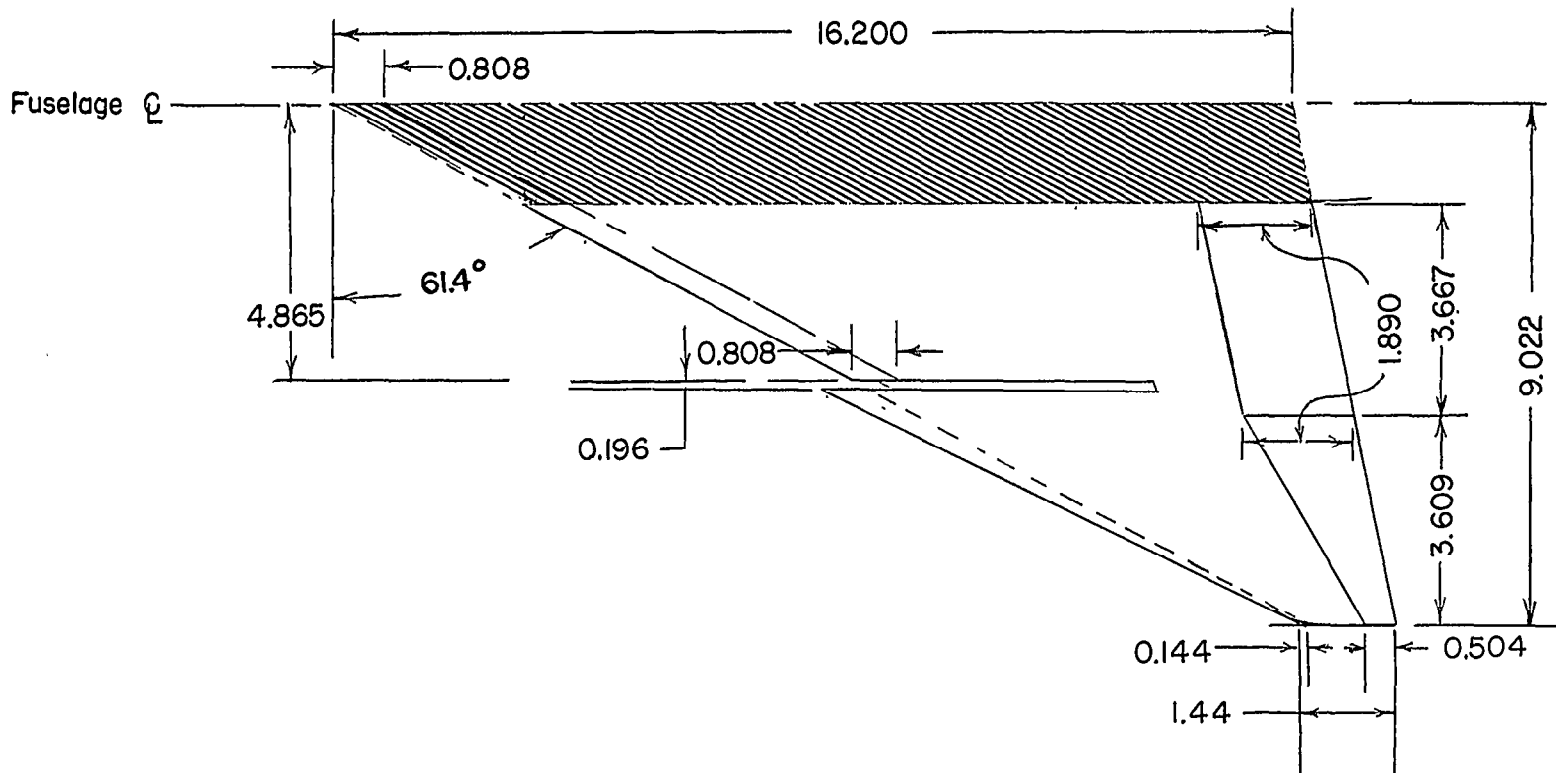
(a) Stability axes.

Figure 1.- Axis notation. Arrows indicate positive directions.



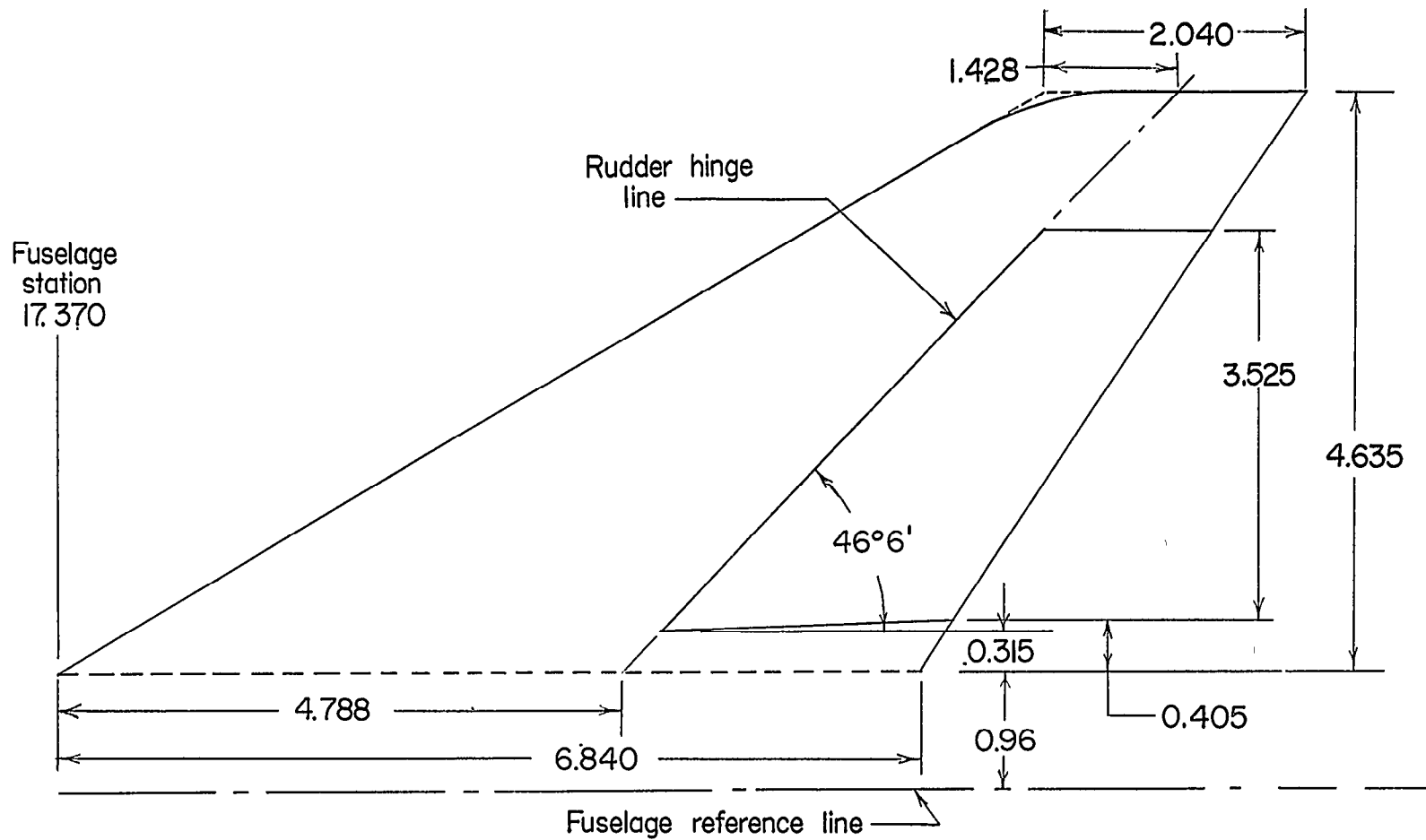
(b) Body axes.

Figure 1.- Concluded.



(b) Details of wing.

Figure 2.- Continued.



(c) Details of vertical tail.

Figure 2.- Concluded.

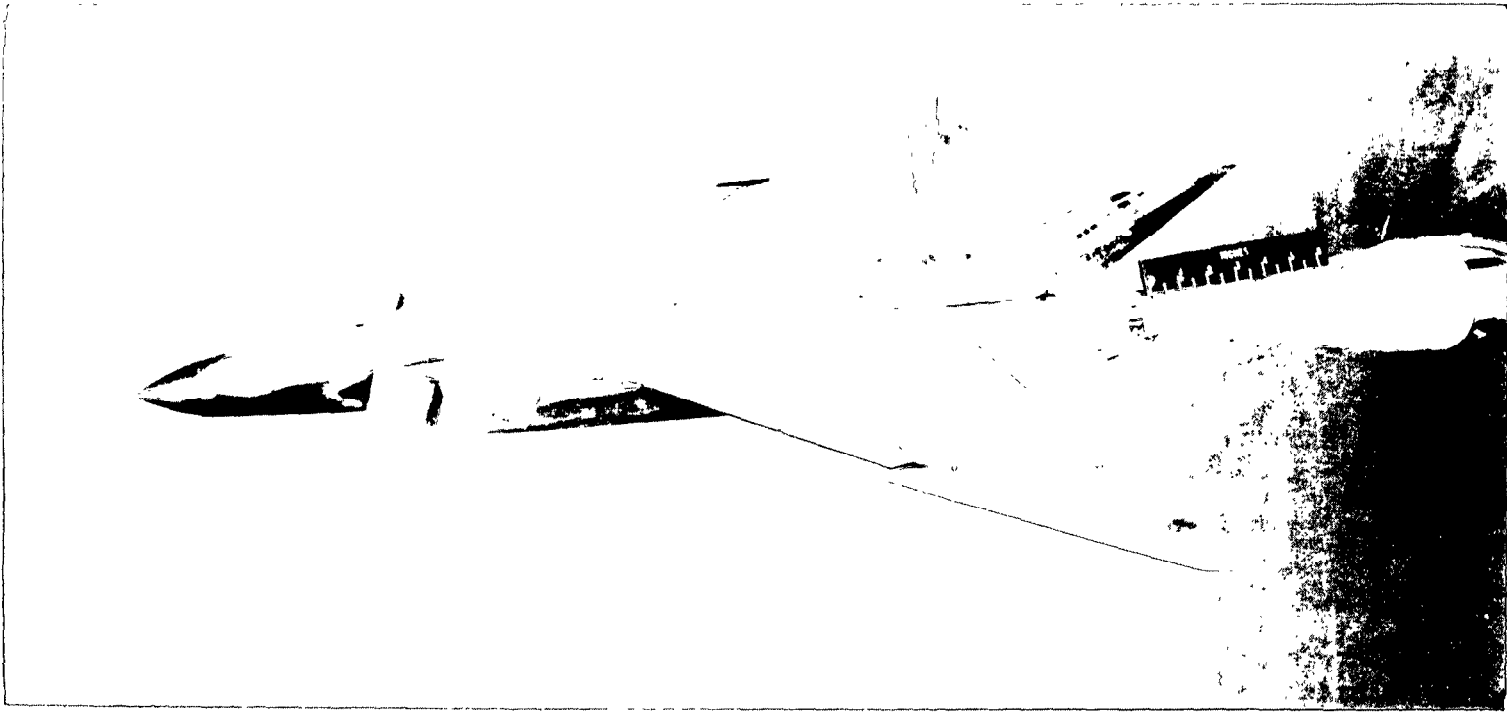


Figure 3.- Photograph of 0.03-scale model of Avro CF-105.

L-93465



L-95757

Figure 4.- Schlieren photograph of inlet; $M = 1.41$, $\alpha = 0^\circ$, $\beta = 0^\circ$.

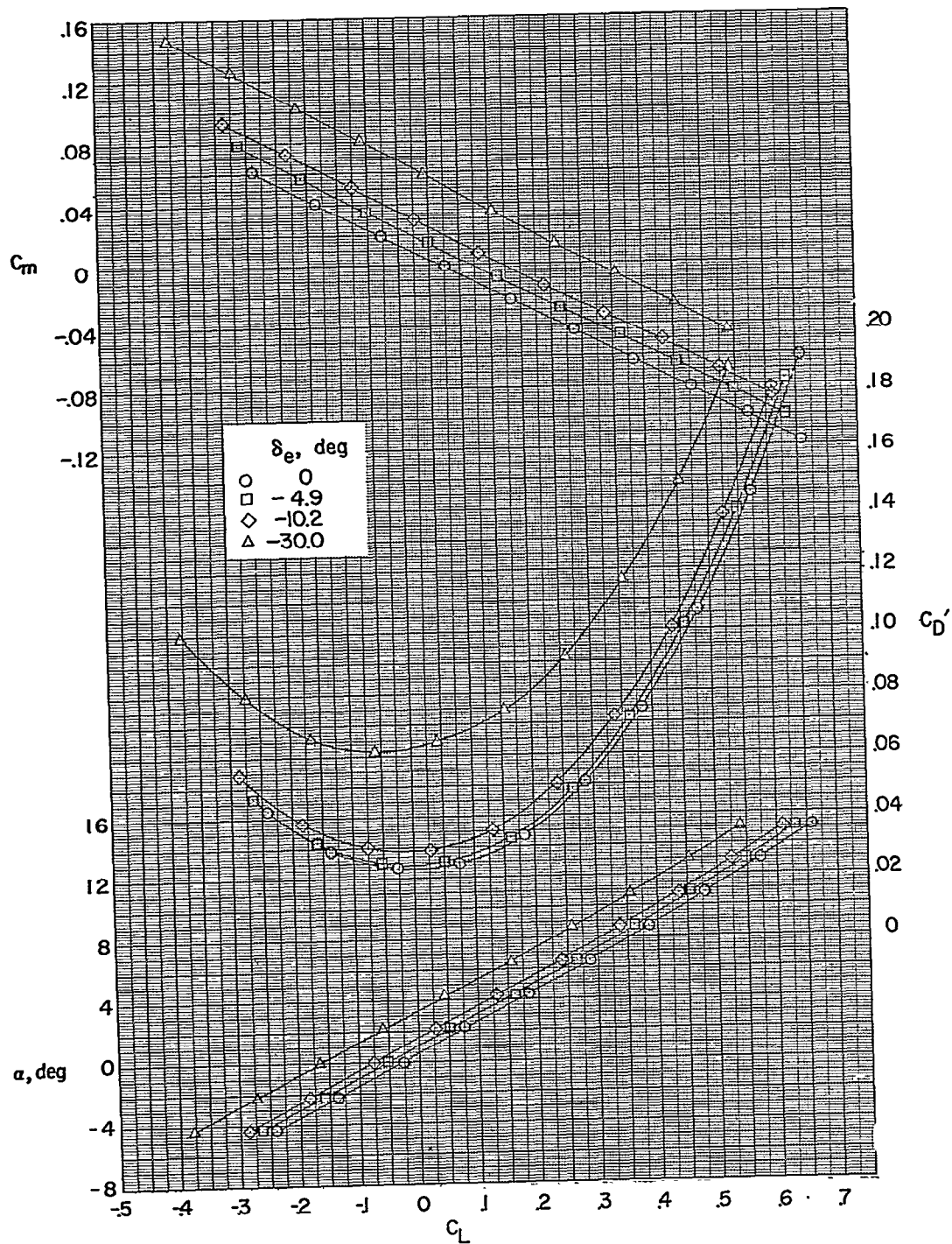


Figure 5.- Effects of elevator deflection on longitudinal characteristics; complete model, $\delta_a = \delta_r = 0^\circ$, $\beta = 0^\circ$.

C_{he}

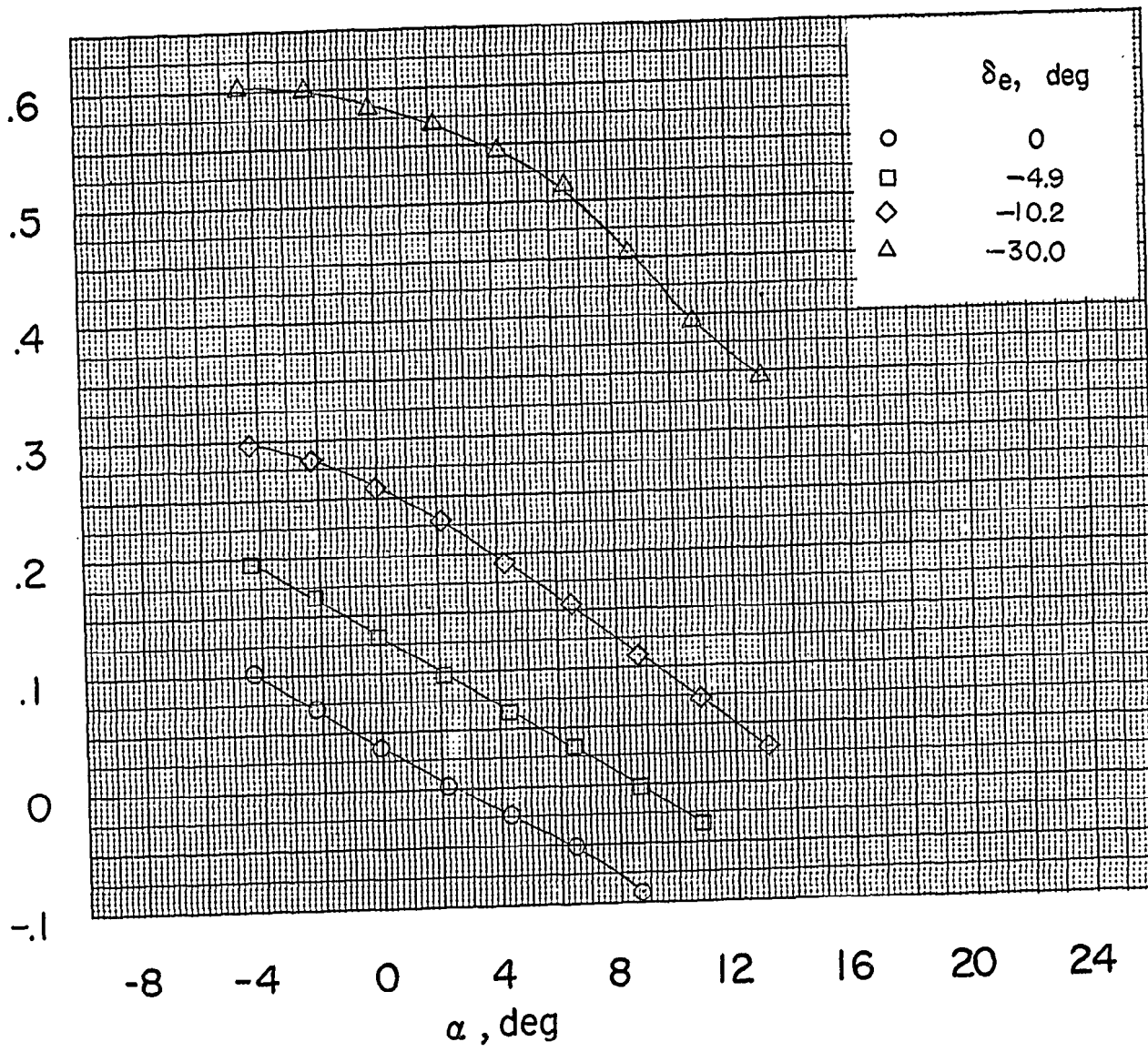


Figure 5.- Concluded.

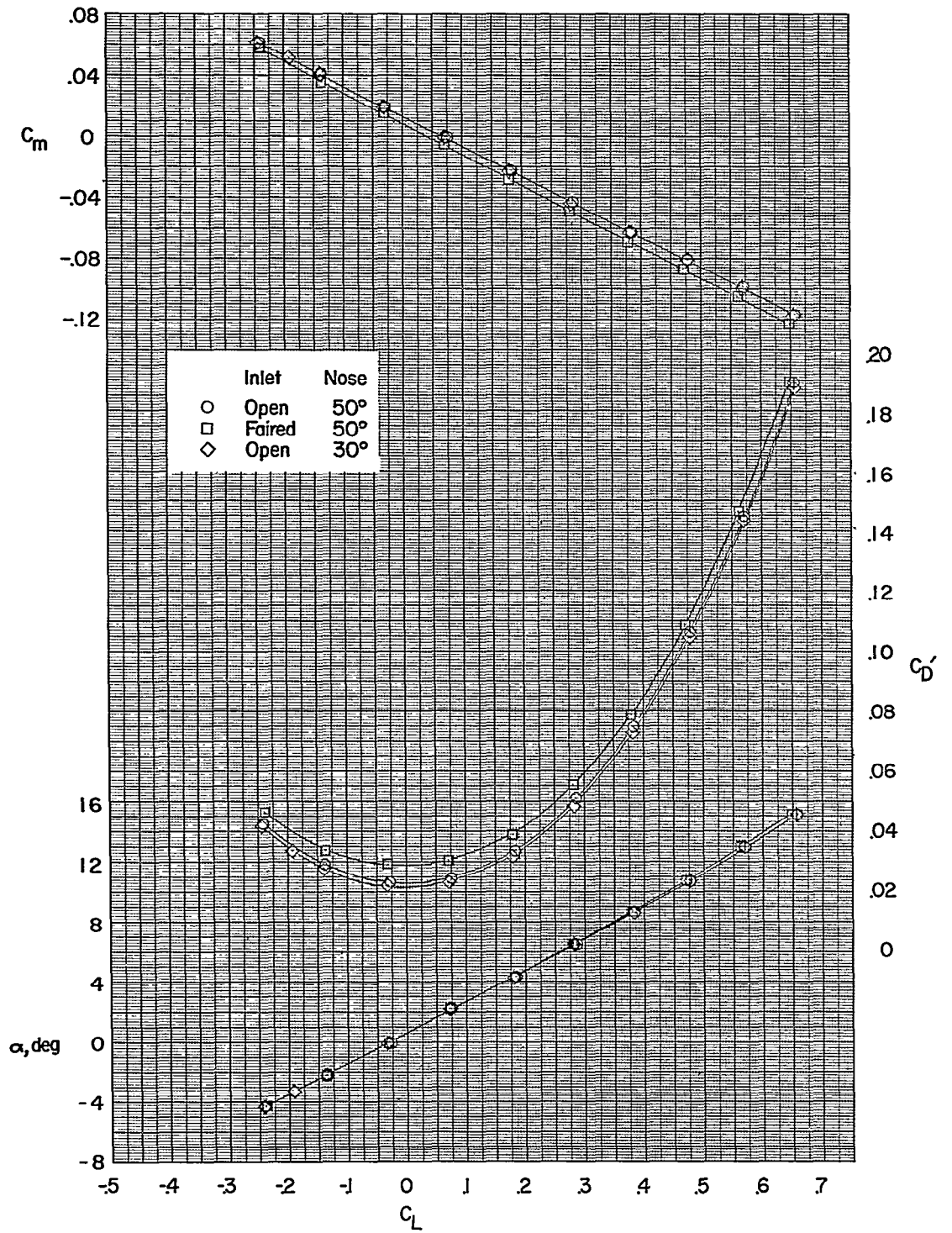
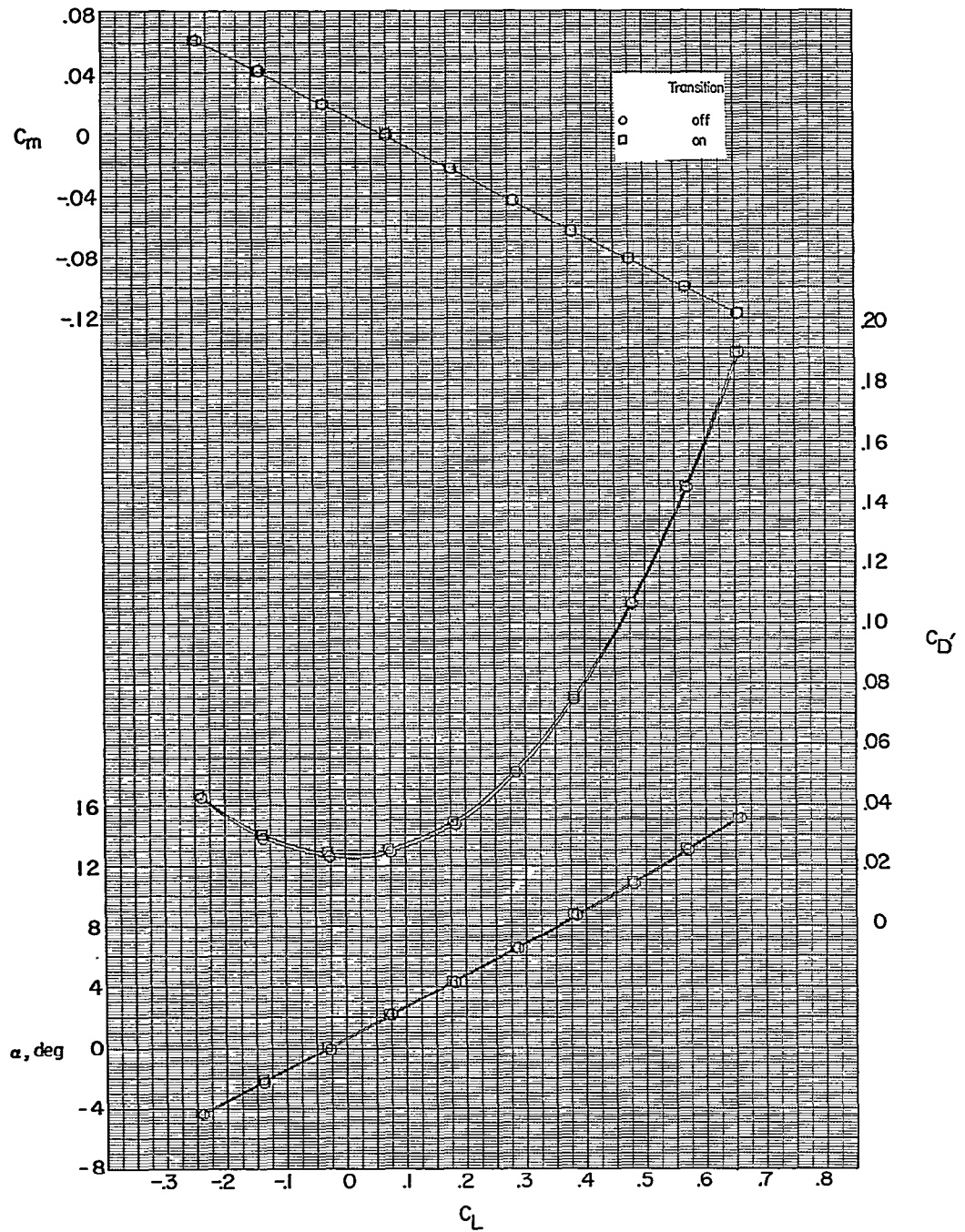
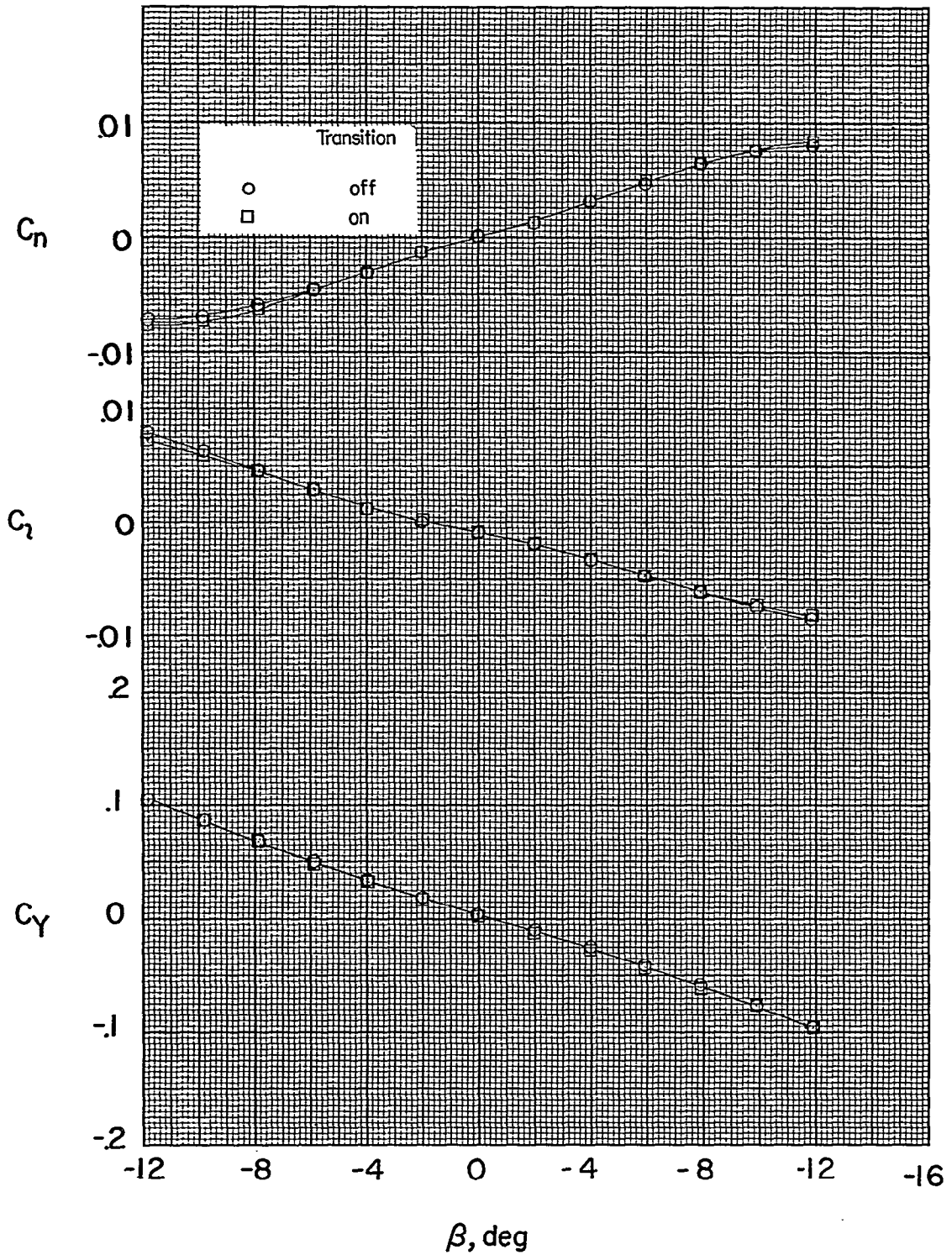


Figure 6.- Effects of fuselage nose and inlet fairings on the longitudinal characteristics; $\delta_a = \delta_e = \delta_r = 0^\circ$, $\beta = 0^\circ$.



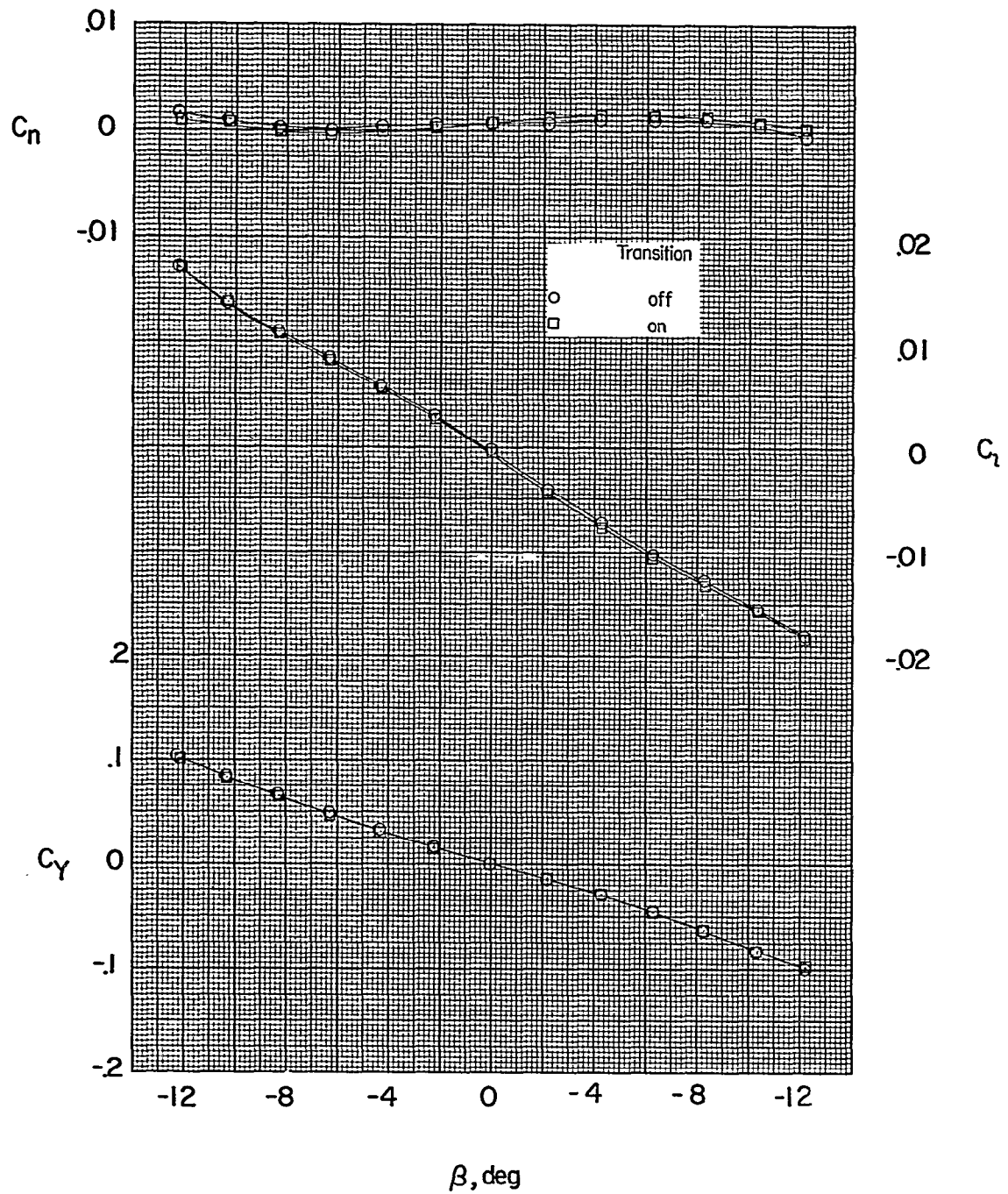
(a) Plot of C_m , C_D' , and α against C_L ; $\beta \approx 0^\circ$.

Figure 7.- Effects of fixed transition on aerodynamic characteristics of complete model in pitch and sideslip; $\delta_e = \delta_a = \delta_r = 0^\circ$.



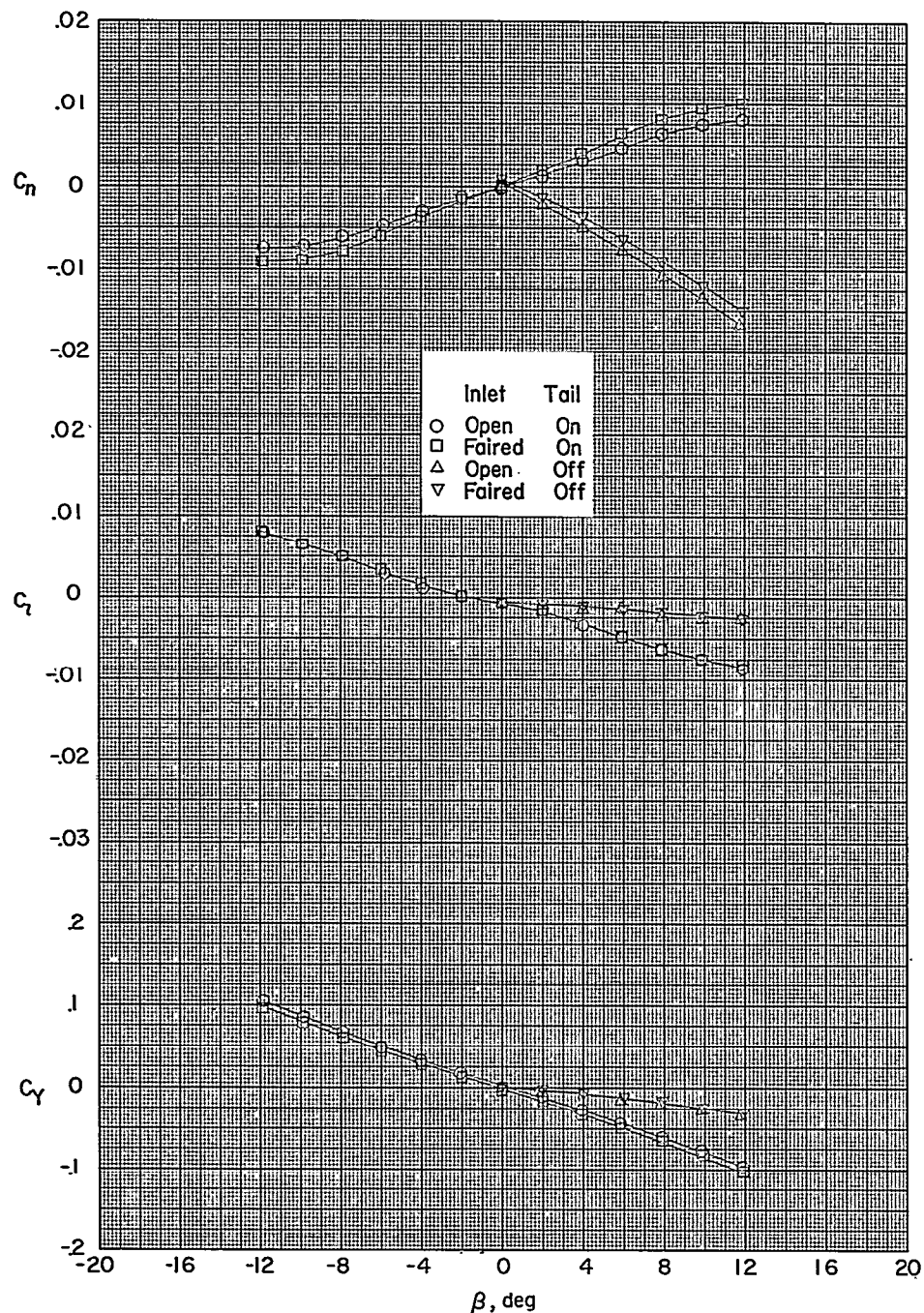
(b) Plot of C_n , C_z , and C_y against β ; $\alpha \approx 0^\circ$.

Figure 7.- Continued.



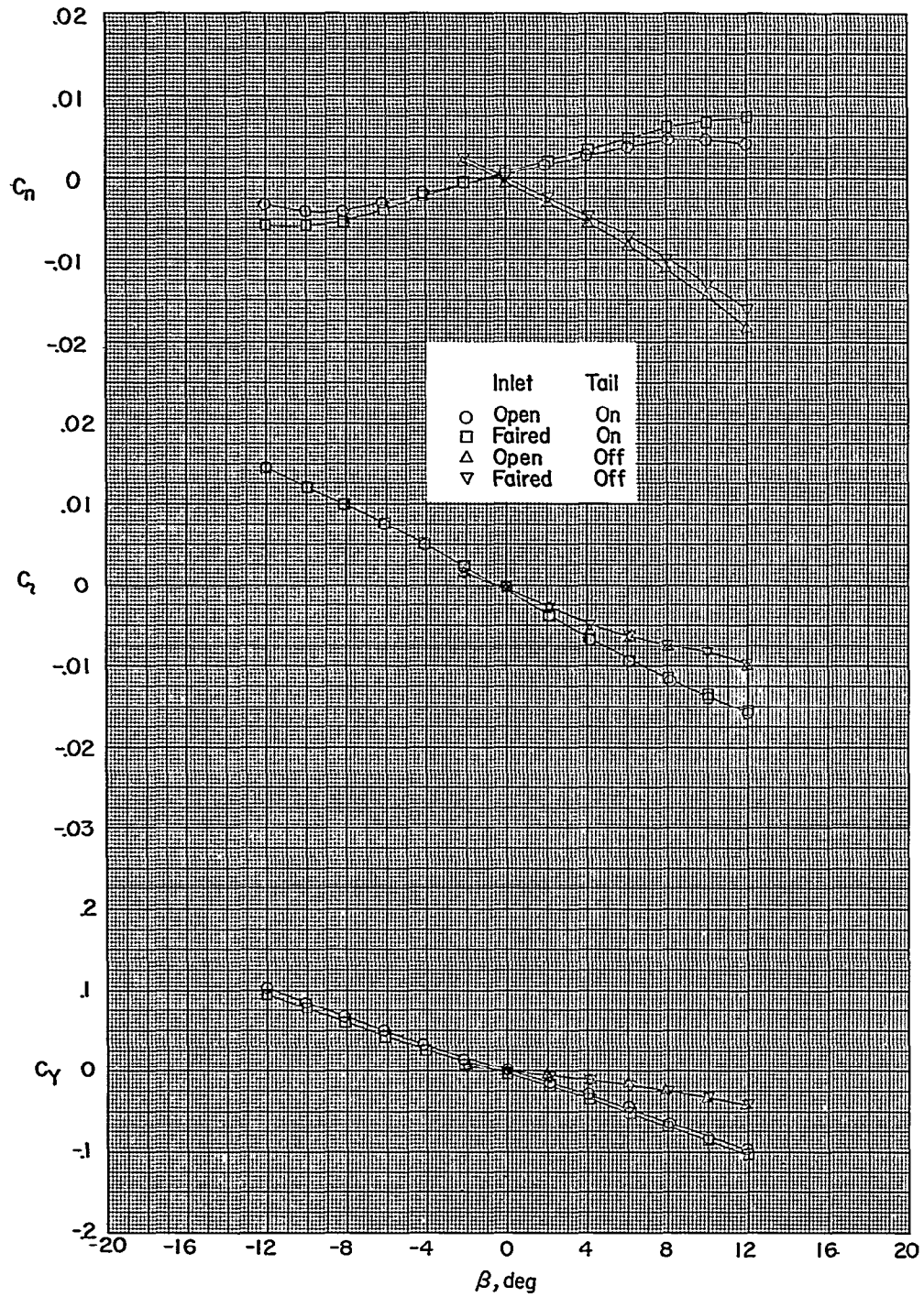
(c) Plot of C_n , C_l , and C_y against β ; $\alpha \approx 8.7^\circ$.

Figure 7.- Concluded.



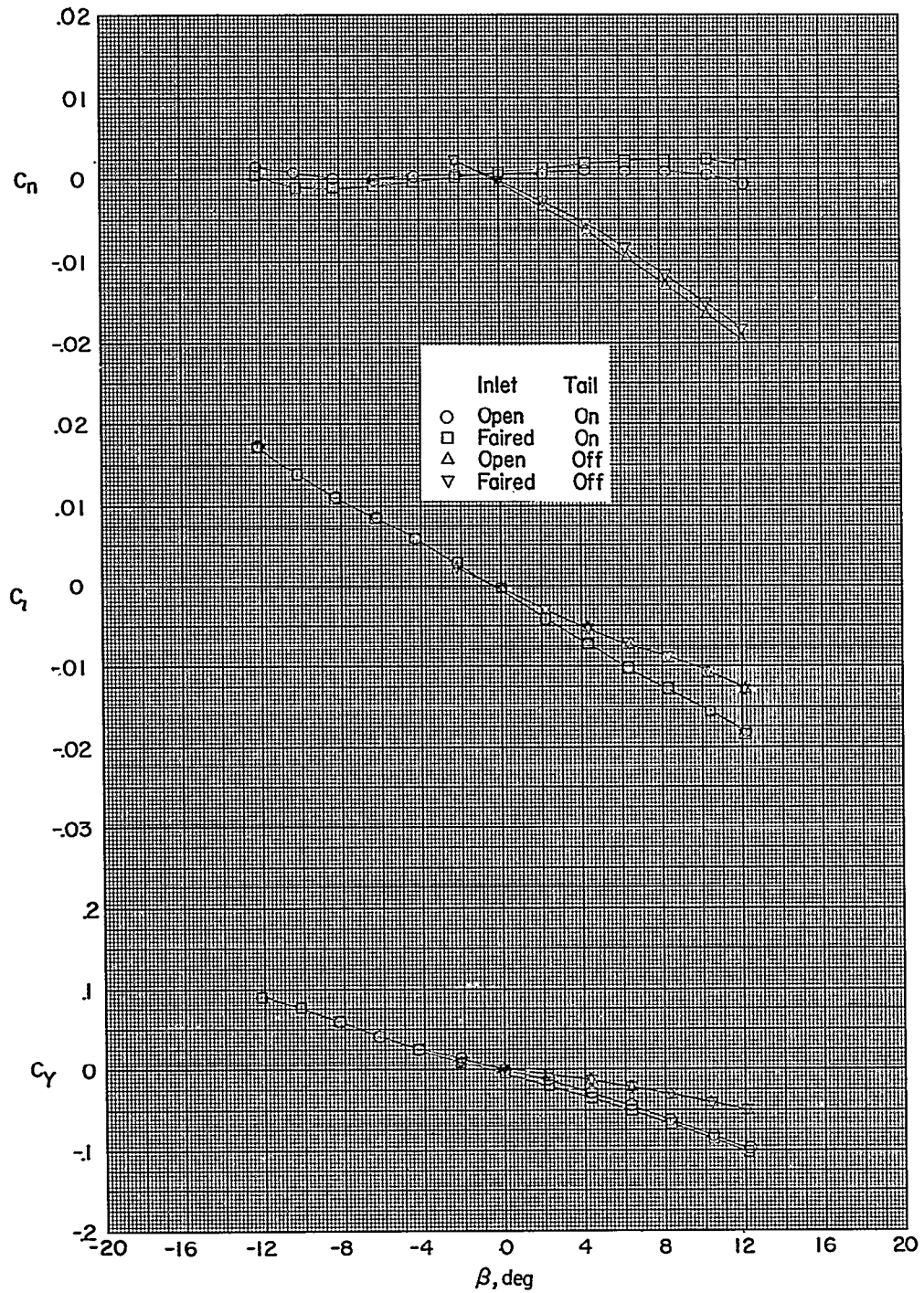
(a) $\alpha \approx 0^\circ$.

Figure 8.- Effects of inlet fairings on aerodynamic characteristics in sideslip of complete model and wing-fuselage combination; $\delta_a = \delta_e = \delta_r = 0^\circ$.



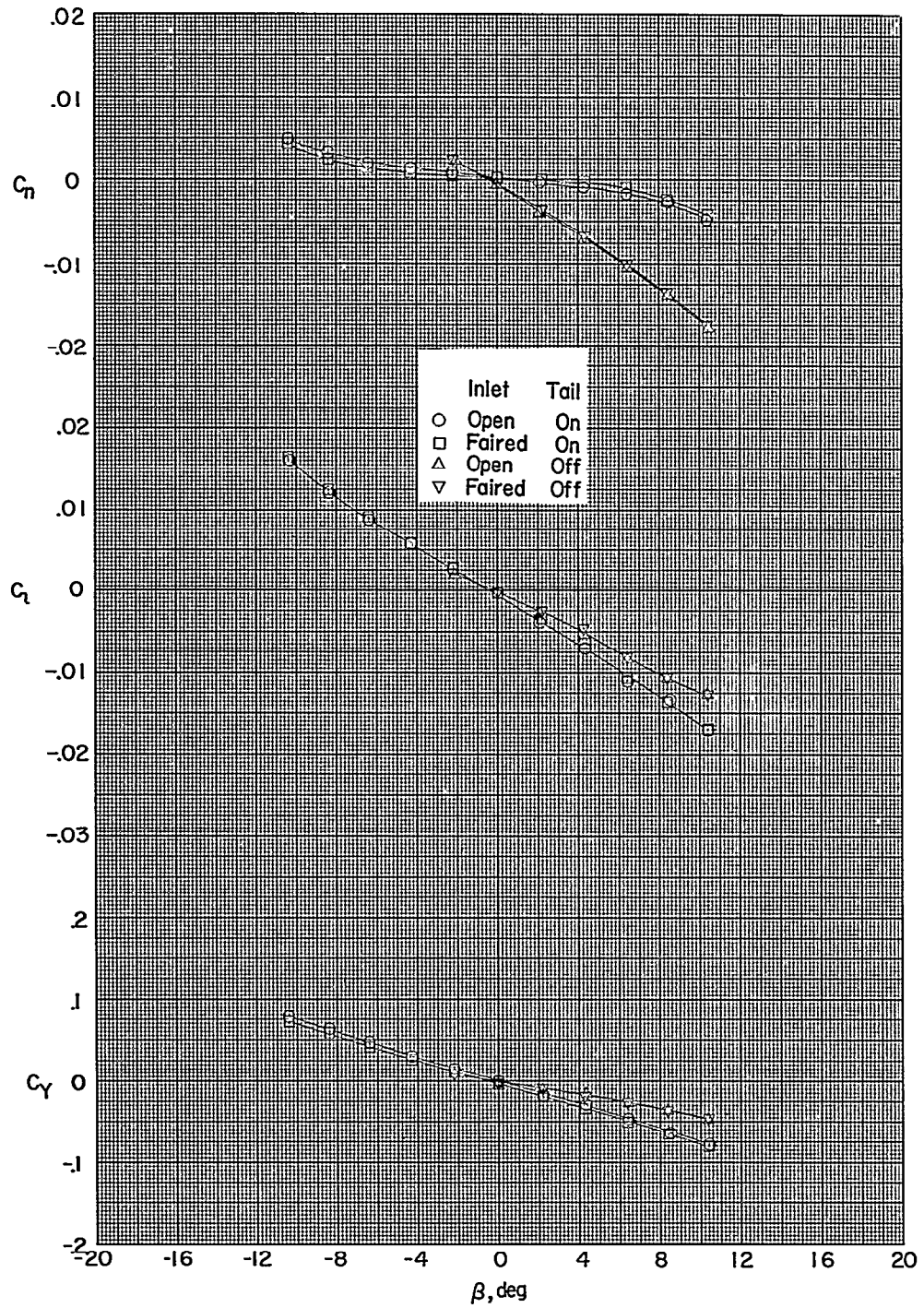
(b) $\alpha \approx 4.3^\circ$.

Figure 8.- Continued.



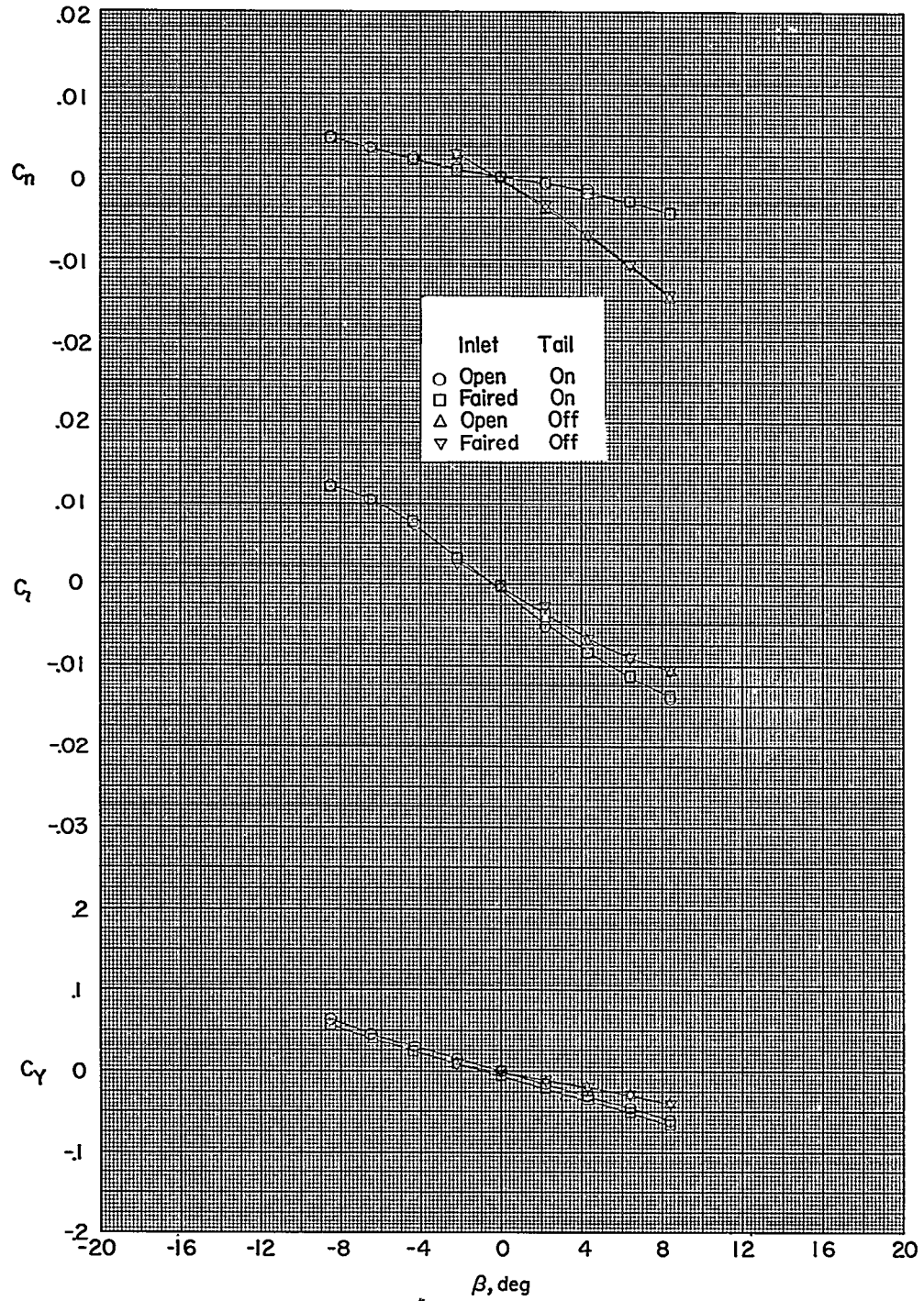
(c) $\alpha = 8.7^\circ$.

Figure 8.- Continued.



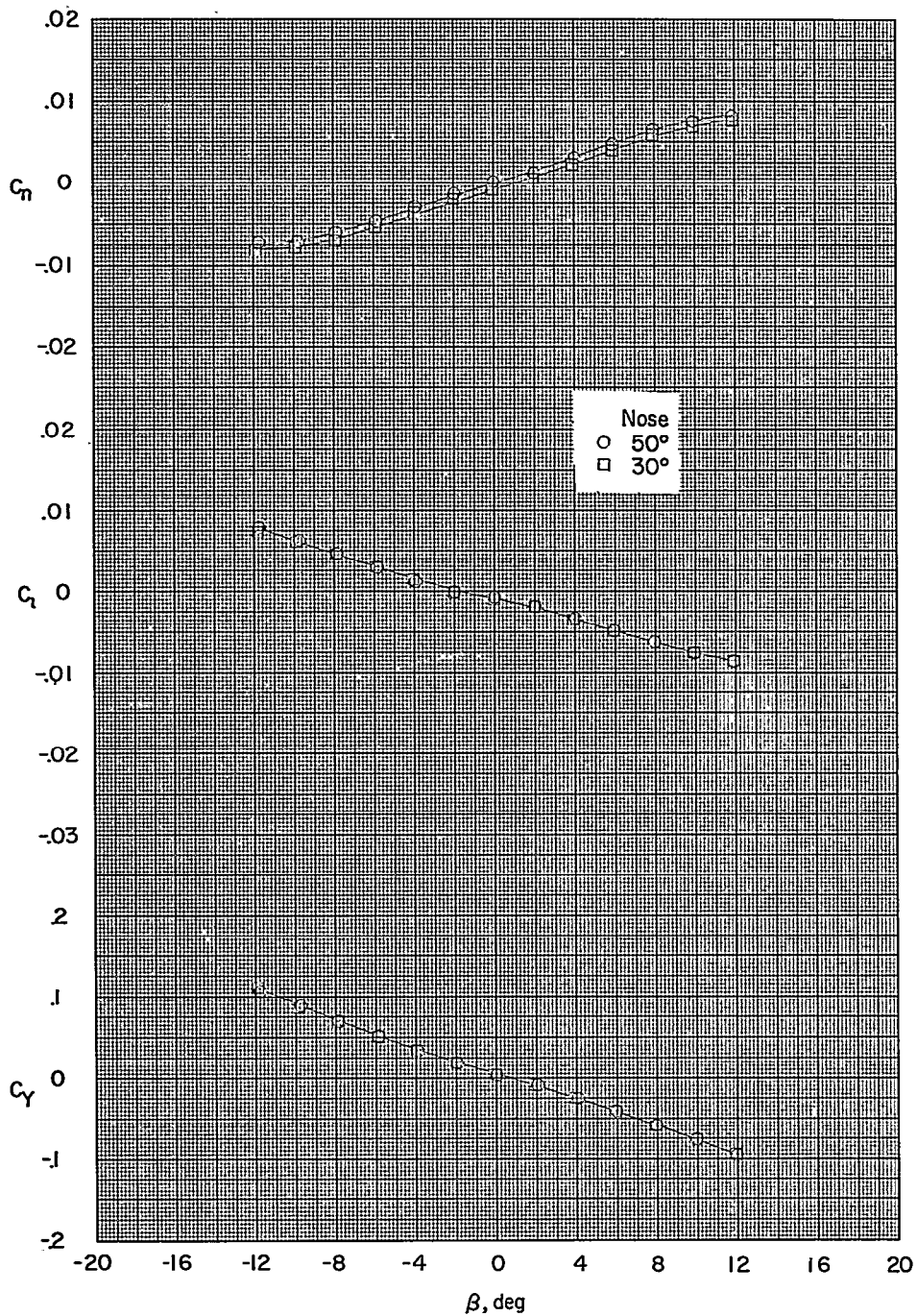
(d) $\alpha \approx 13^\circ$.

Figure 8.- Continued.



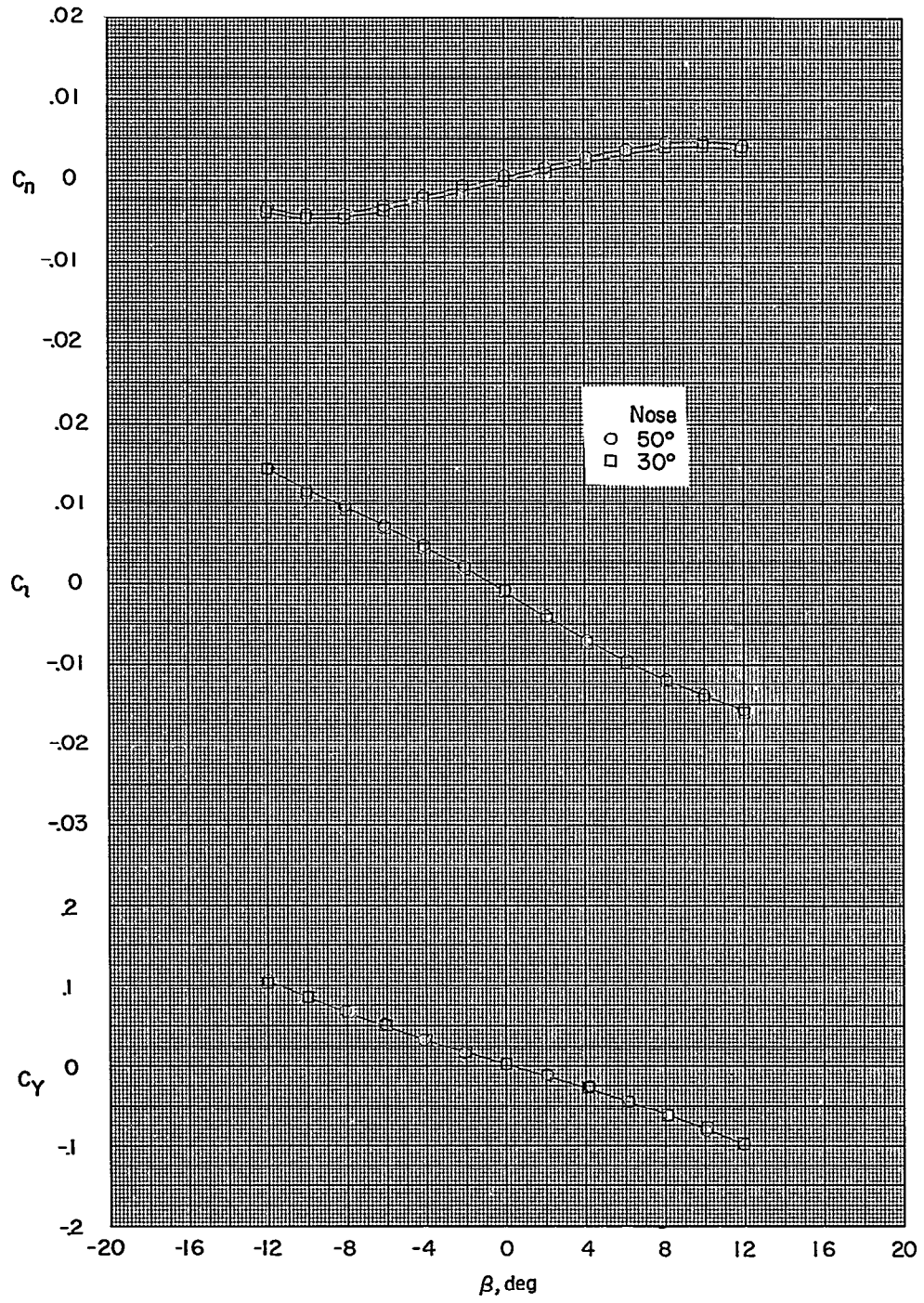
(e) $\alpha \approx 15.2^\circ$.

Figure 8.- Concluded.



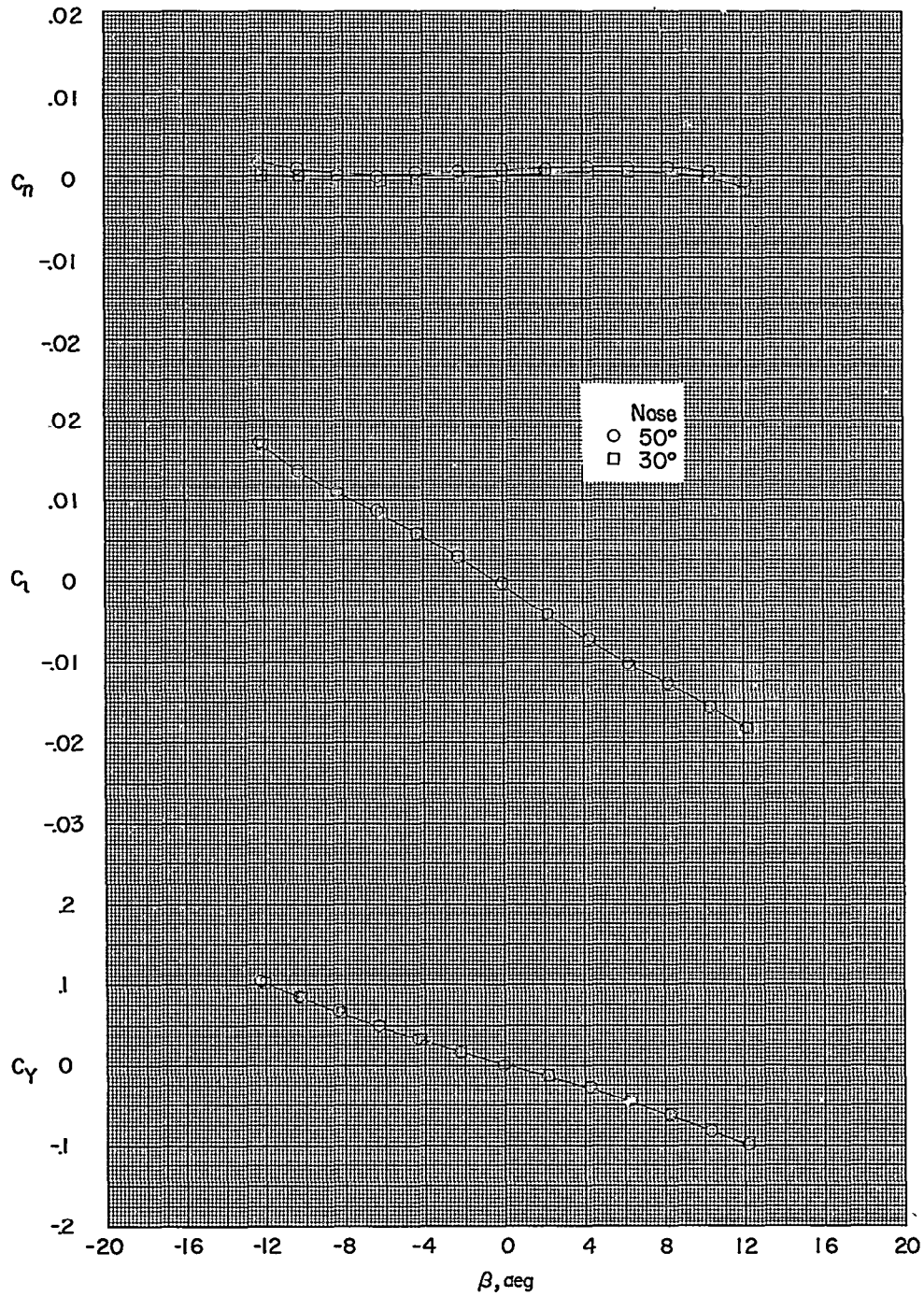
(a) $\alpha \approx 0^\circ$.

Figure 9.- Effects of fuselage nose shape on aerodynamic characteristics in sideslip of various angles of attack; complete model, $\delta_a = \delta_e = \delta_r = 0^\circ$.



(b) $\alpha \approx 4.3^\circ$.

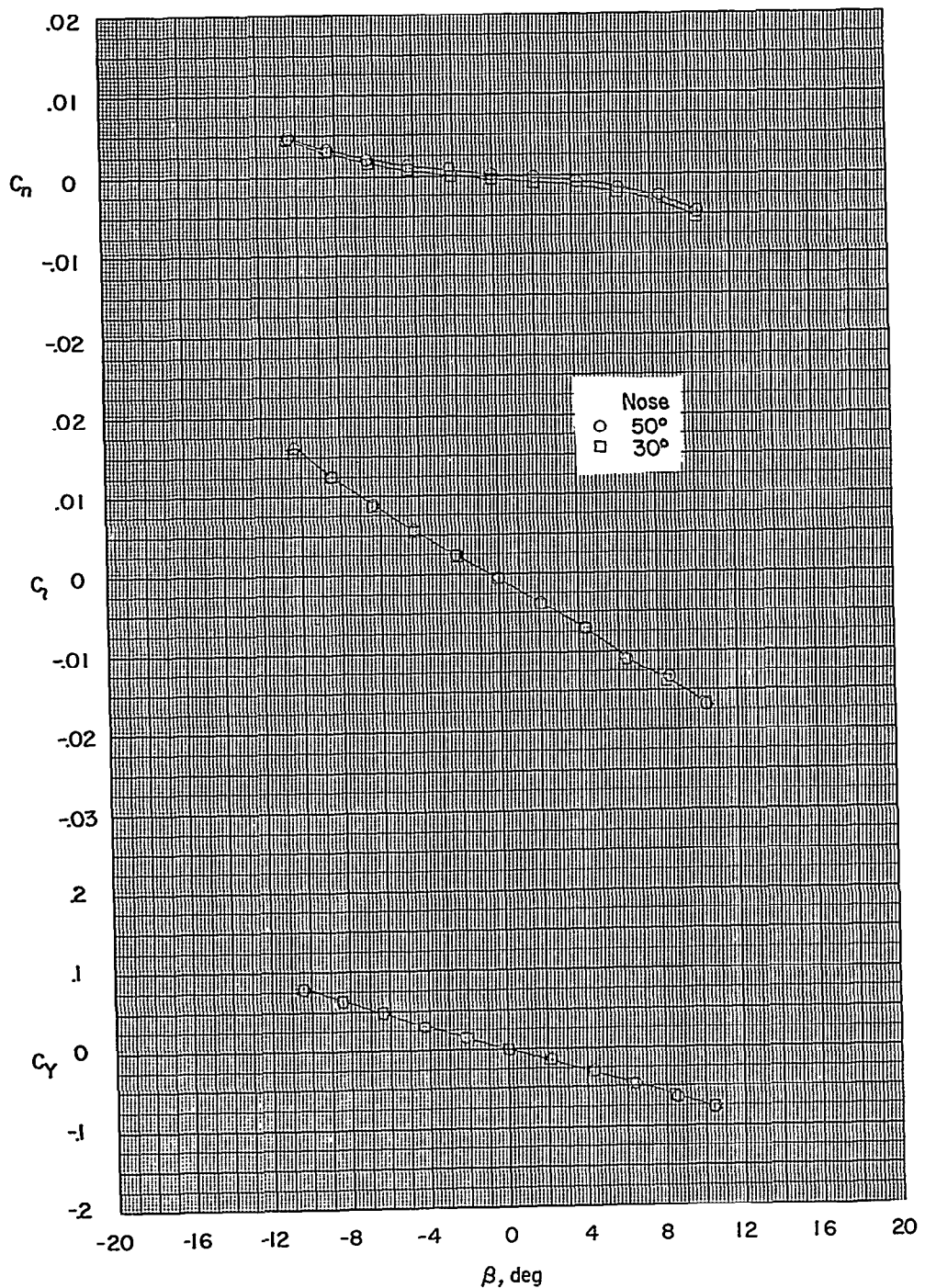
Figure 9.- Continued.



(c) $\alpha \approx 8.7^\circ$.

Figure 9.- Continued.

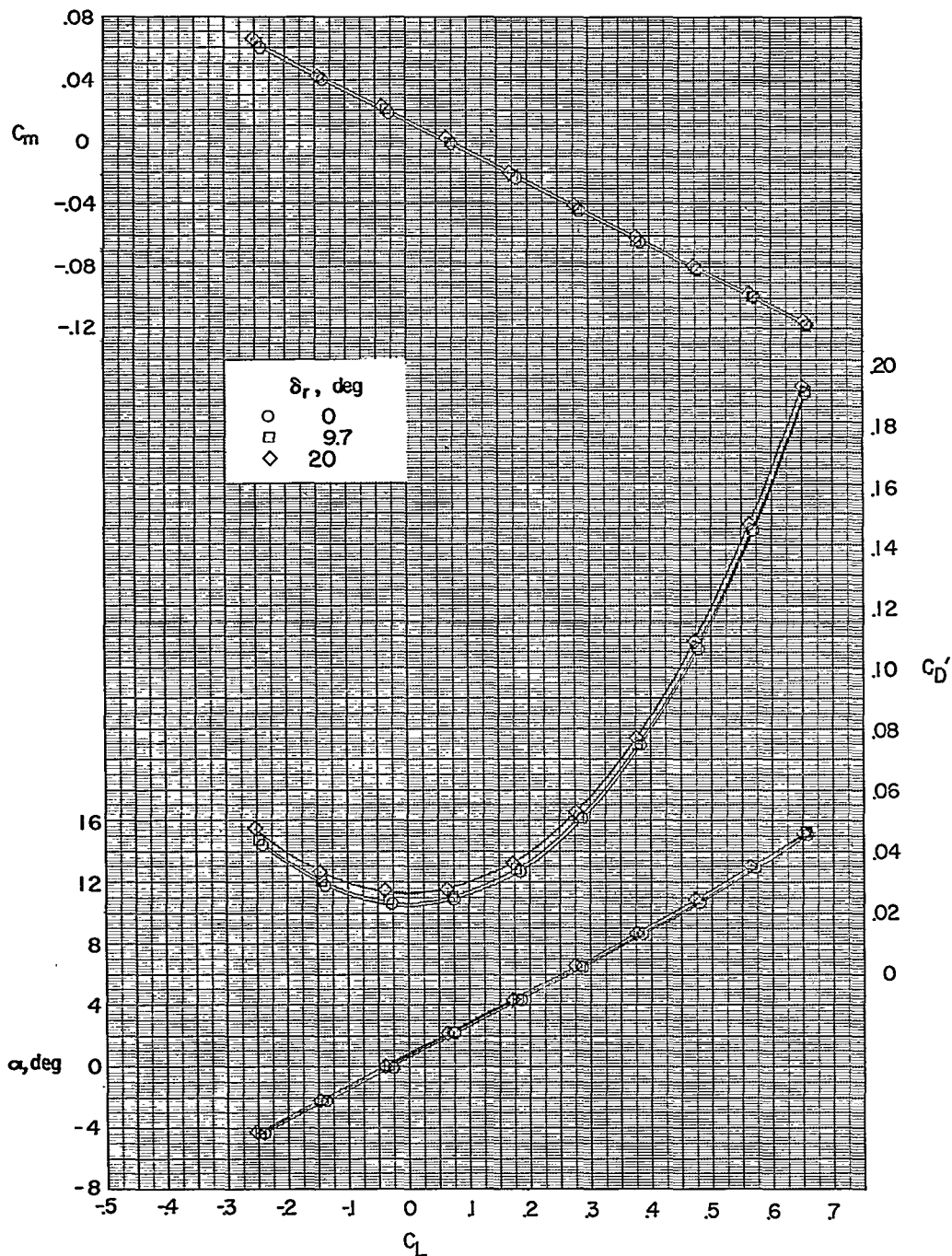
~~CONFIDENTIAL~~



(d) $\alpha \approx 13.0^\circ$.

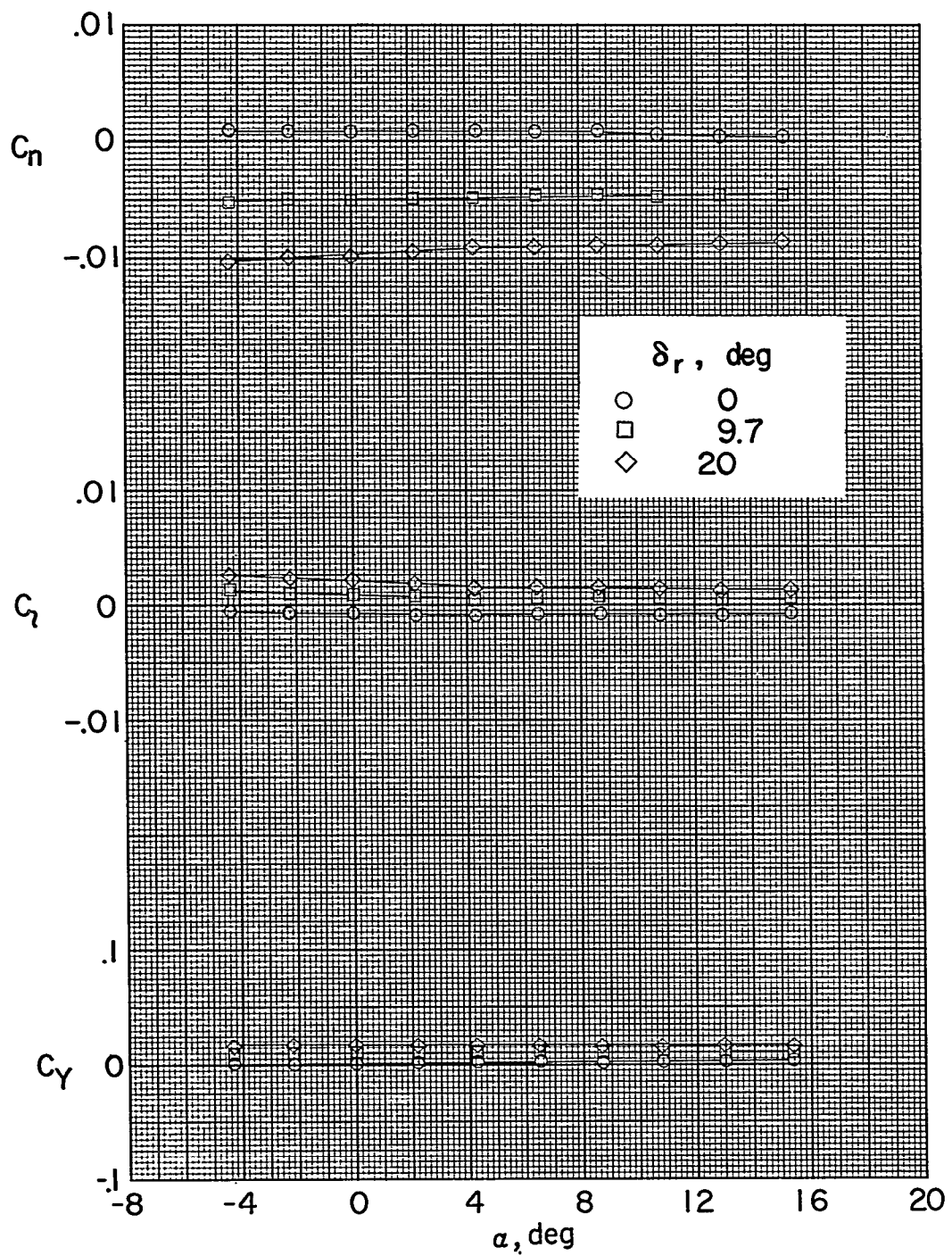
Figure 9.- Concluded.

~~CONFIDENTIAL~~



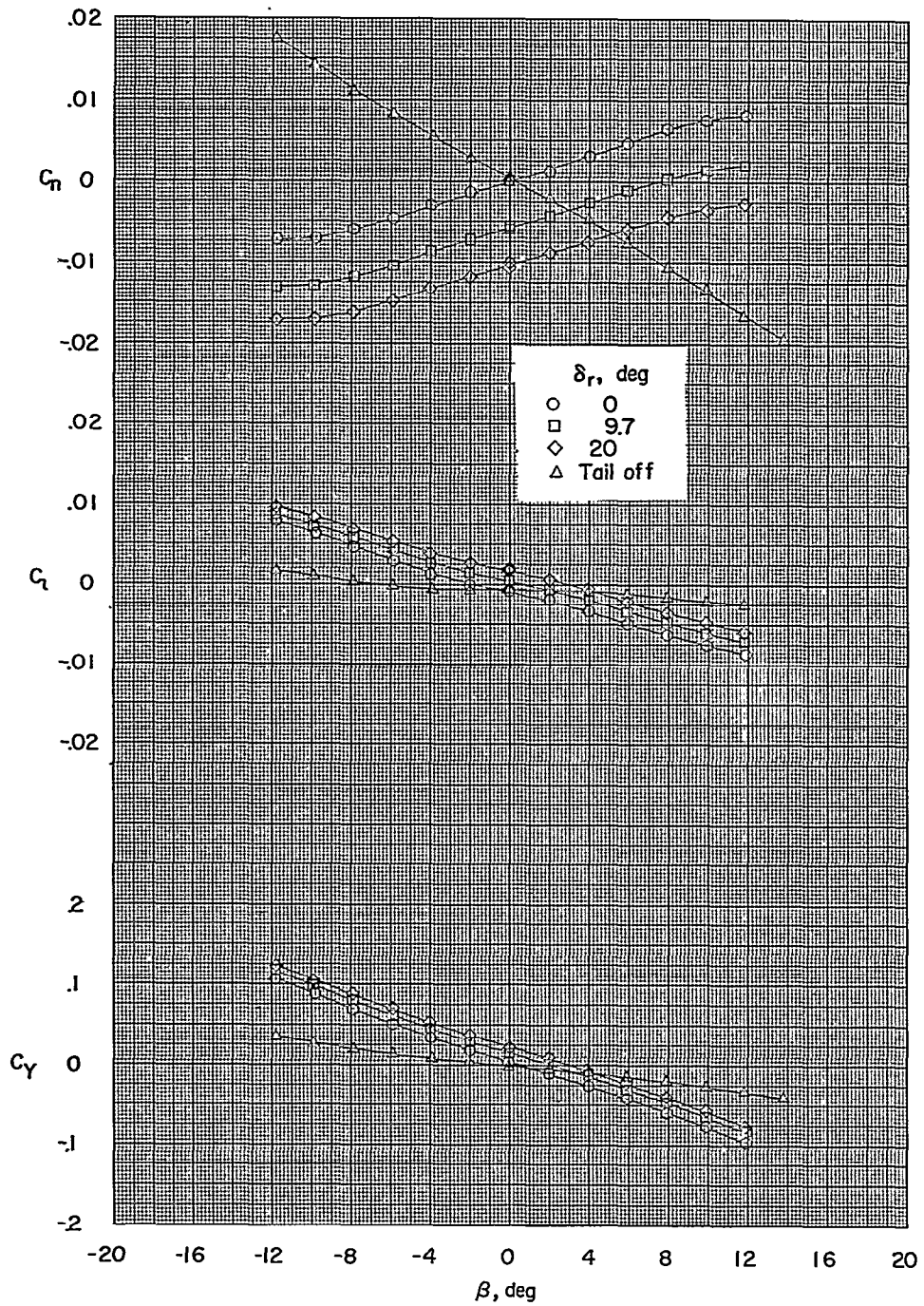
(a) Plot of C_m , C_D' , and α against C_L .

Figure 10.- Effects of rudder deflection on aerodynamic characteristics in pitch; complete model, $\delta_a = \delta_e = 0^\circ$, $\beta = 0^\circ$.



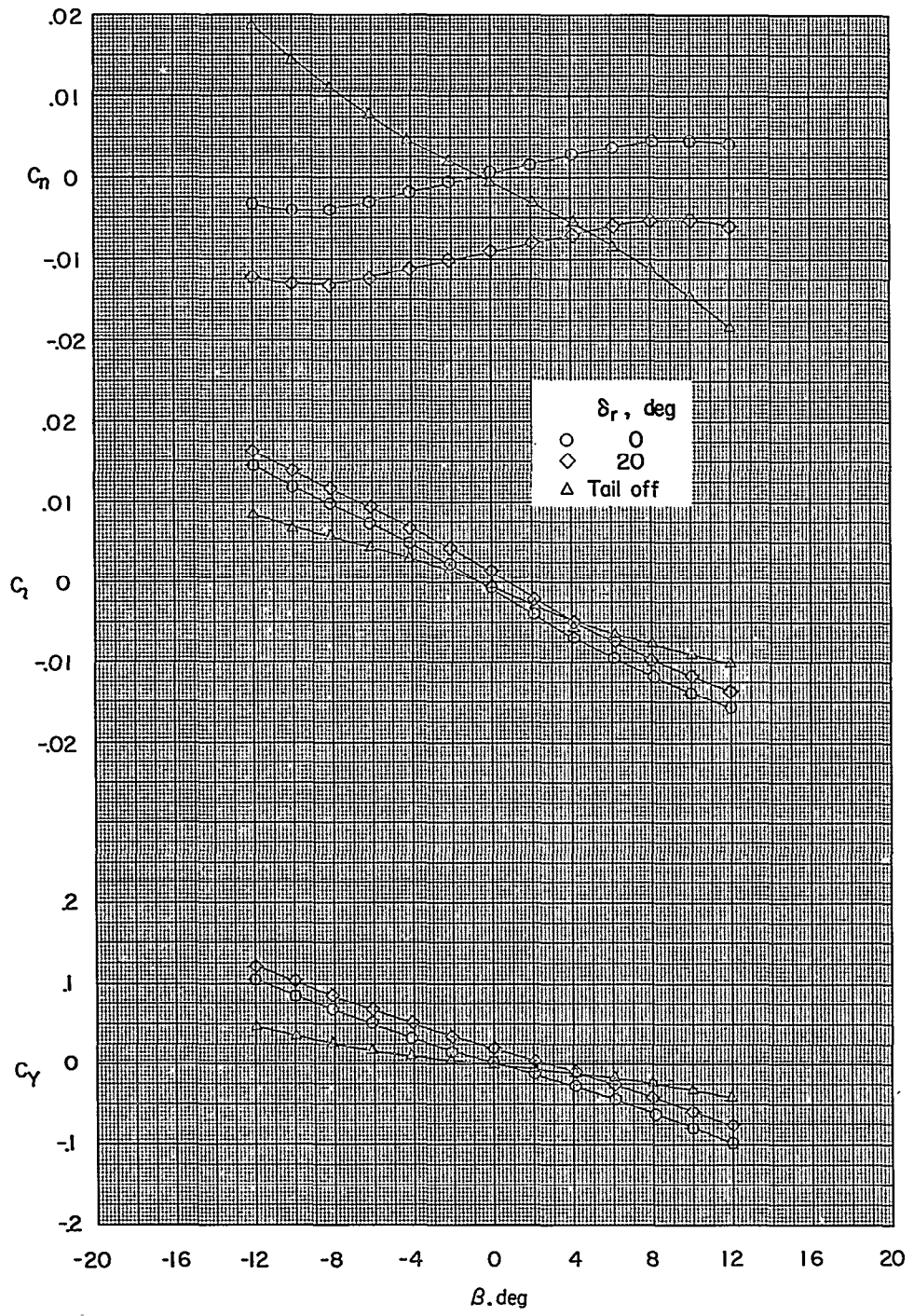
(b) Plot of C_n , C_z , and C_y against α .

Figure 10.- Concluded.



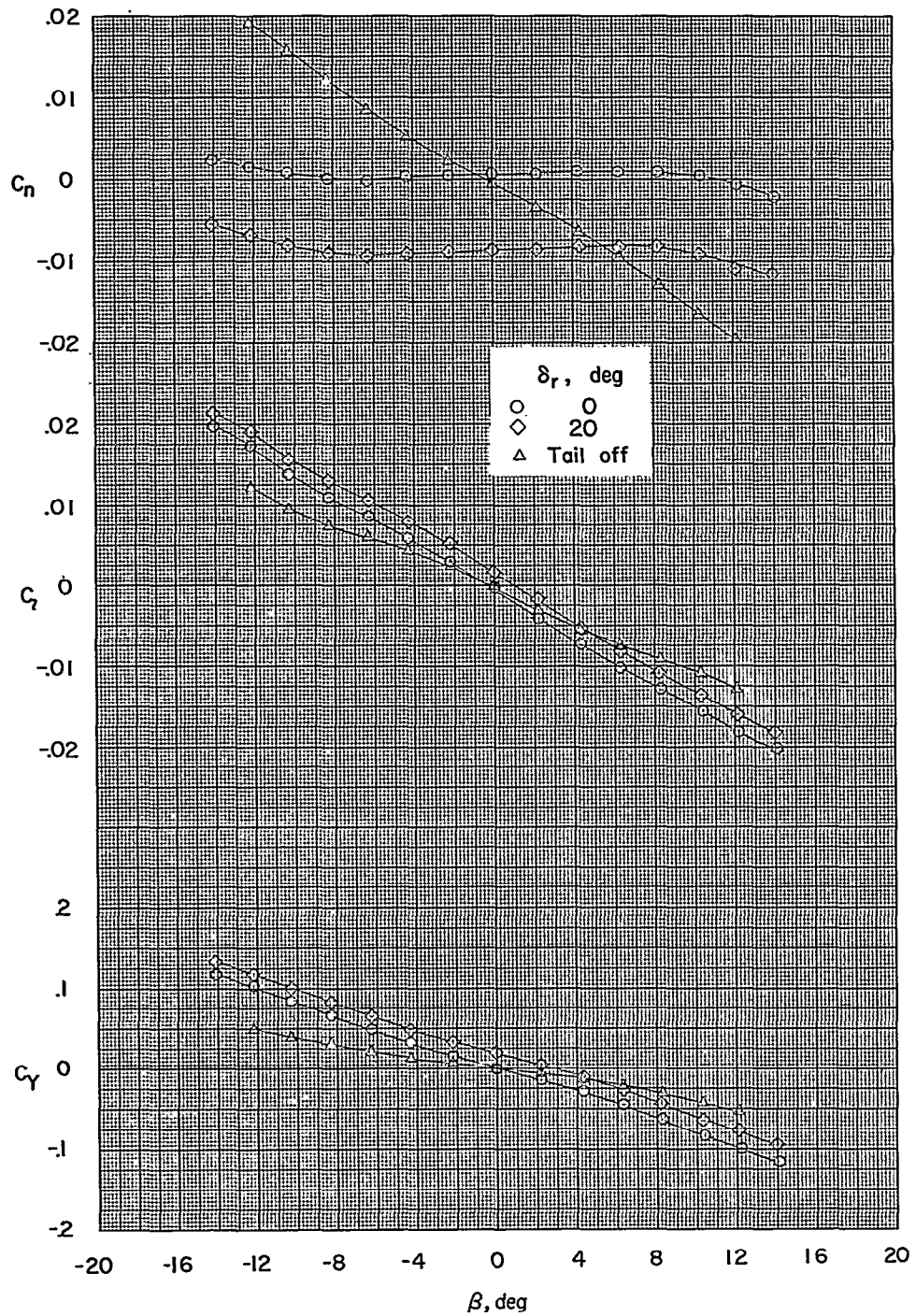
(a) $\alpha \approx 0^\circ$.

Figure 11.- Aerodynamic characteristics in sideslip at several angles of attack of complete model with various rudder deflections of wing-fuselage combination; $\delta_a = \delta_e = 0^\circ$.



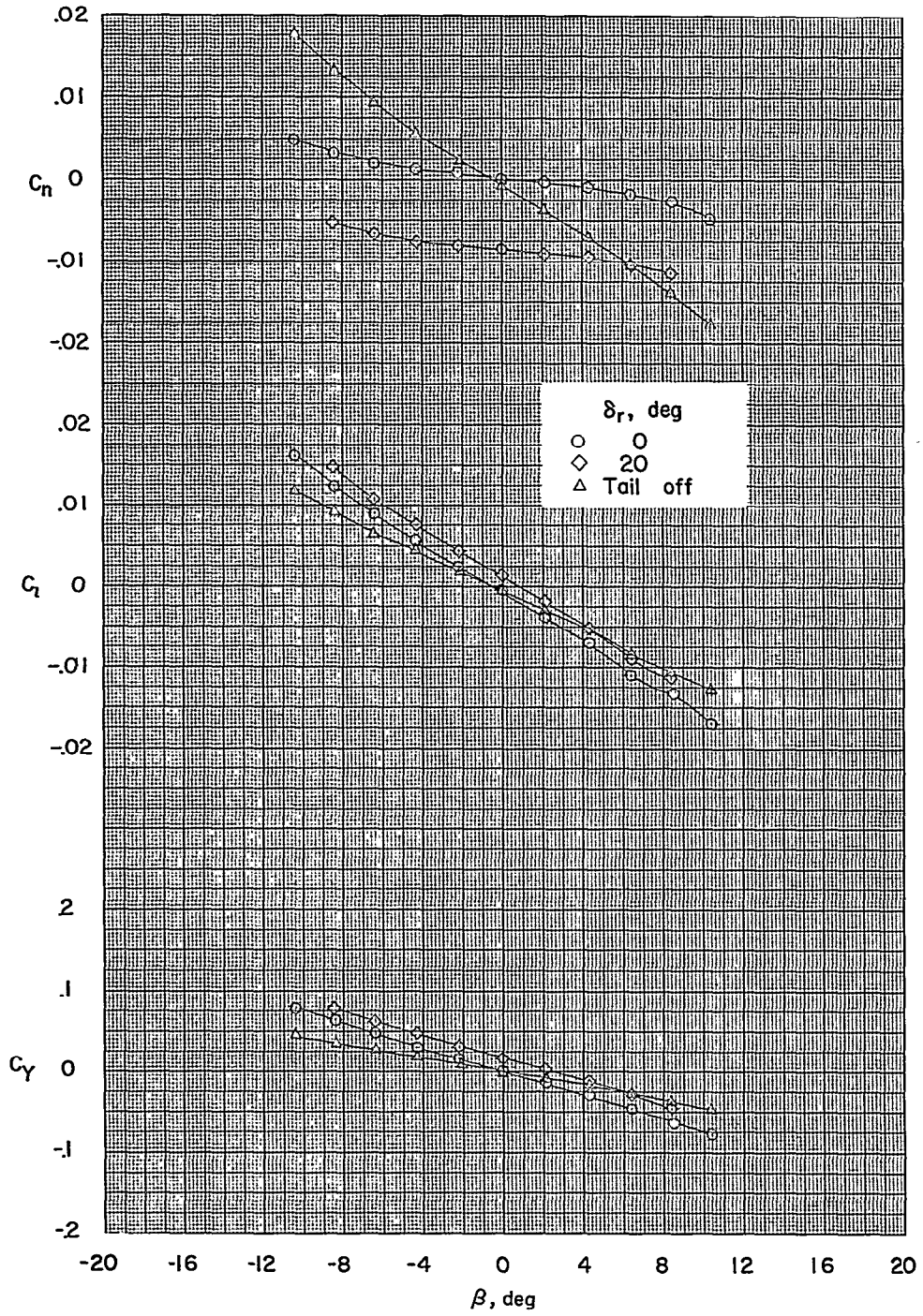
(b) $\alpha \approx 4.3^\circ$.

Figure 11.- Continued.



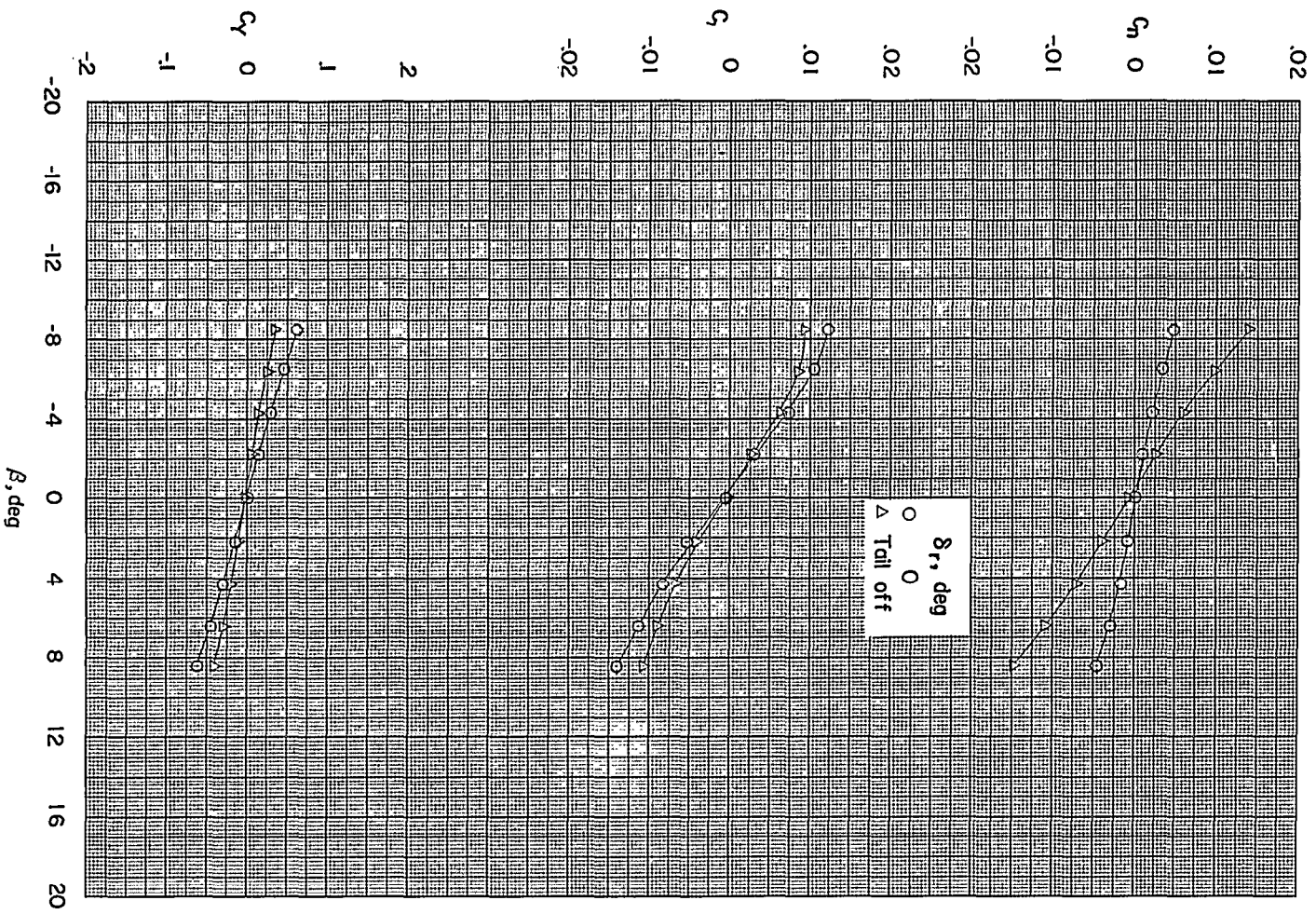
(c) $\alpha \approx 8.7^\circ$.

Figure 11.- Continued.



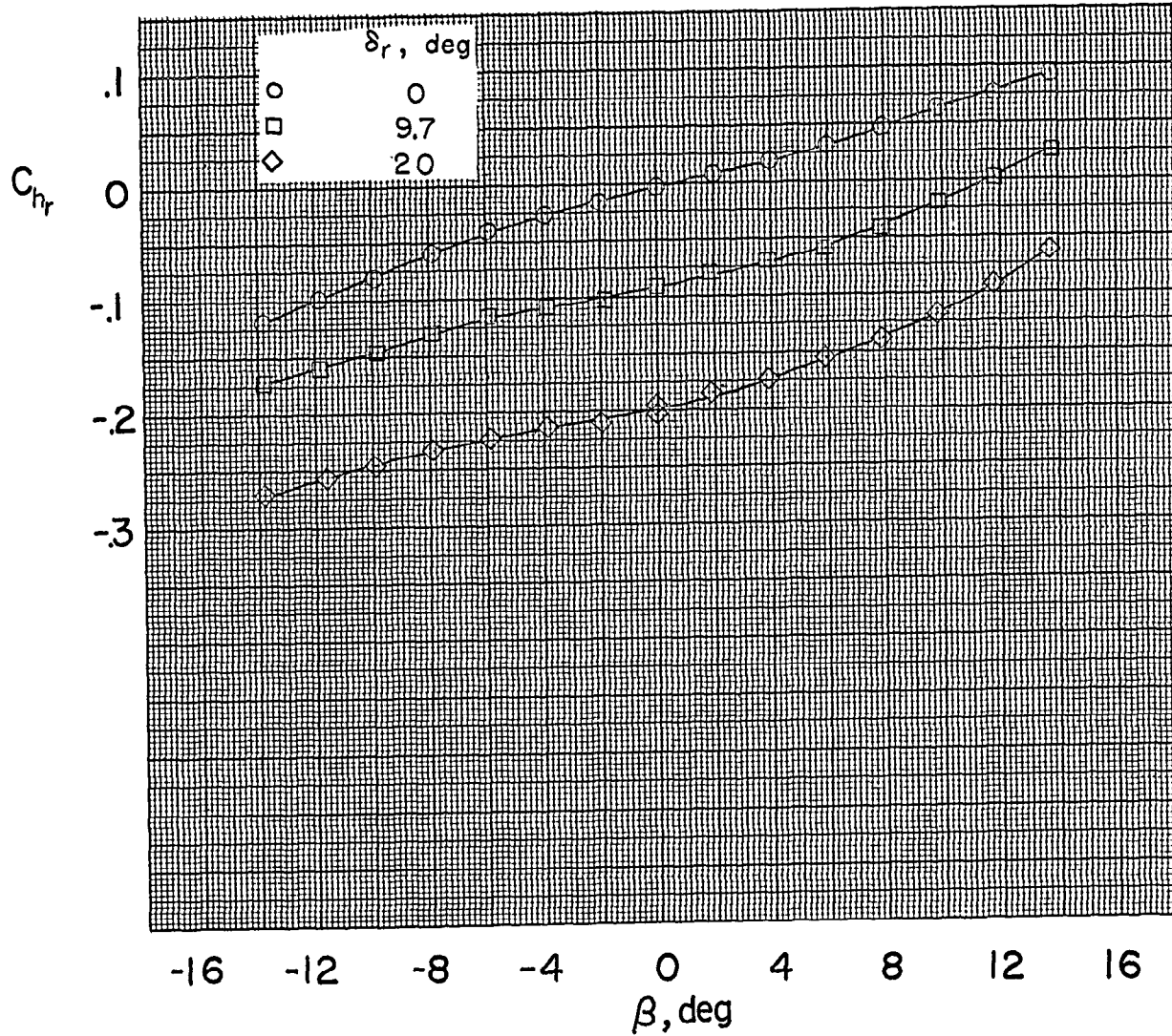
(d) $\alpha \approx 13.0^\circ$.

Figure 11.- Continued.



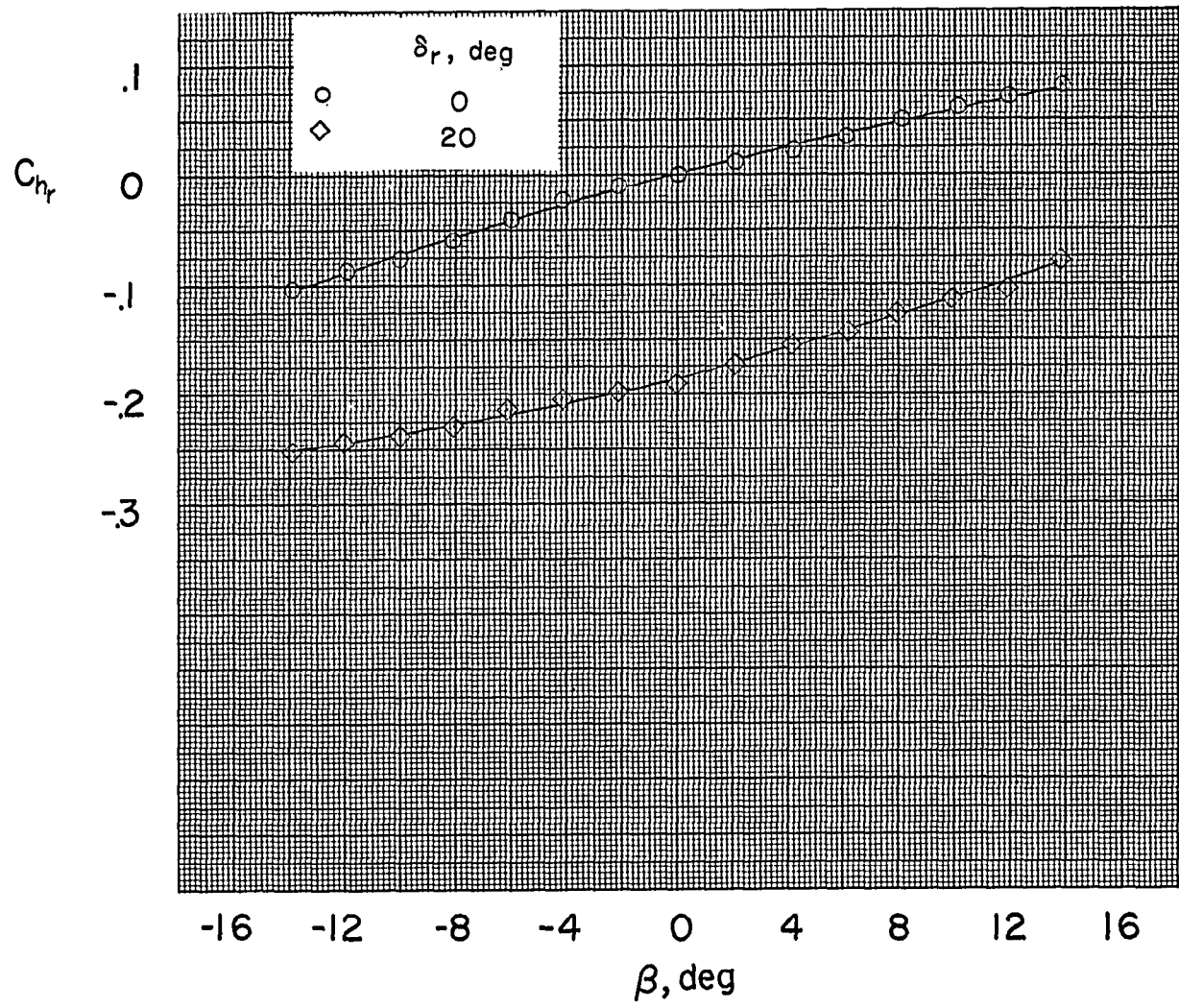
(e) $\alpha \approx 15.20^\circ$.

Figure 11.- Concluded.



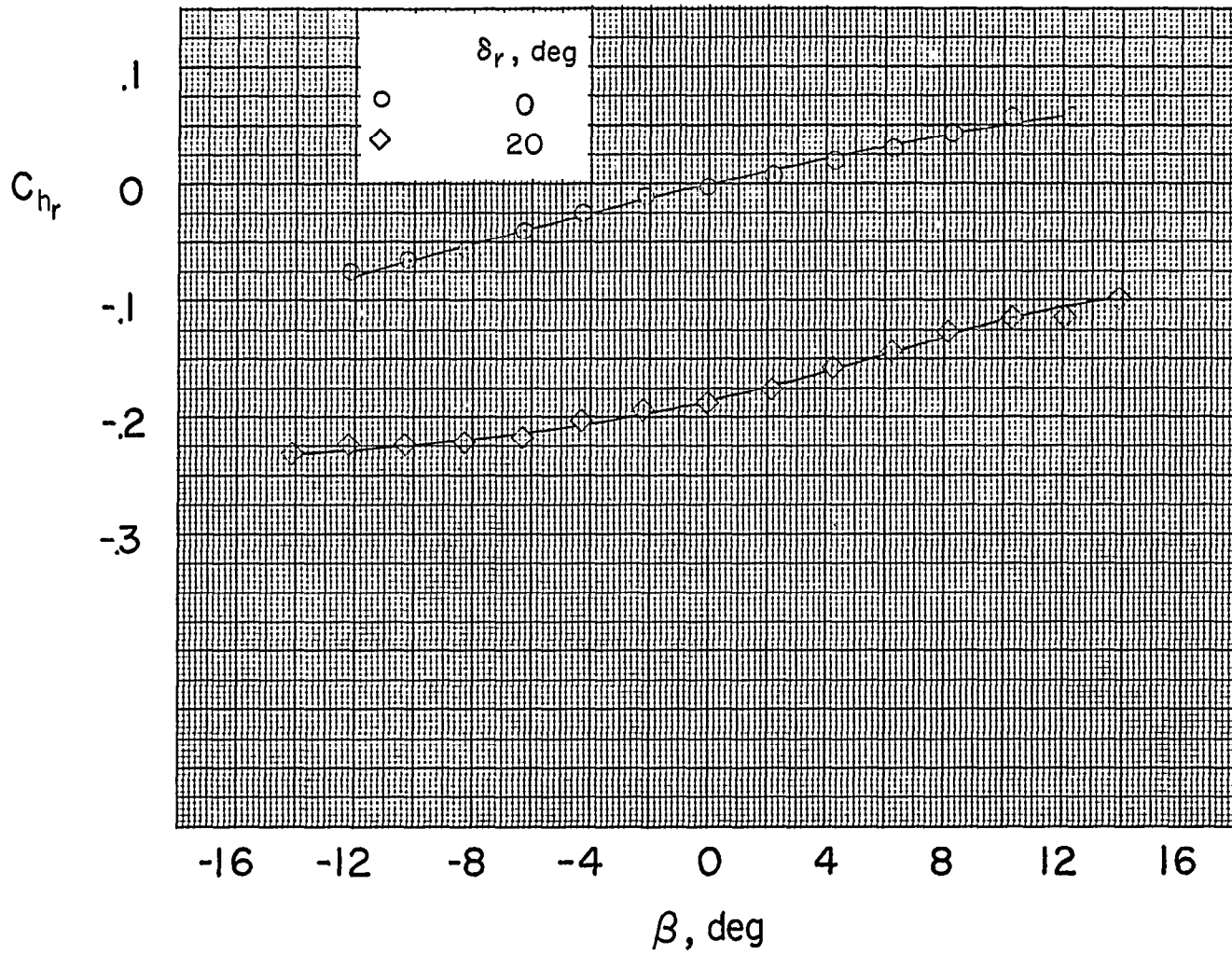
(a) $\alpha \approx 0^\circ$.

Figure 12.- Rudder hinge-moment characteristics in sideslip at several angles of attack; $\delta_e = \delta_a = 0^\circ$.



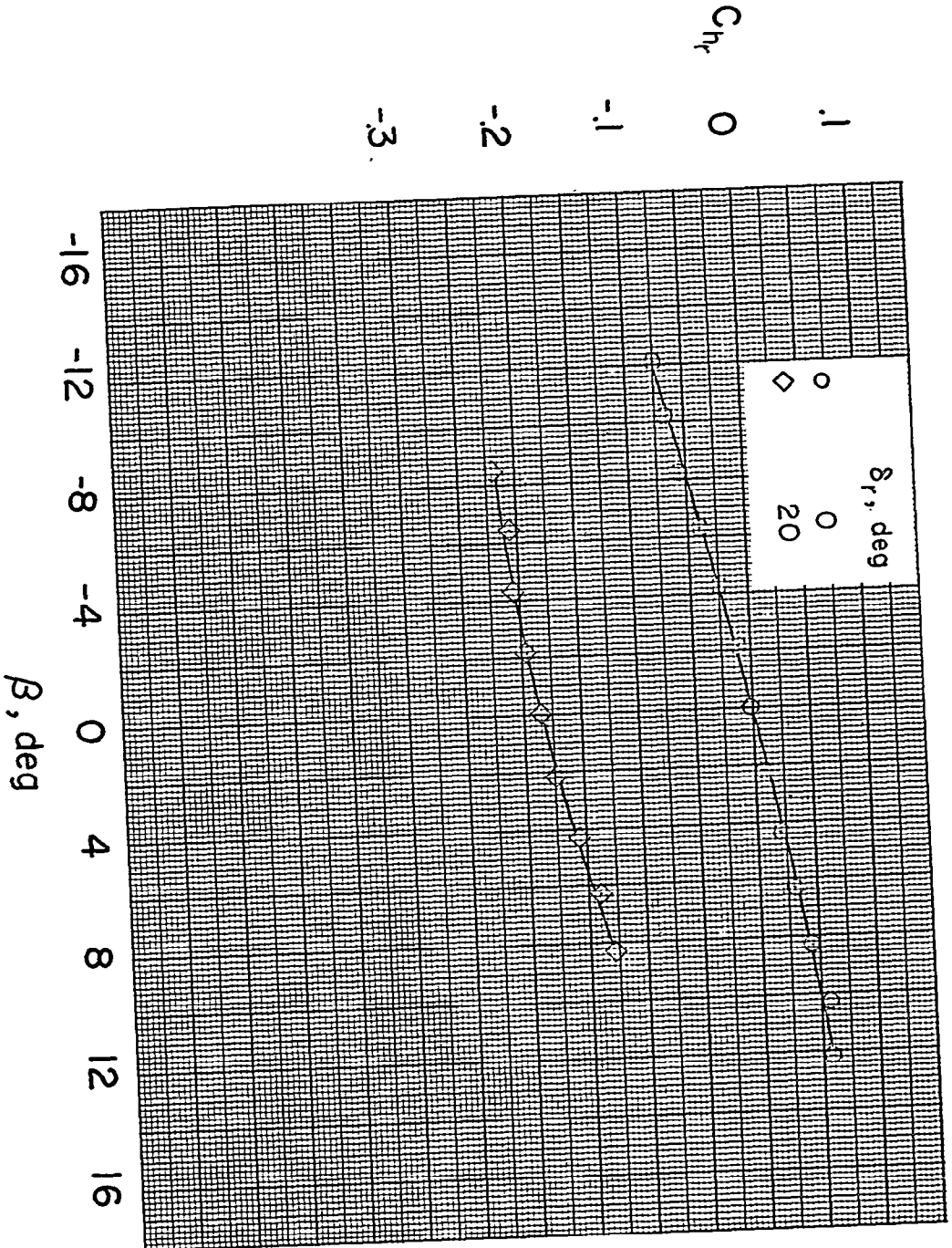
(b) $\alpha \approx 4.3^\circ$.

Figure 12.- Continued.



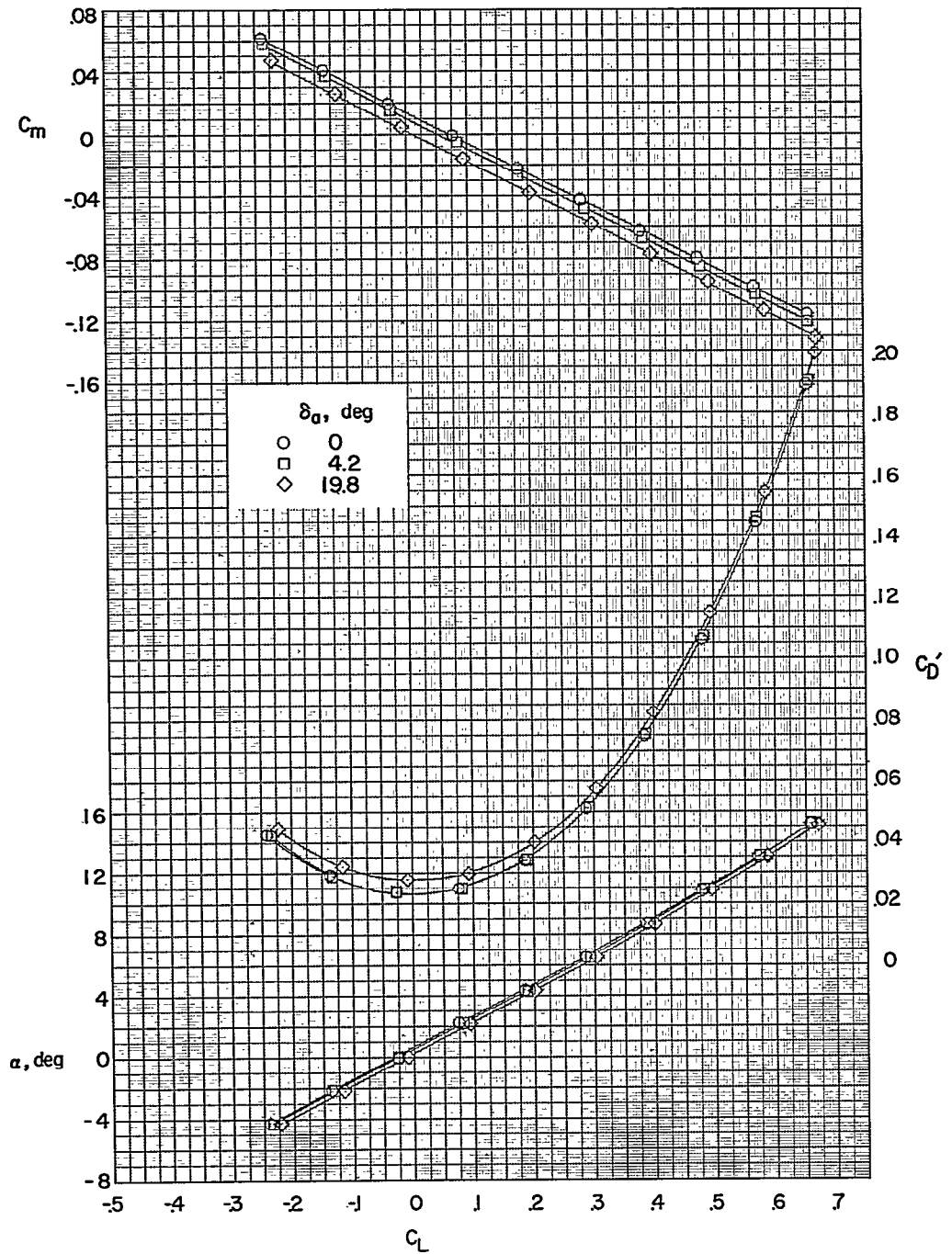
(c) $\alpha \approx 8.7^\circ$.

Figure 12.- Continued.



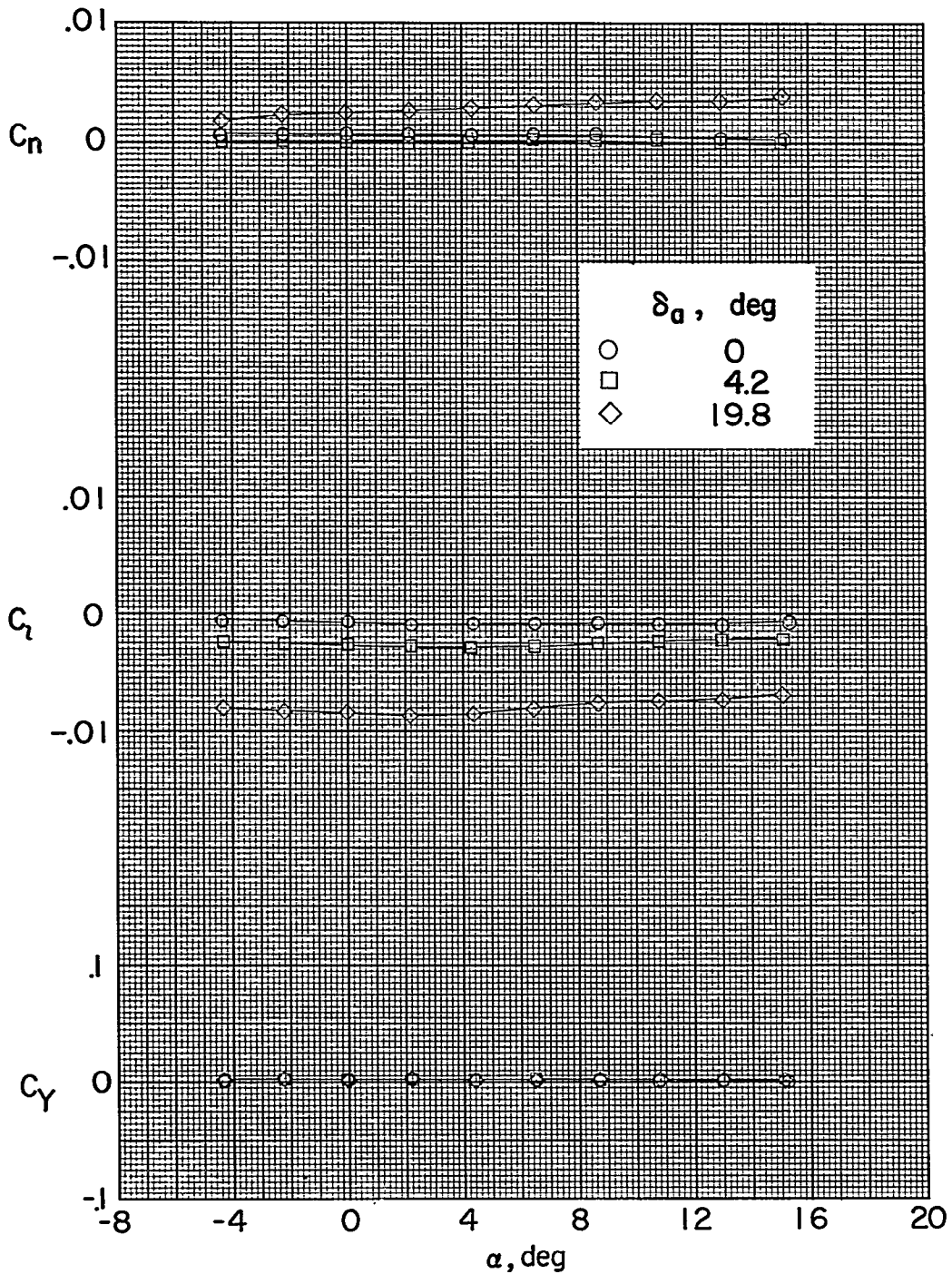
(a) $\alpha \approx 13.0^\circ$.

Figure 12.- Concluded.



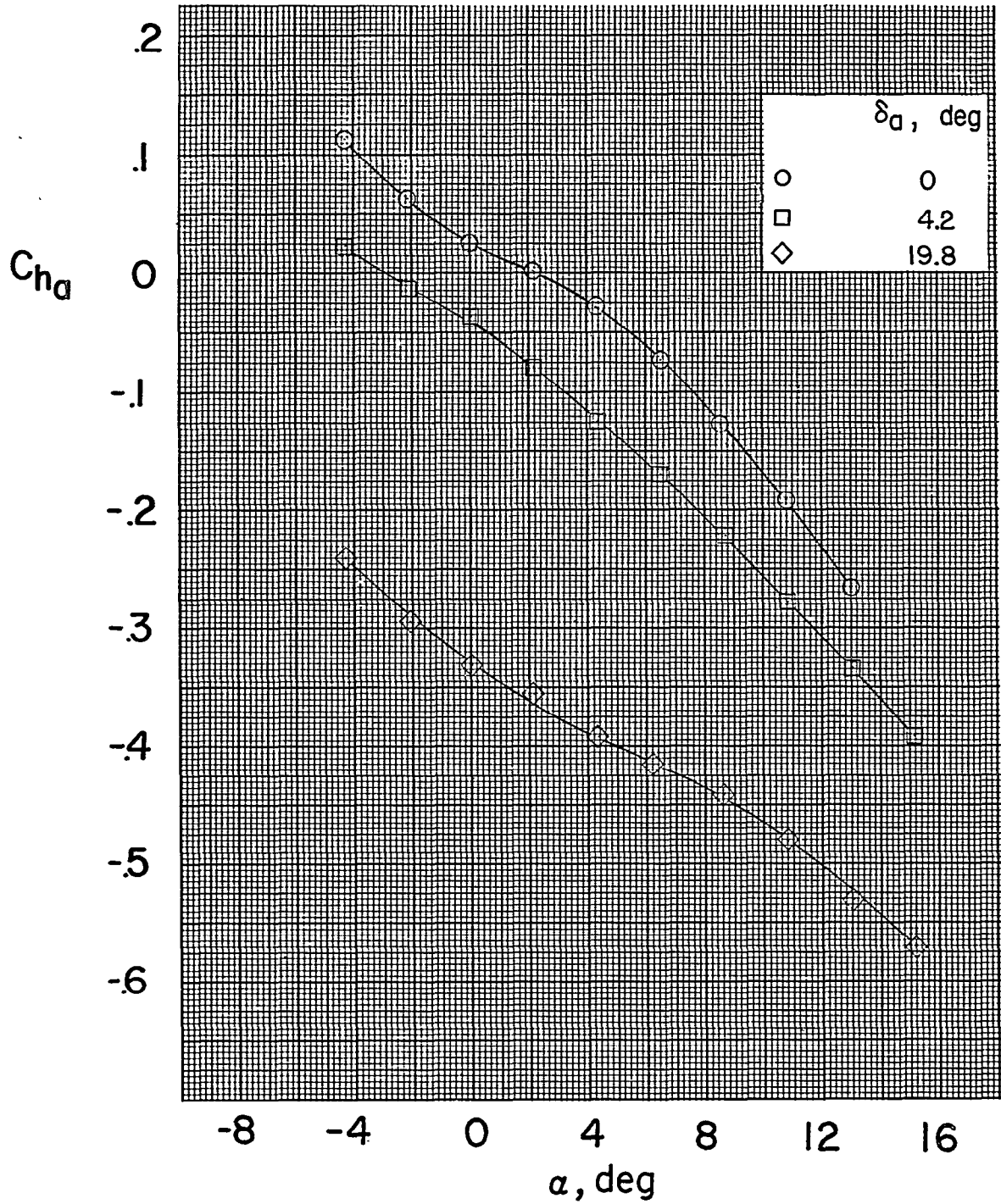
(a) Plot of C_m , C_D' , and α against C_L .

Figure 13.- Effects of aileron deflection on aerodynamic characteristics in pitch; complete model, $\delta_e = \delta_r = 0^\circ$, $\beta = 0^\circ$.



(b) Plot of C_n , C_z , and C_y against α .

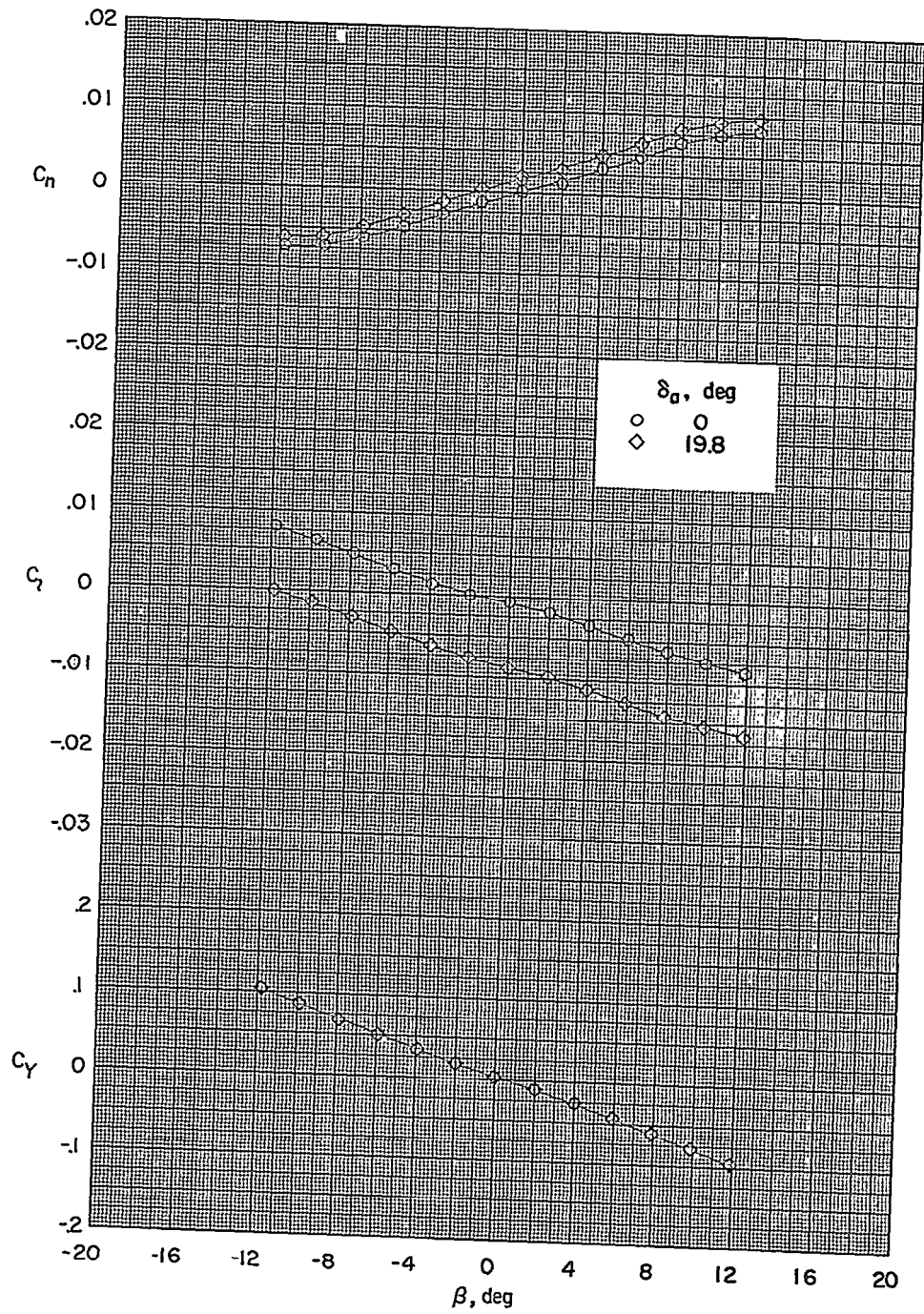
Figure 13.- Continued.



(c) Plot of C_{h_a} against α .

Figure 13.- Concluded.

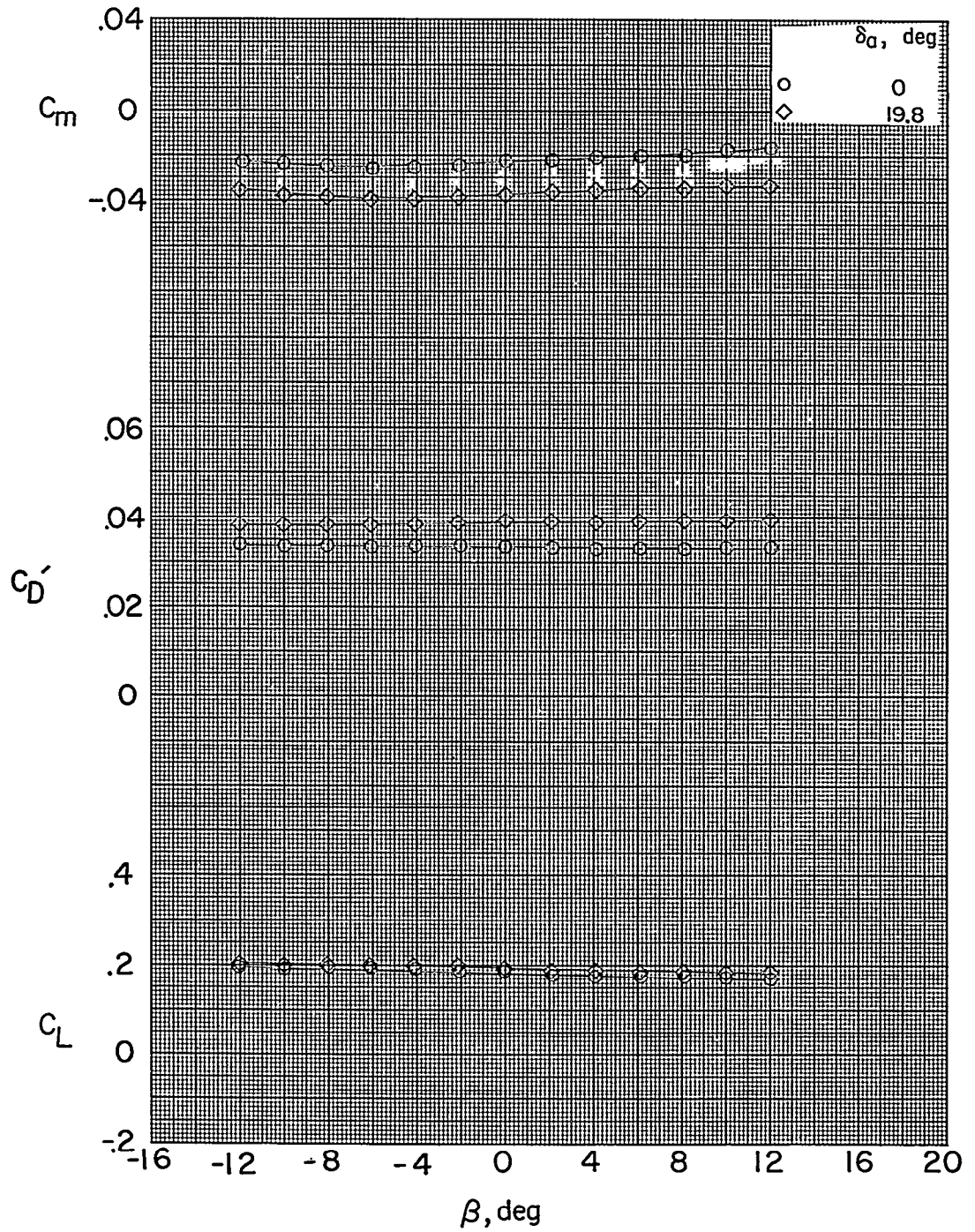
~~CONFIDENTIAL~~



(a) $\alpha \approx 0^\circ$.

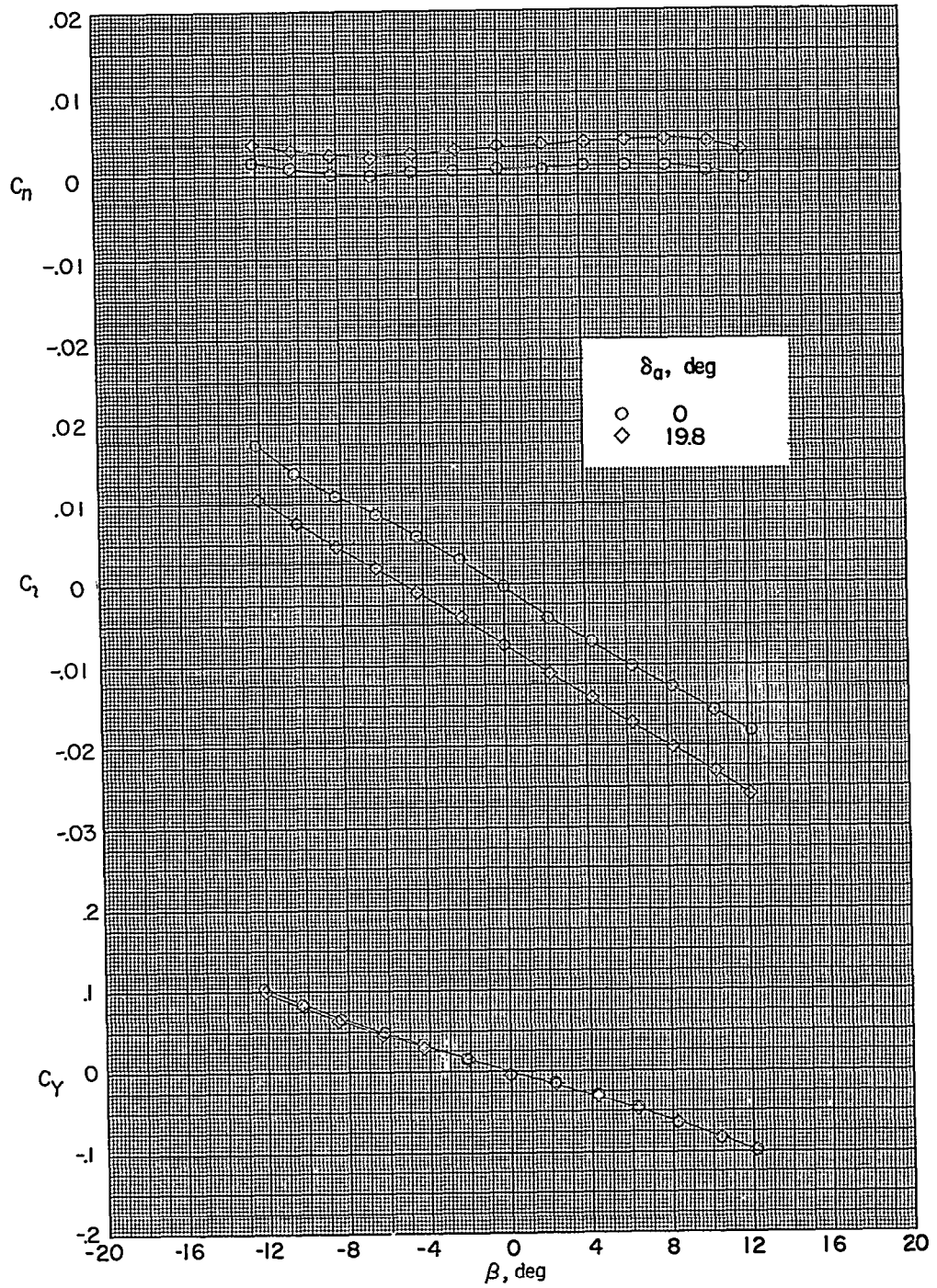
Figure 14.- Effect of aileron deflection on aerodynamic characteristics in sideslip for various angles of attack; $\delta_e = \delta_r = 0^\circ$.

~~CONFIDENTIAL~~



(b) Concluded.

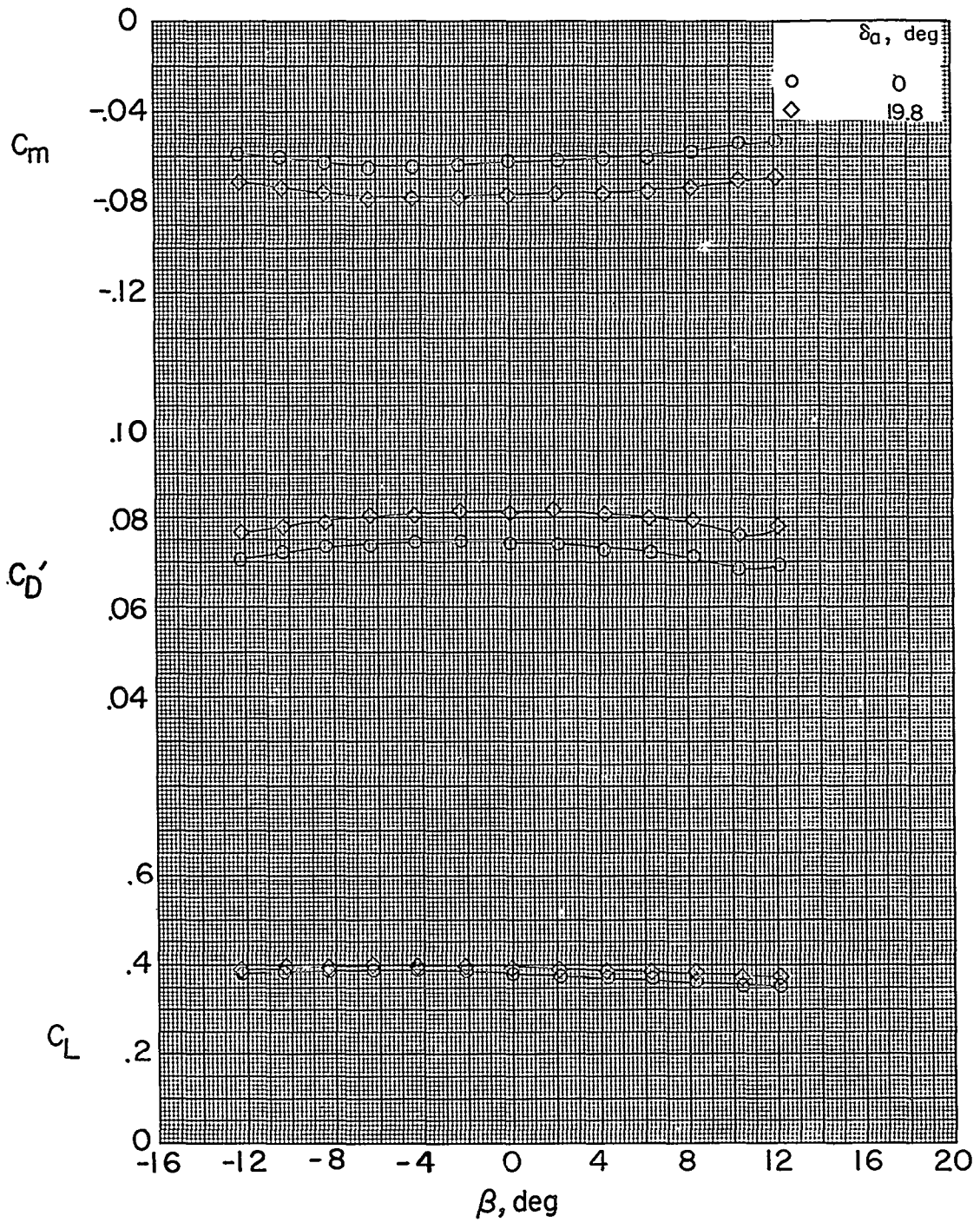
Figure 14.- Continued.



(c) $\alpha \approx 8.7^\circ$.

Figure 14.- Continued.

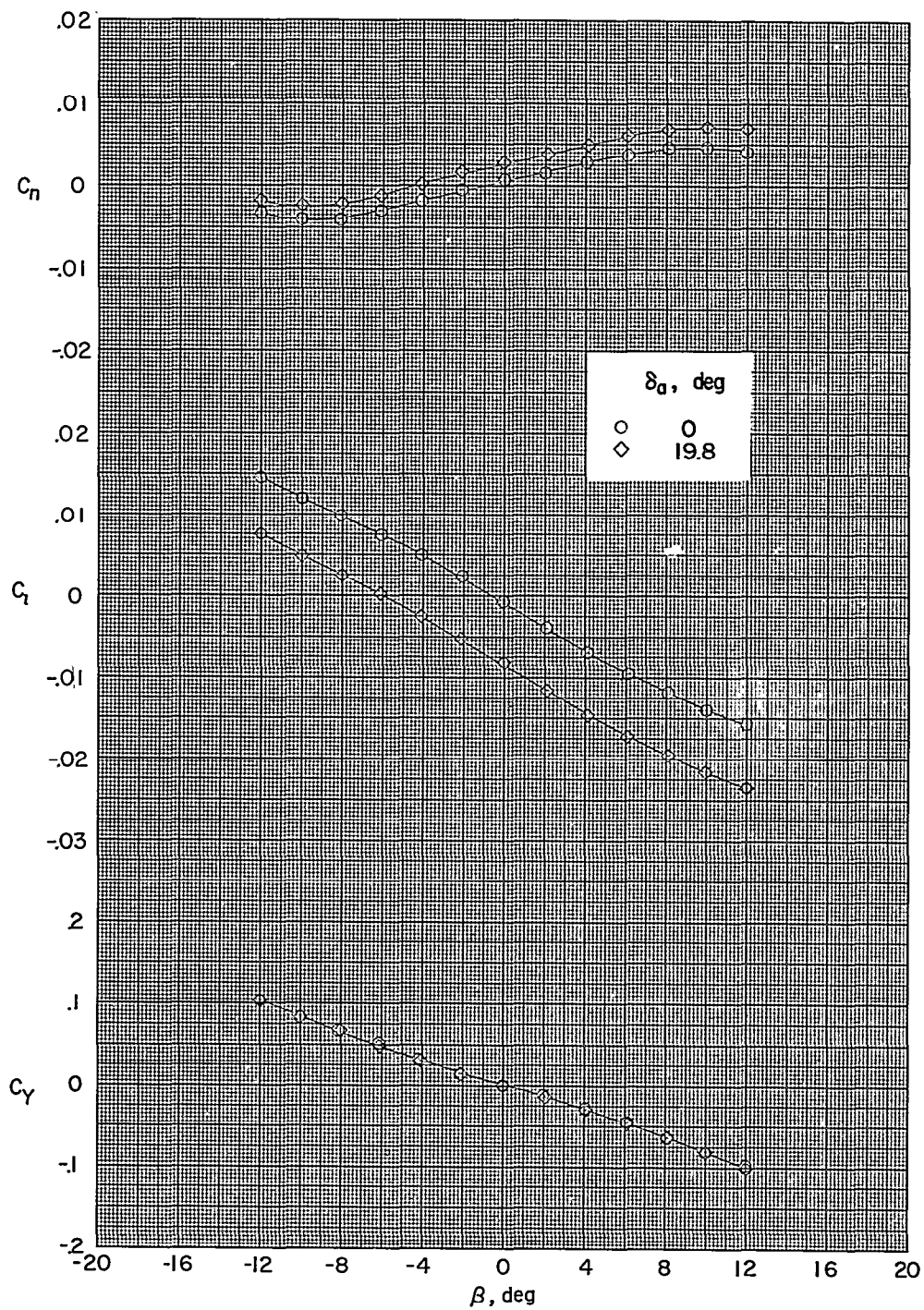
~~CONFIDENTIAL~~



(c) Concluded.

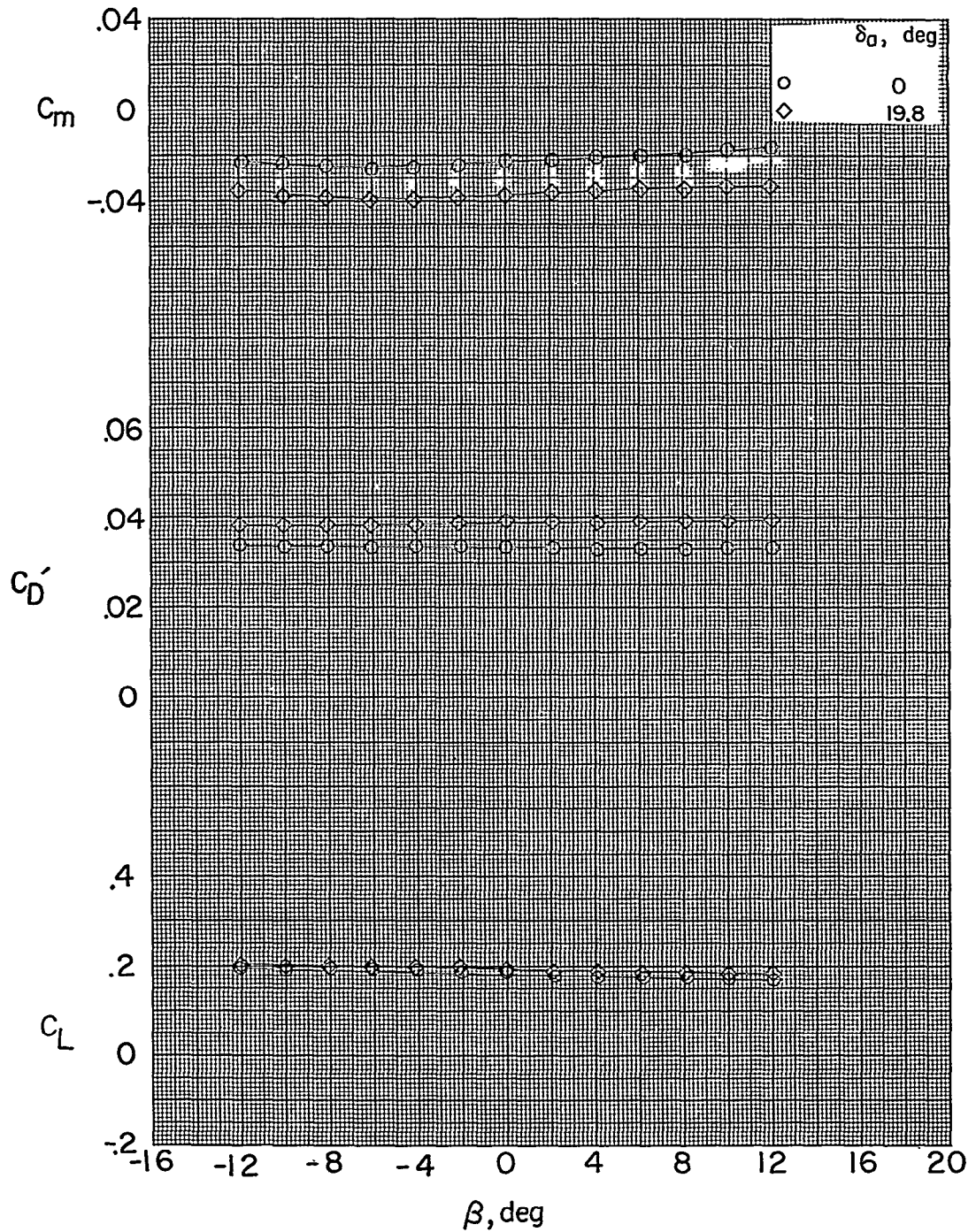
Figure 14.- Continued.

~~CONFIDENTIAL~~



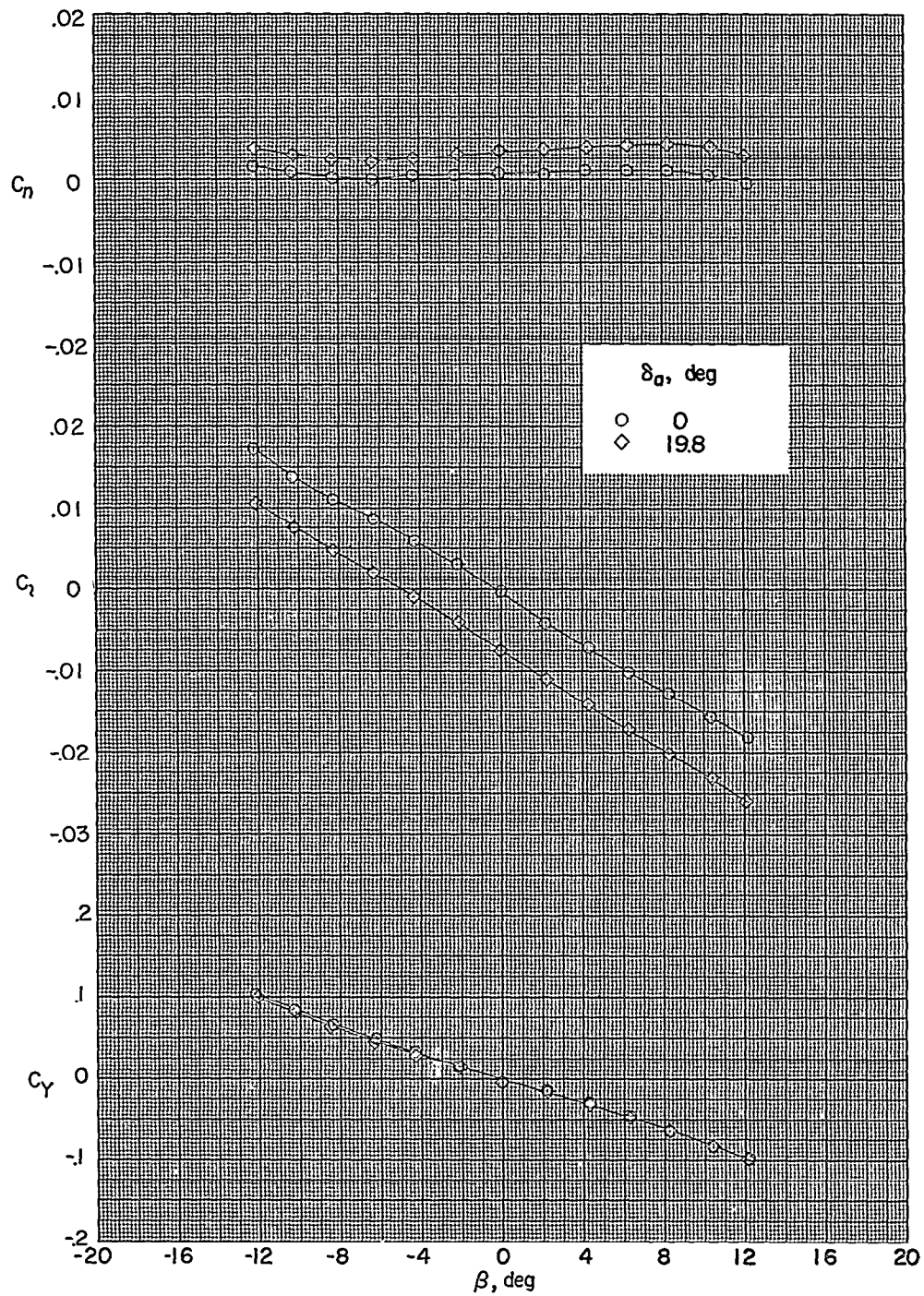
(b) $\alpha \approx 4.3^\circ$.

Figure 14.- Continued.



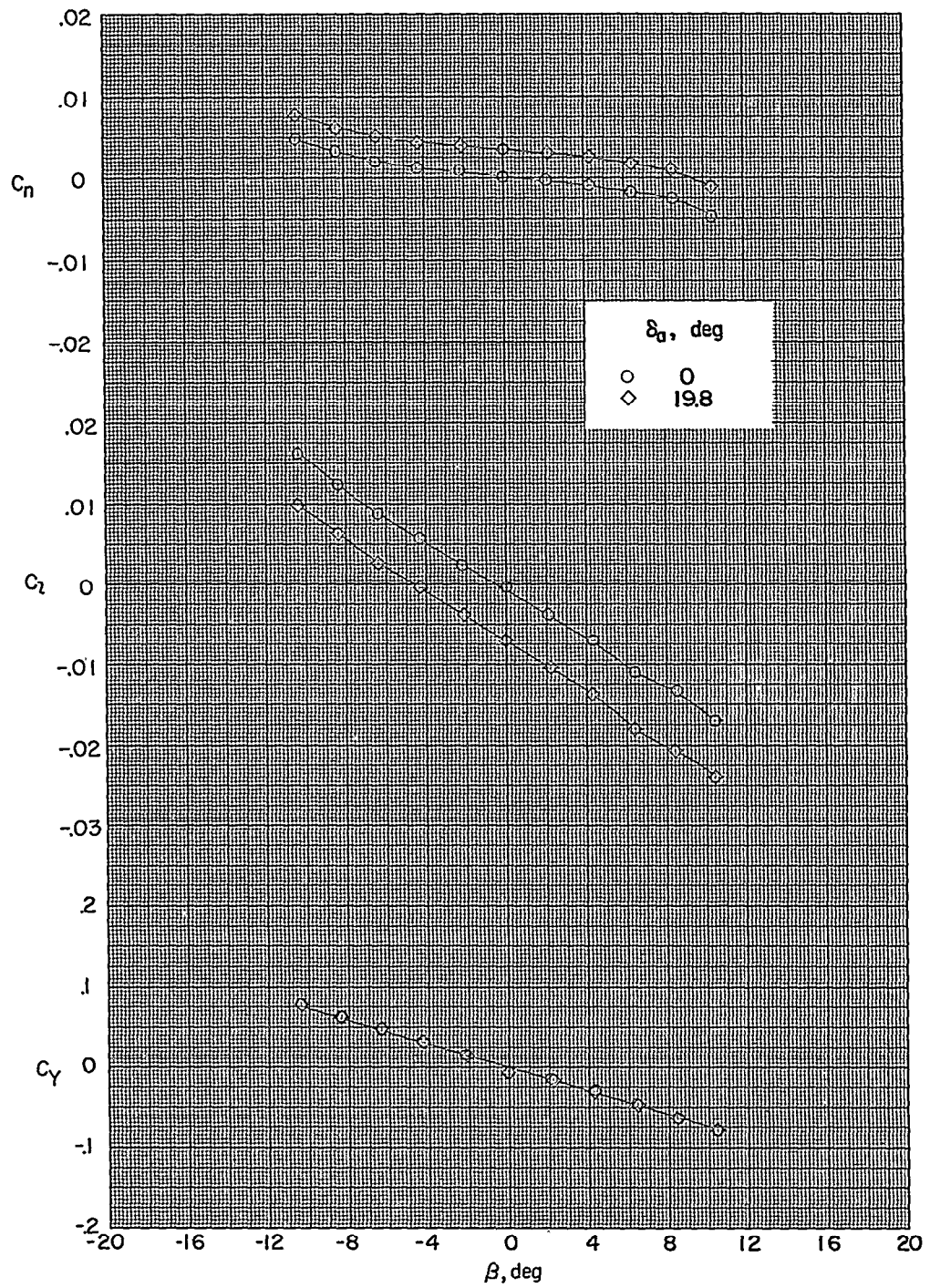
(b) Concluded.

Figure 14.- Continued.



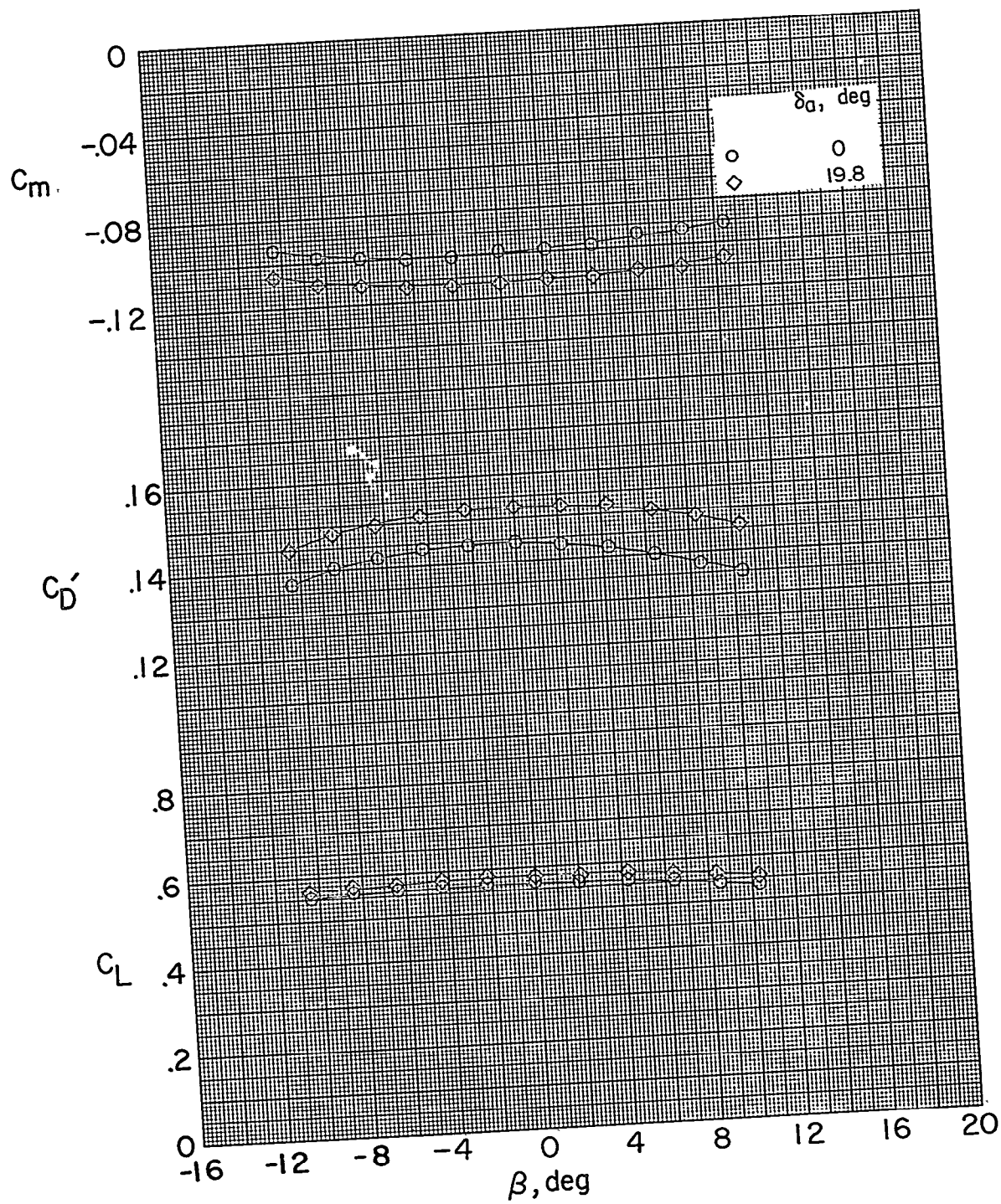
(c) $\alpha \approx 8.7^\circ$.

Figure 14.- Continued.



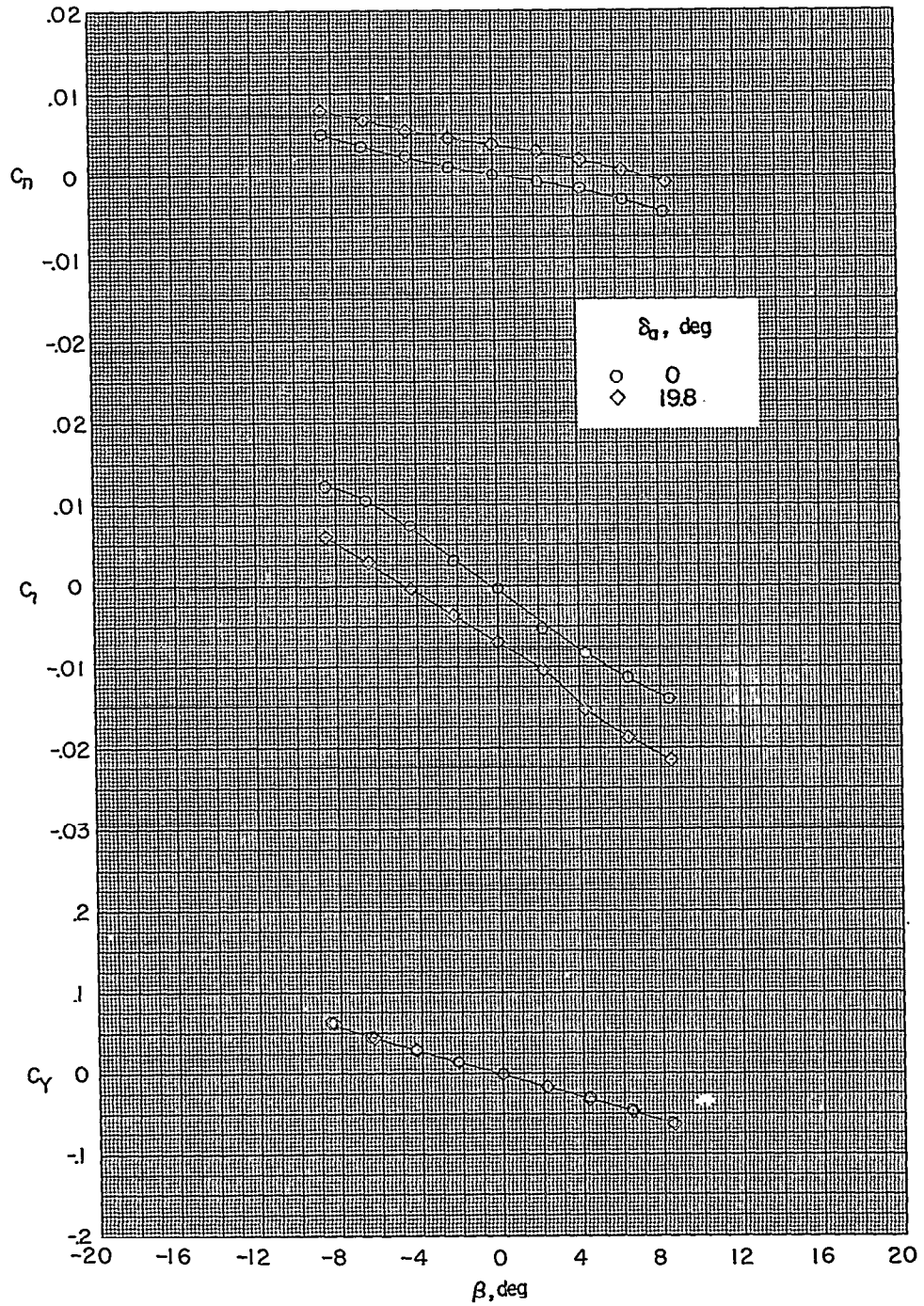
(d) $\alpha \approx 13.0^\circ$.

Figure 14.- Continued.



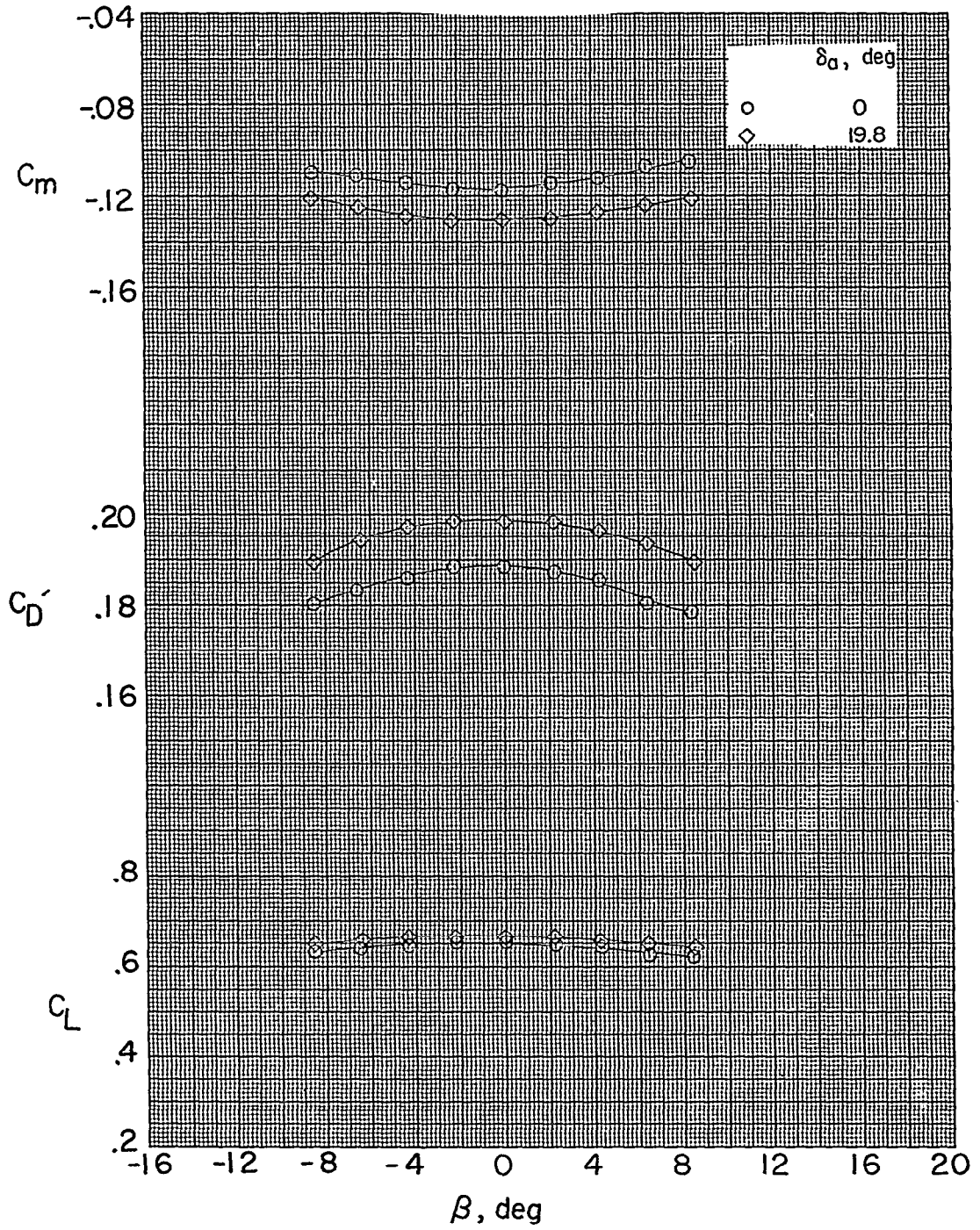
(a) Concluded.

Figure 14.- Continued.



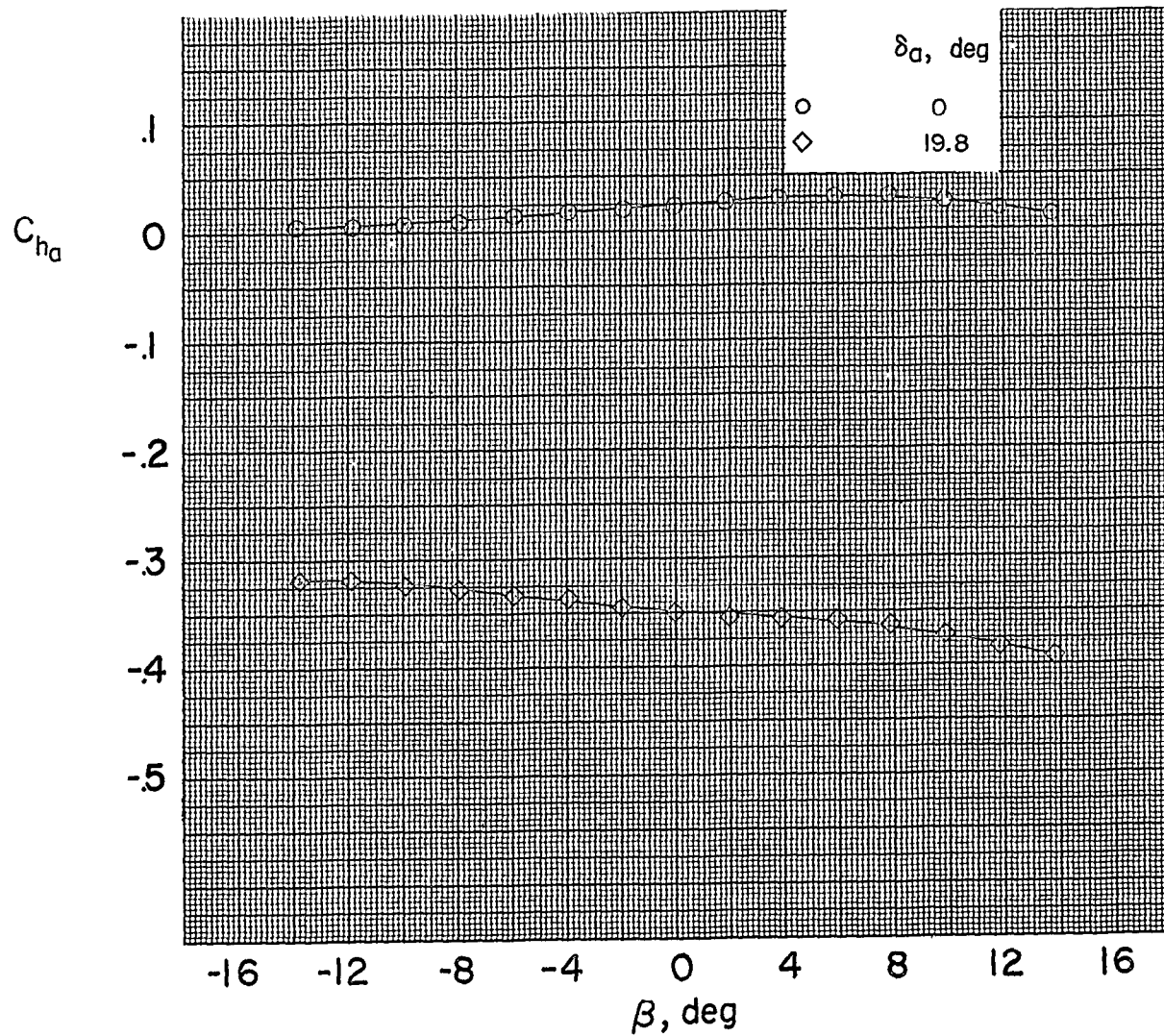
(e) $\alpha \approx 15.2^\circ$.

Figure 14.- Continued.



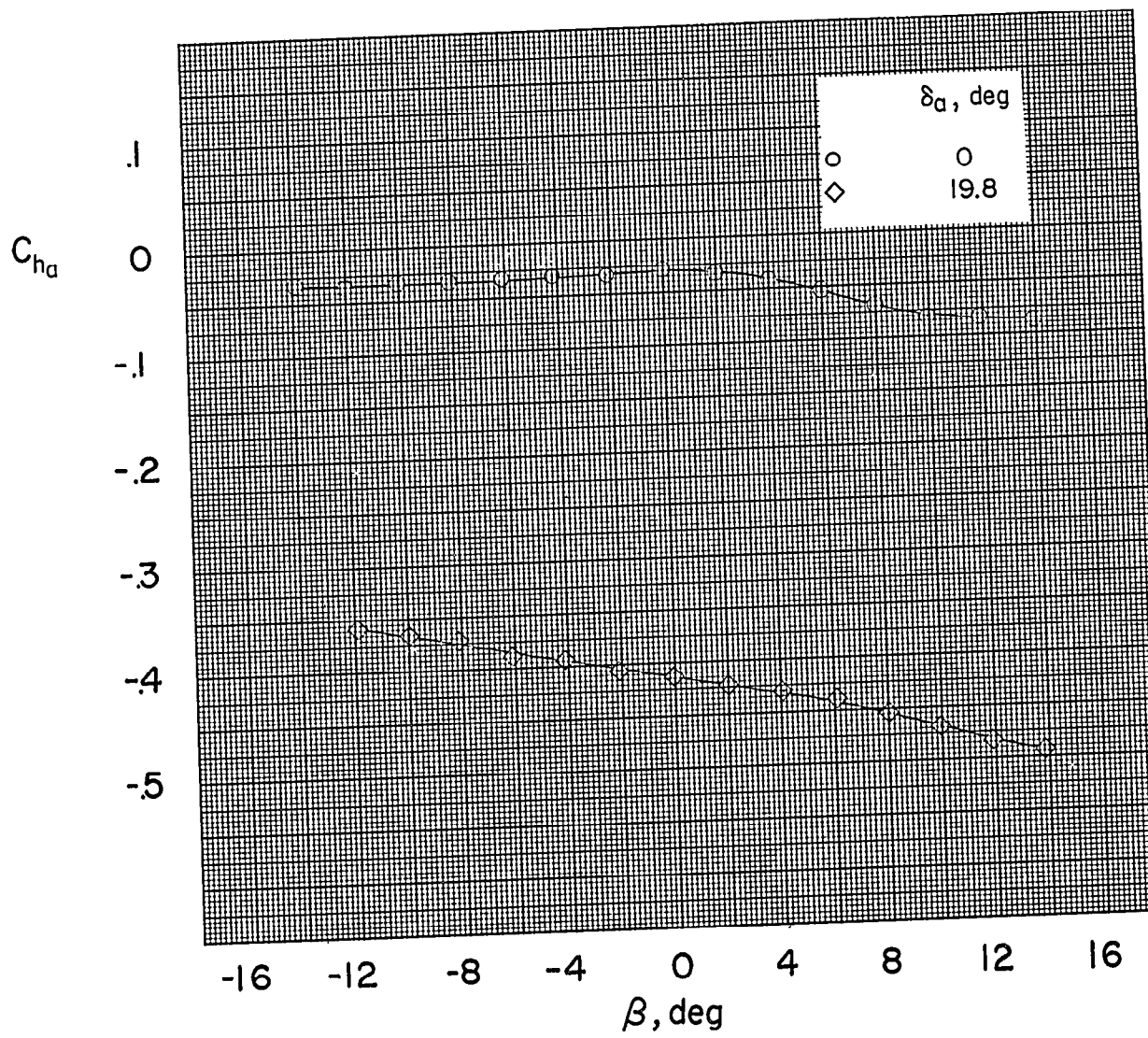
(e) Concluded.

Figure 14.- Concluded.



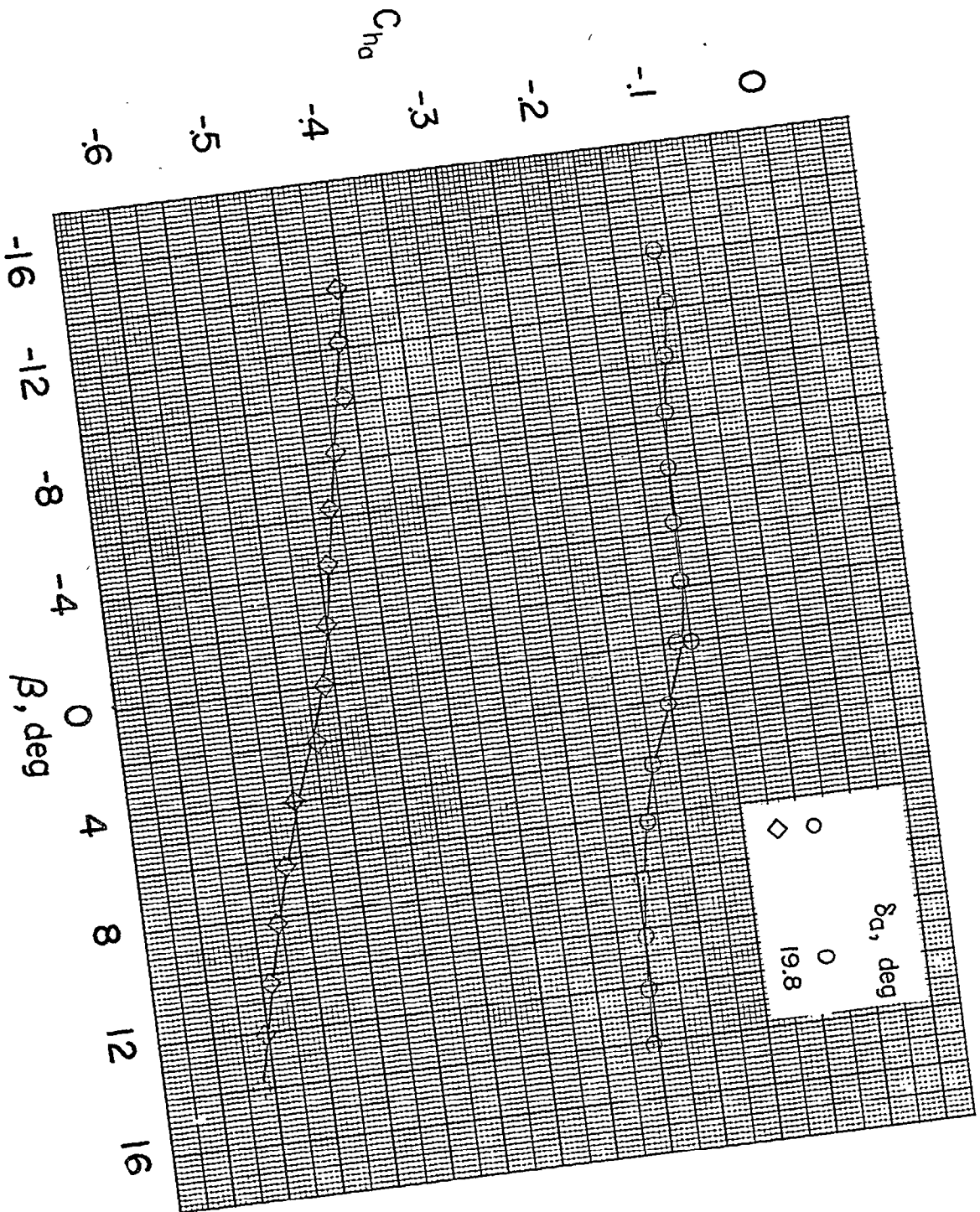
(a) $\alpha \approx 0^\circ$.

Figure 15.-- Aileron hinge-moment characteristics in sideslip; complete model, $\delta_e = \delta_r = 0^\circ$.



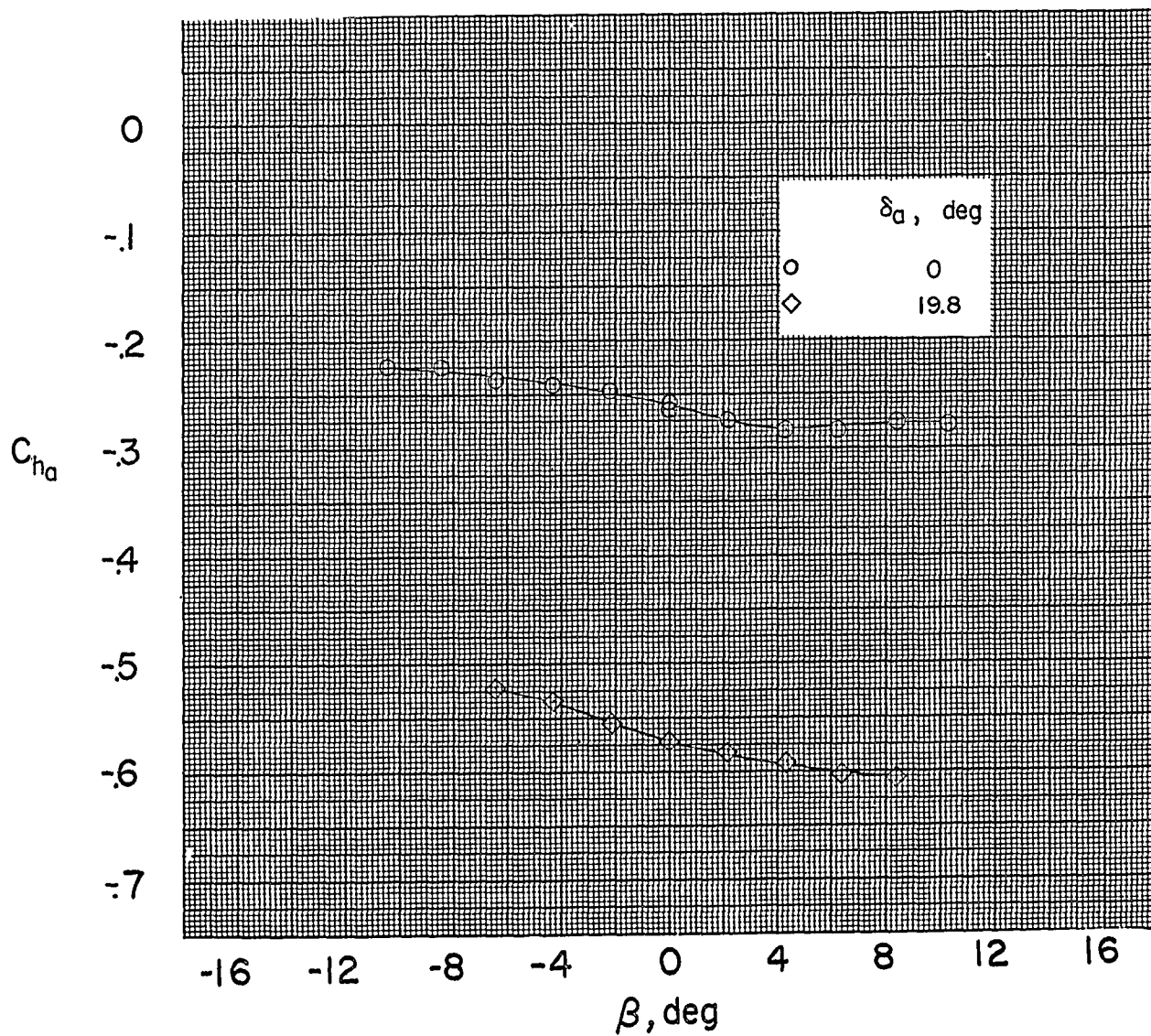
(b) $\alpha \approx 4.3^\circ$.

Figure 15.- Continued.



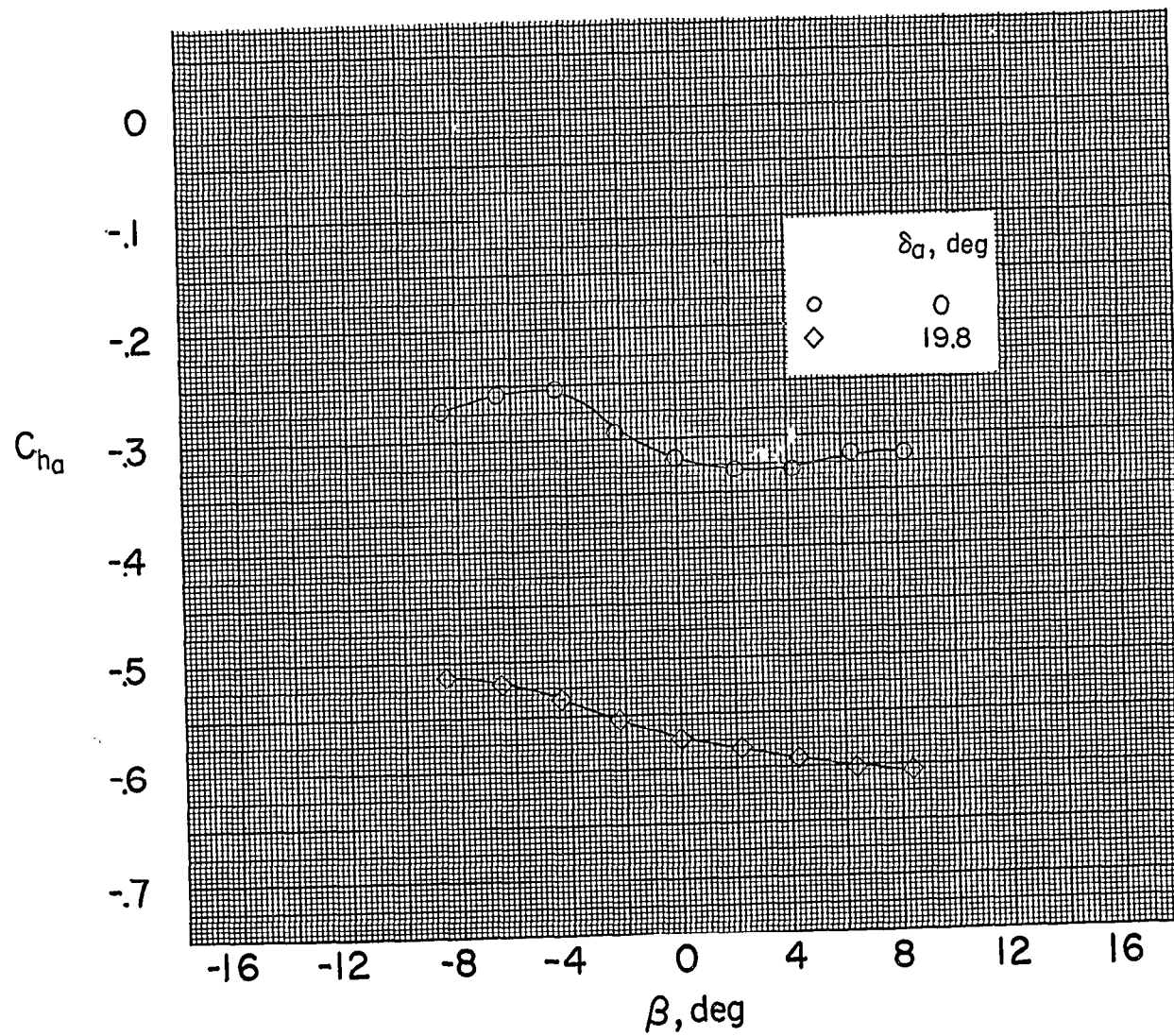
(c) $\alpha \approx 8.7^\circ$.

Figure 15.- Continued.



(d) $\alpha \approx 13.0^\circ$.

Figure 15.- Continued.



(e) $\alpha \approx 15.2^\circ$.

Figure 15.- Concluded.

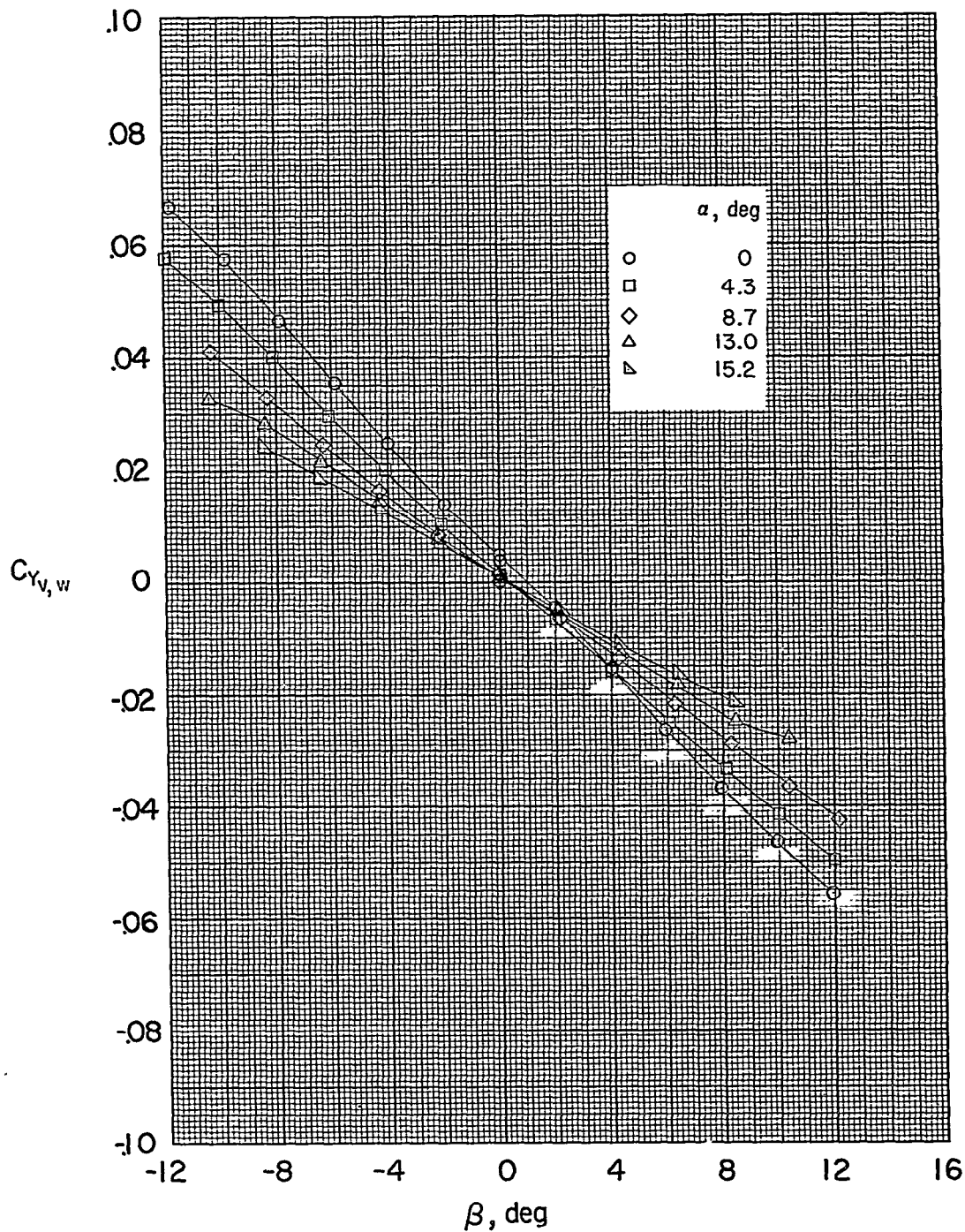
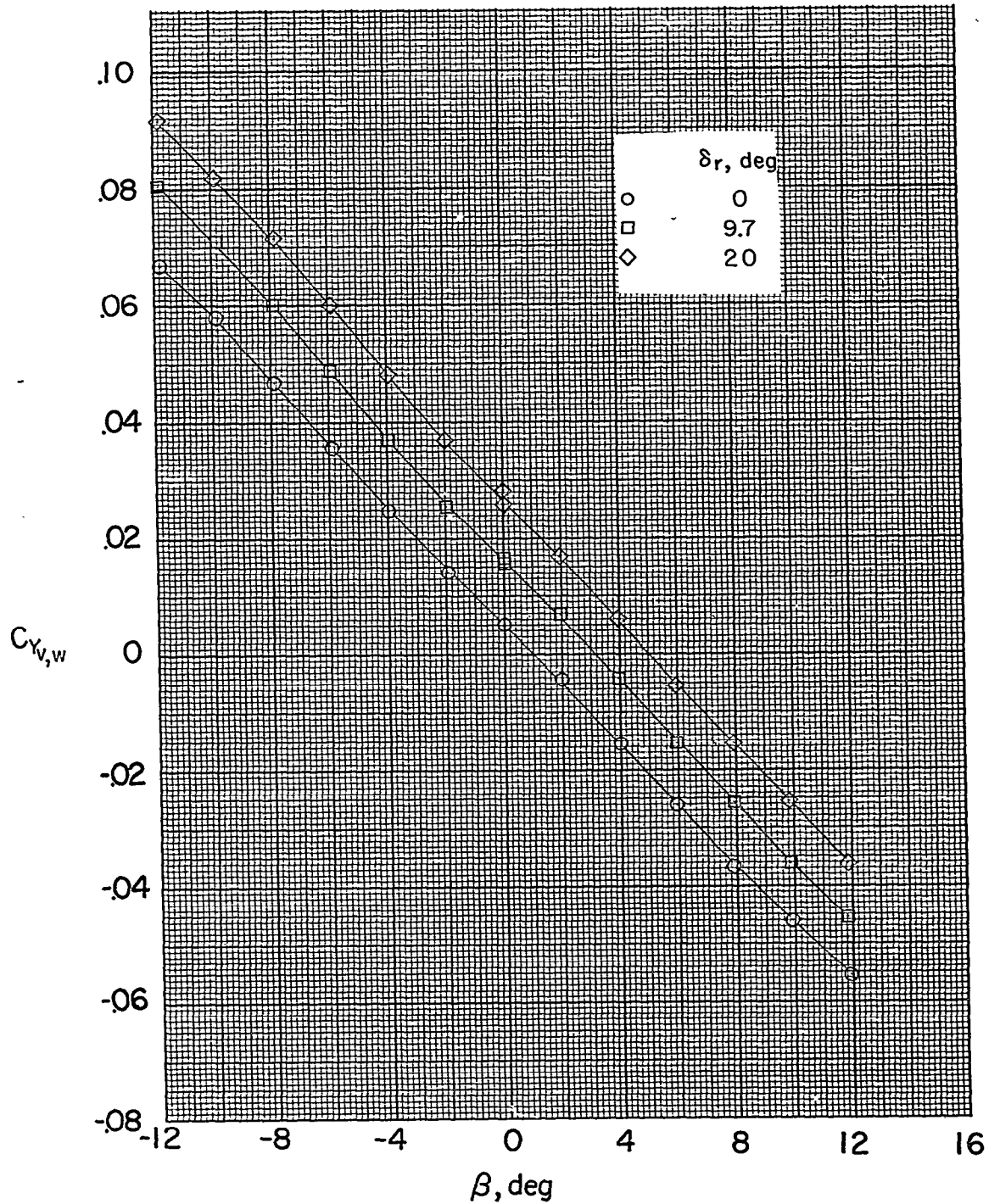
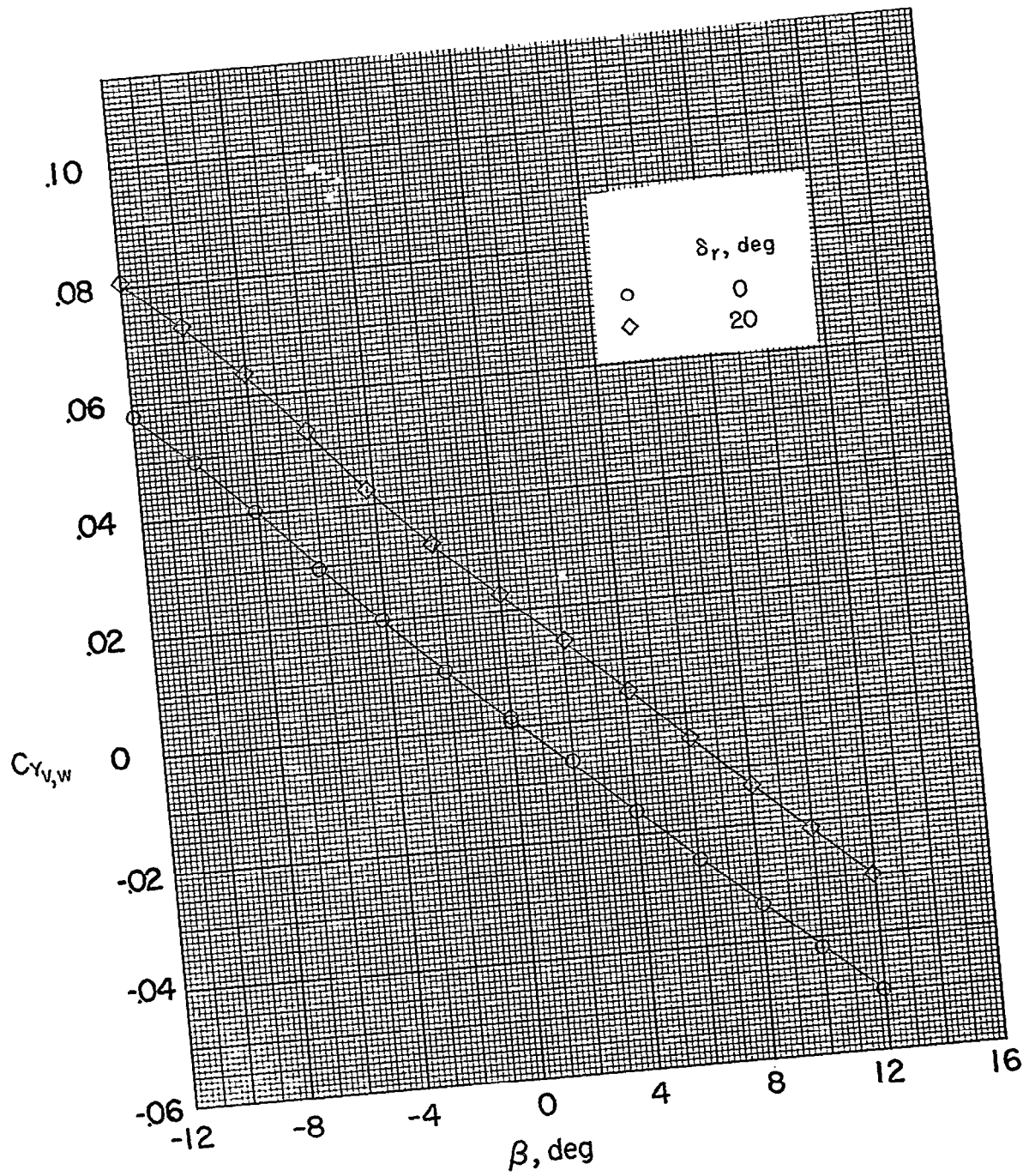


Figure 16.- Effect of angle of attack on variation of side-force coefficient of vertical tail based on wing area with angle of sideslip; $\delta_e = \delta_a = \delta_r = 0^\circ$.



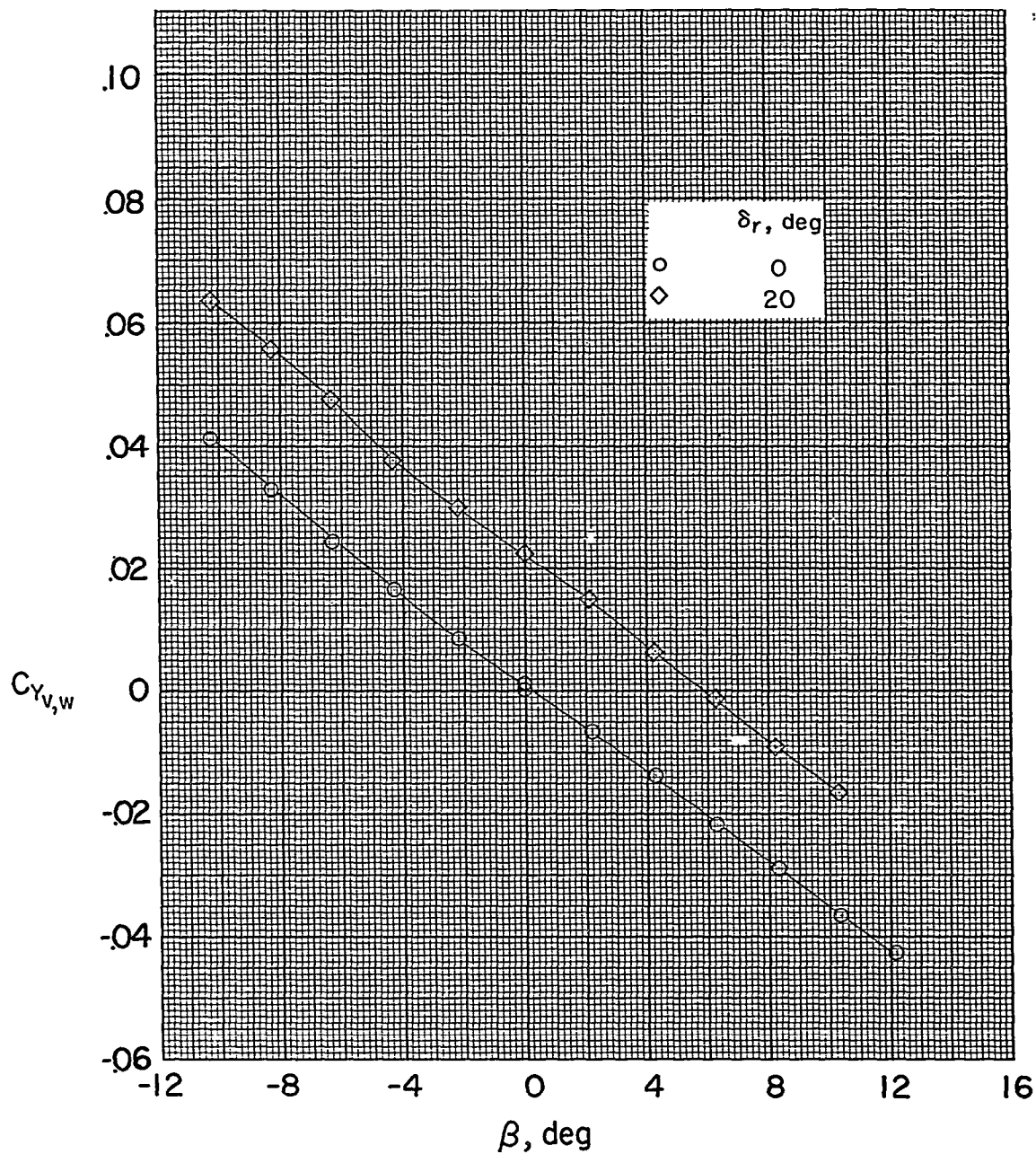
(a) $\alpha \approx 0^\circ$.

Figure 17.- Effect of rudder deflection on variation of side-force coefficient of vertical tail based on wing area with angle of sideslip for various angles of attack.



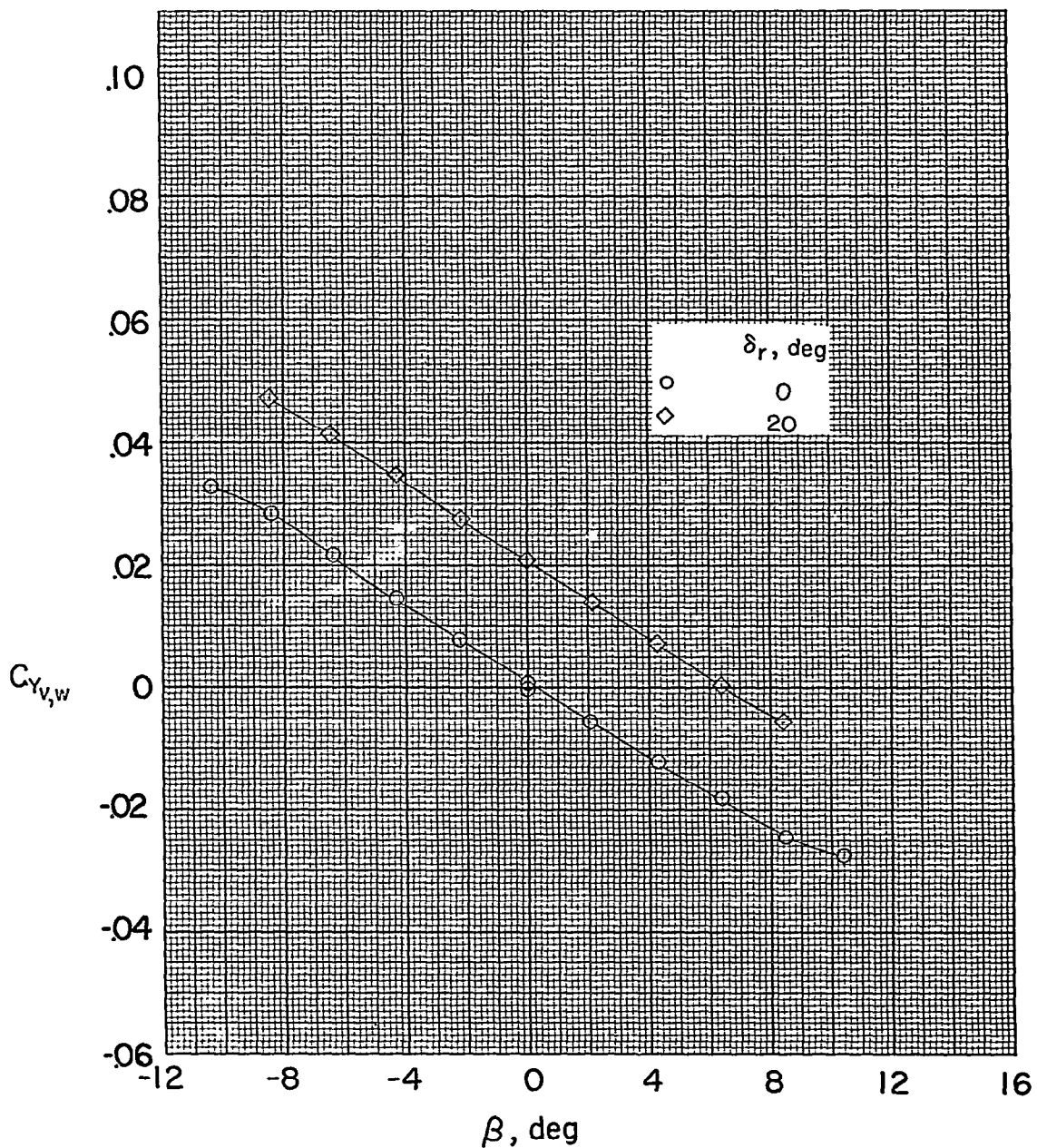
(b) $\alpha \approx 4.3^\circ$.

Figure 17.- Continued.



(c) $\alpha \approx 8.7^\circ$.

Figure 17.- Continued.



(d) $\alpha \approx 13^\circ$.

Figure 17.- Concluded.

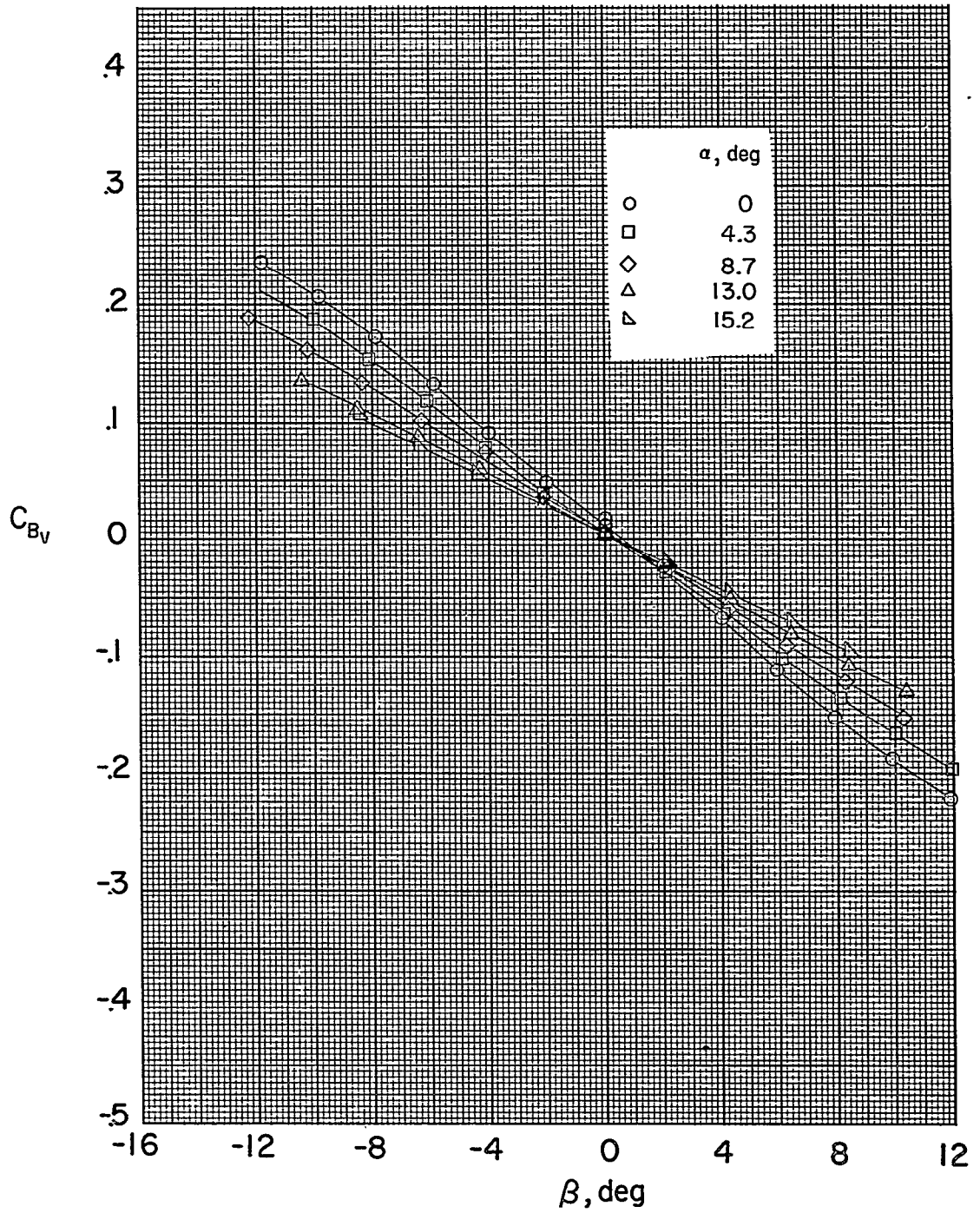
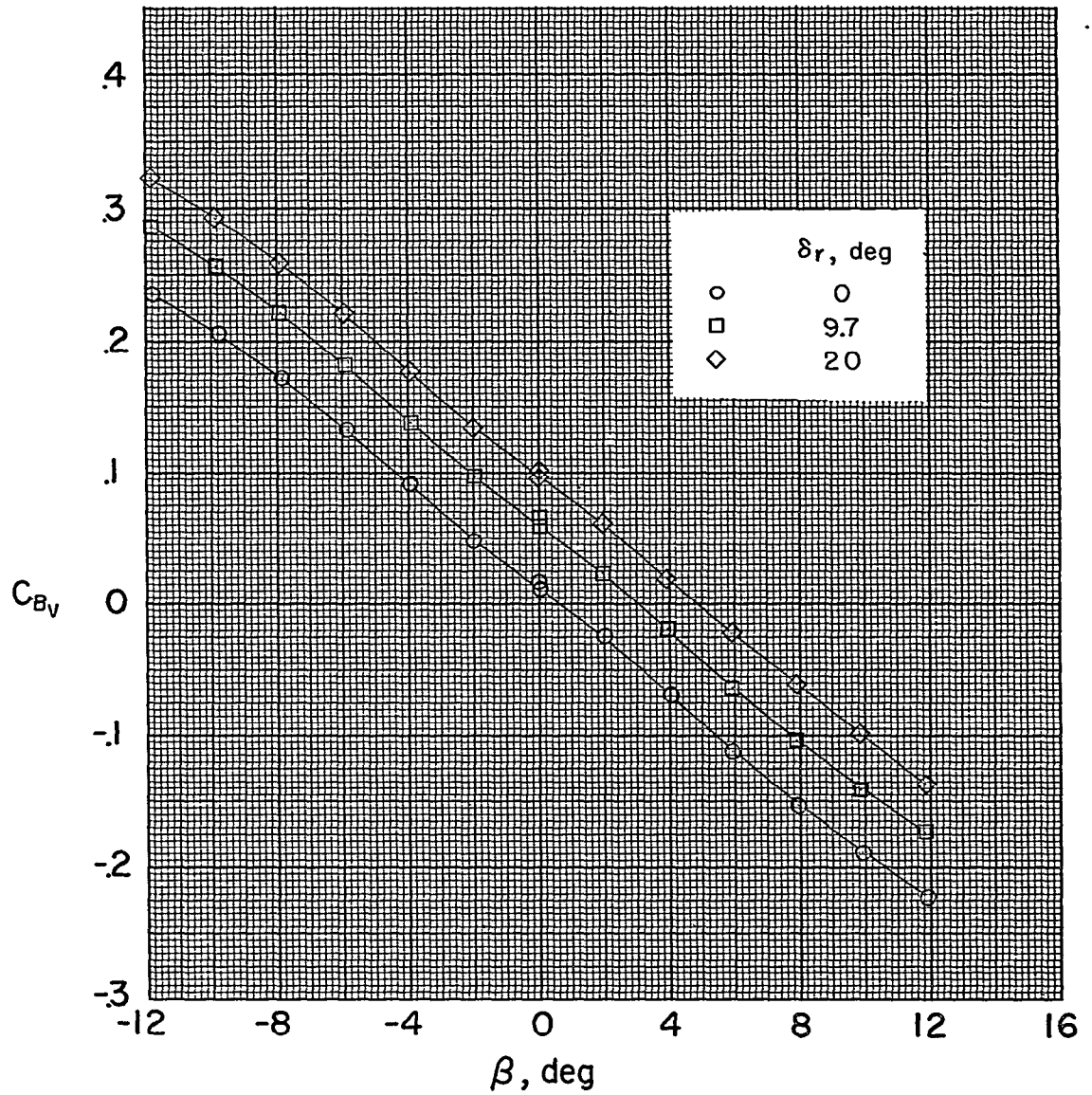
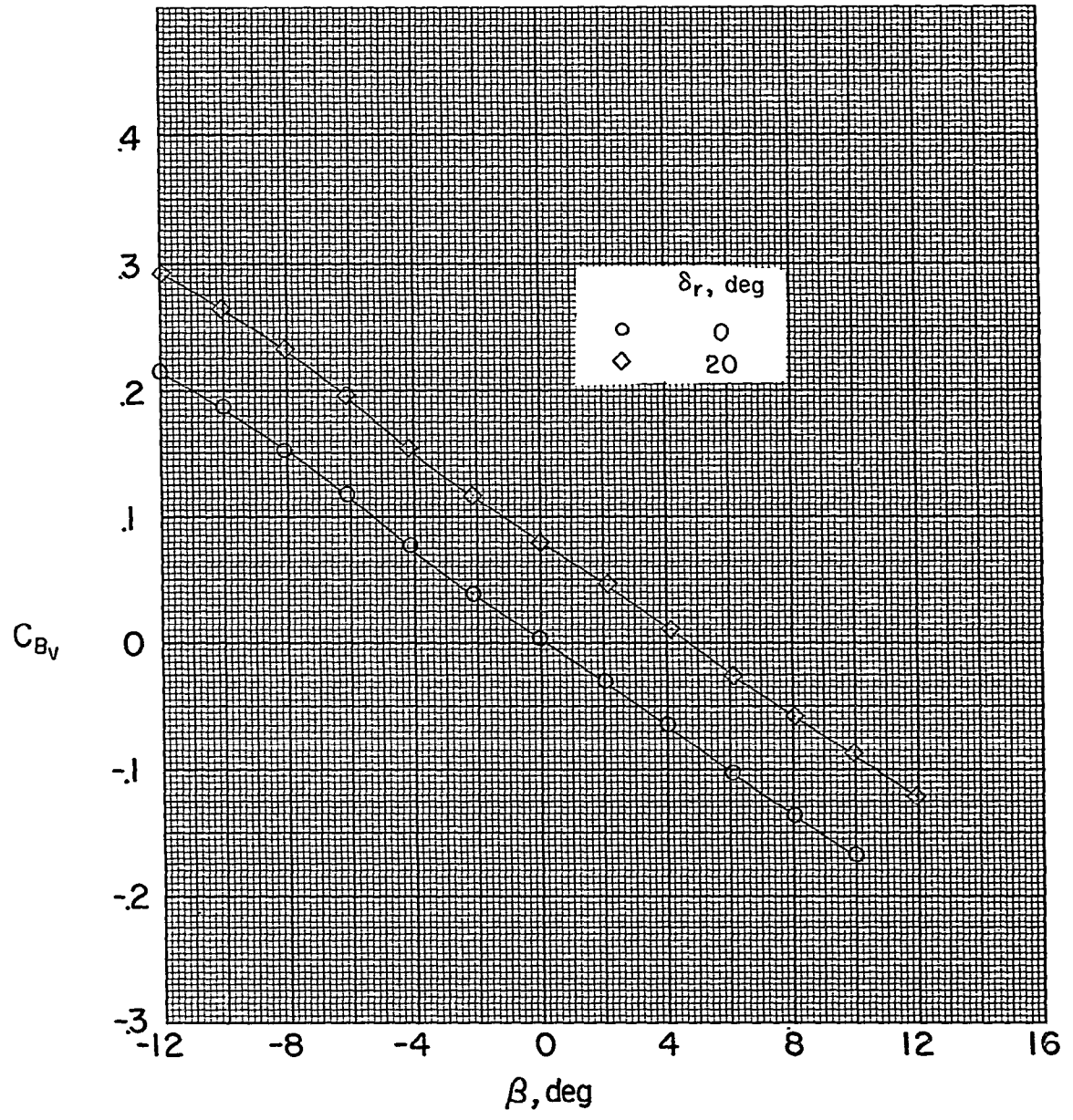


Figure 18.- Effect of angle of attack on variation of root-bending-moment coefficient of vertical tail with angle of sideslip; $\delta_e = \delta_a = \delta_r = 0^\circ$.



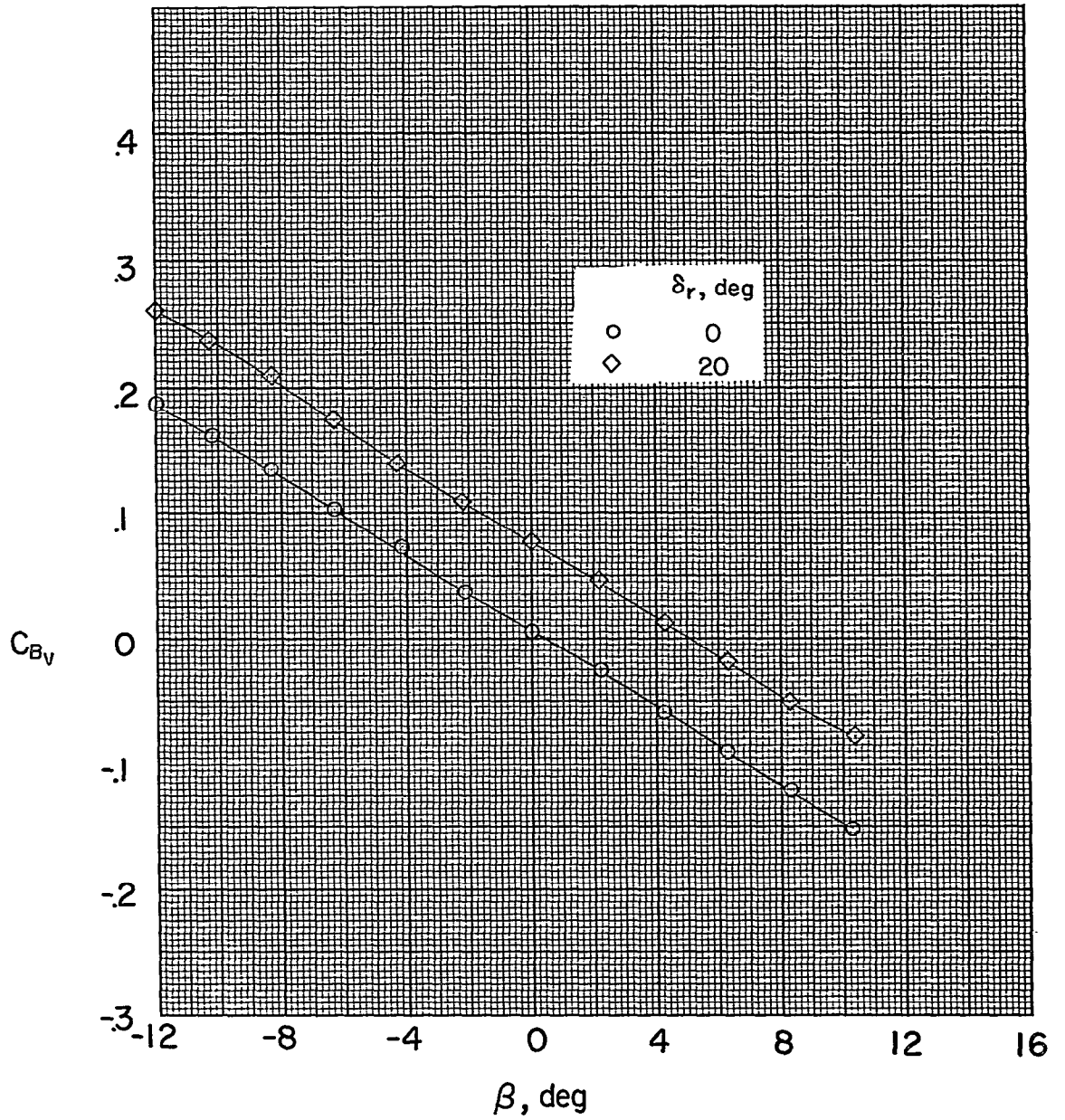
(a) $\alpha \approx 0^\circ$.

Figure 19.- Effect of rudder deflection on variation of root-bending-moment coefficient of vertical tail with angle of sideslip for various angles of attack.



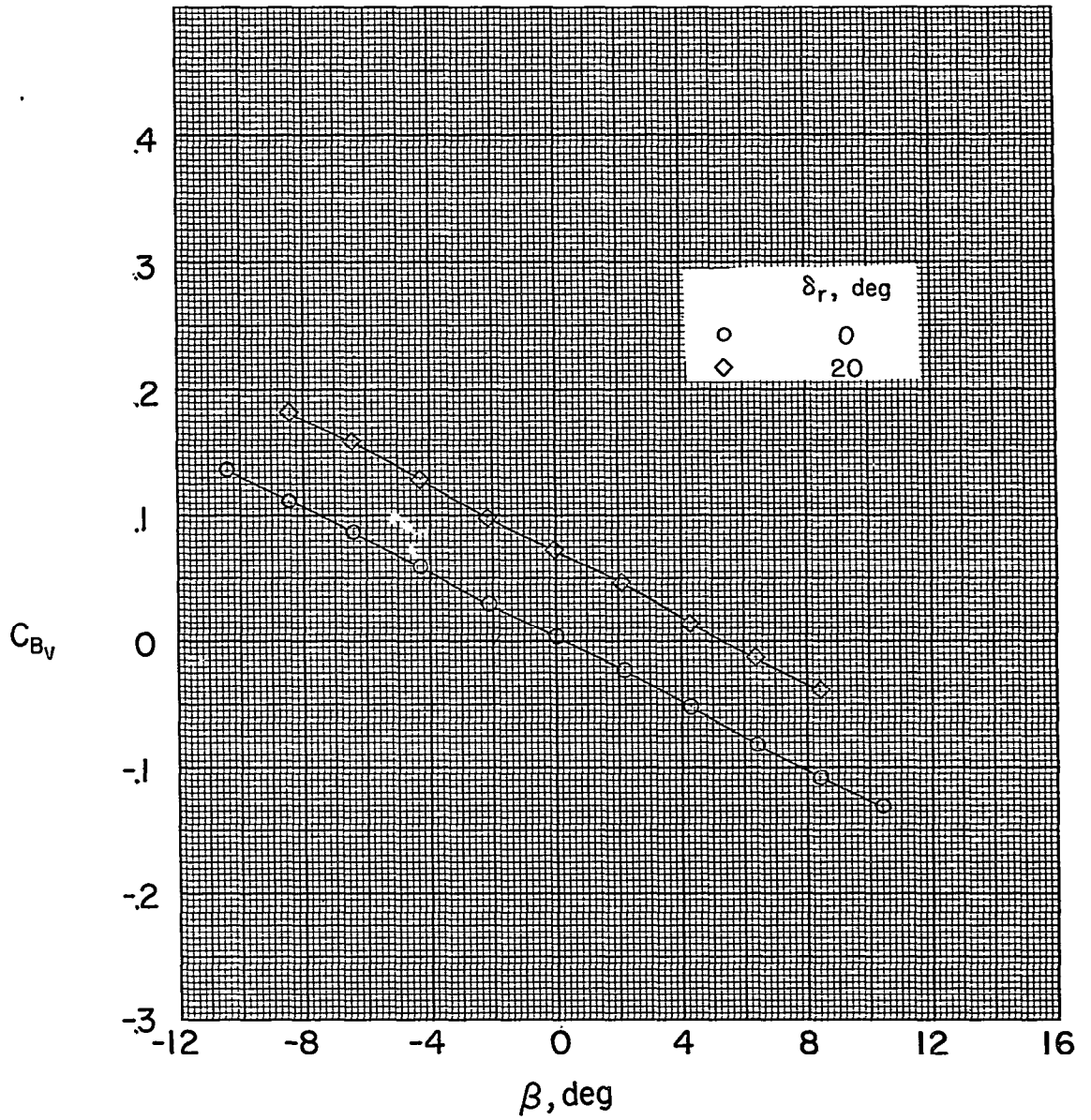
(b) $\alpha \approx 4.3^\circ$.

Figure 19.- Continued.



(c) $\alpha \approx 8.7^\circ$.

Figure 19.- Continued.



(d) $\alpha \approx 13^\circ$.

Figure 19.- Concluded.

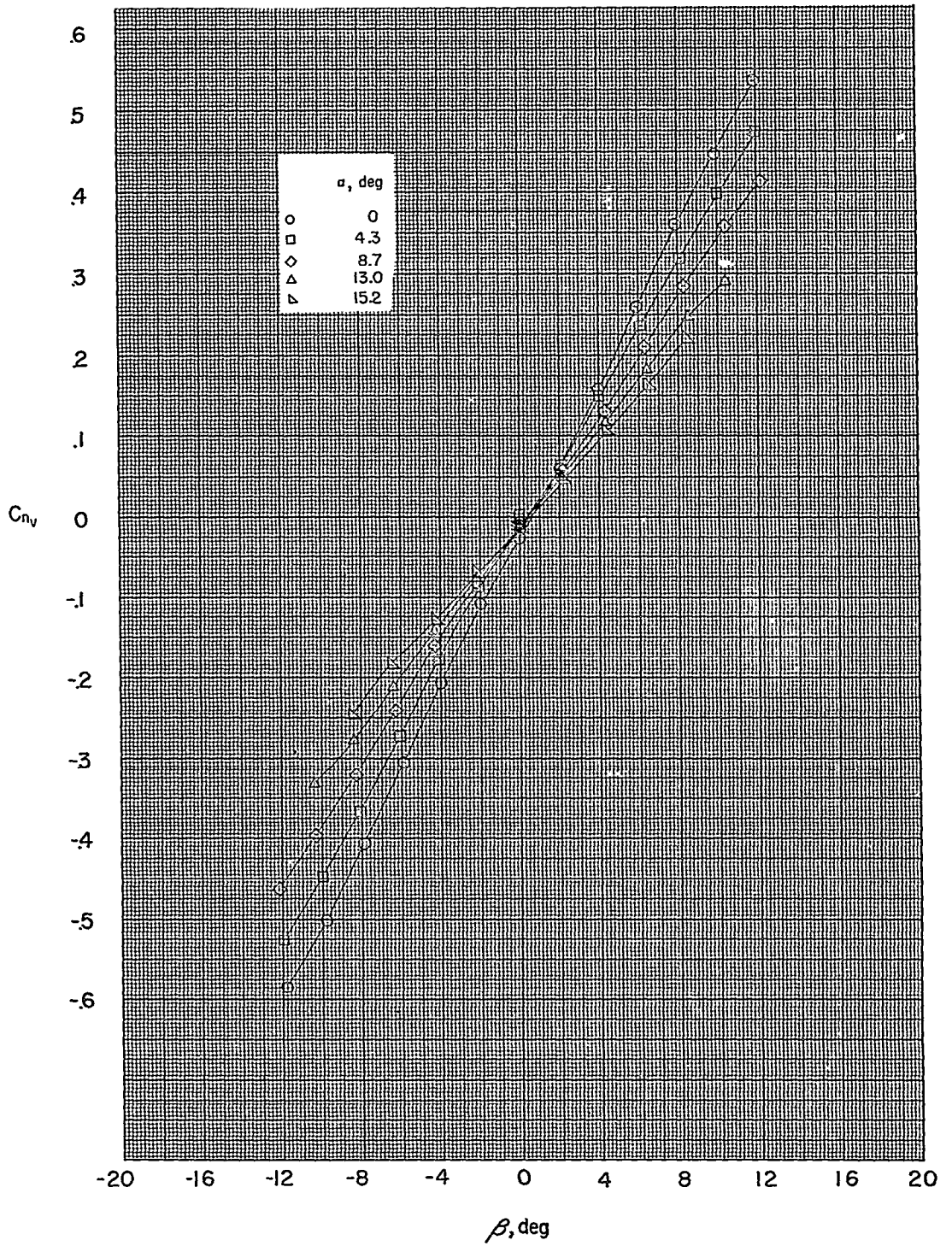
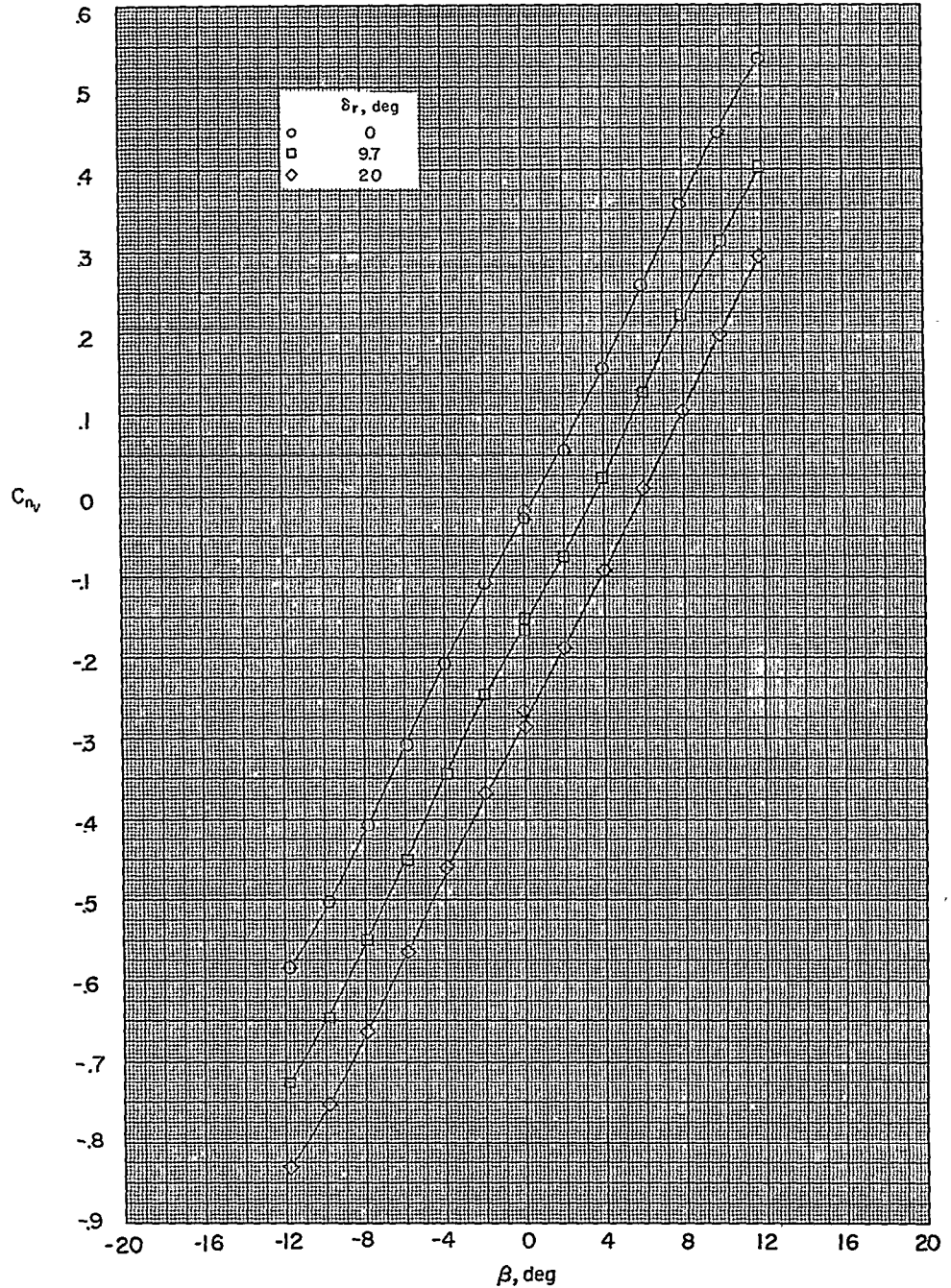
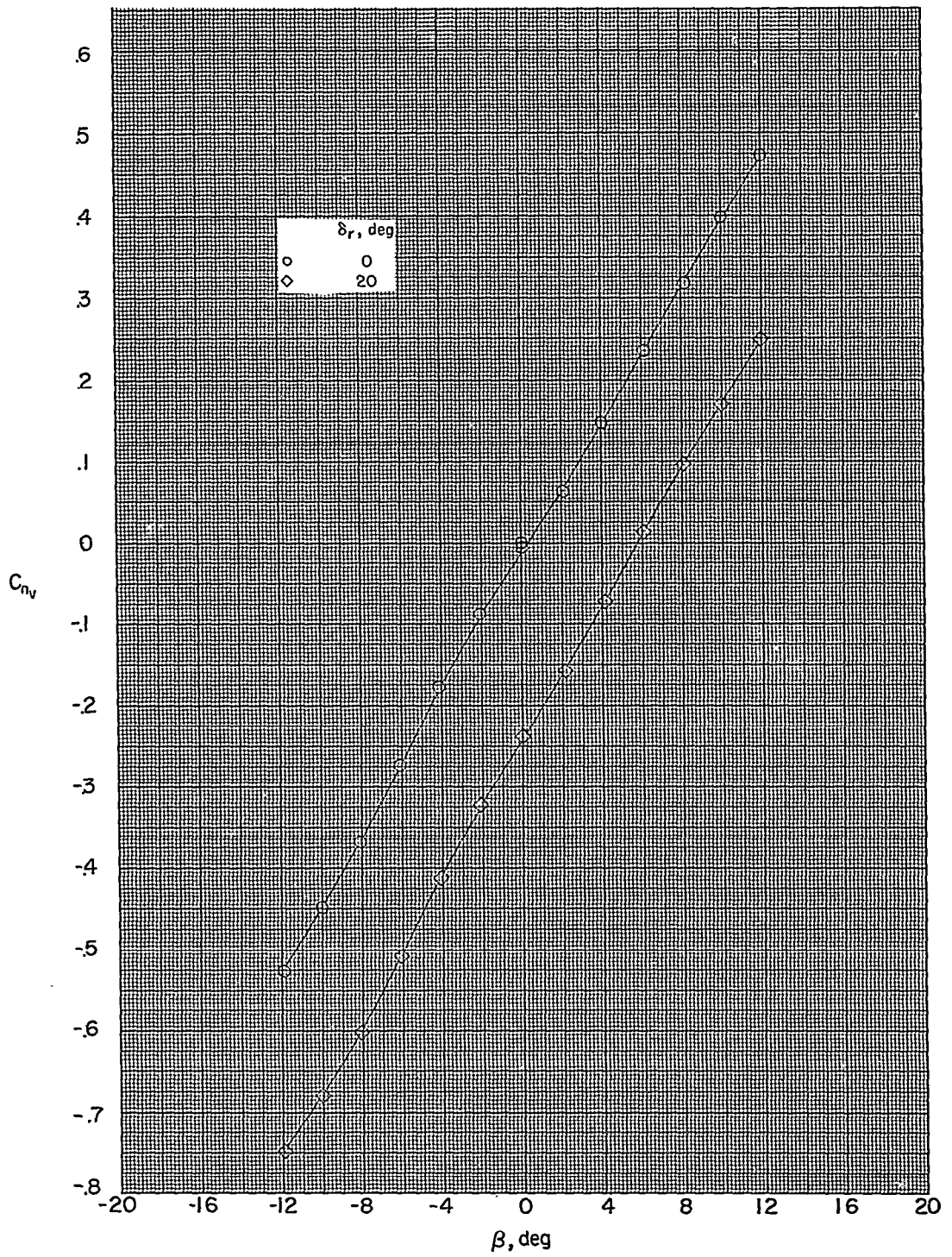


Figure 20.- Effect of angle of attack on variation of yawing-moment coefficient of vertical tail with angle of sideslip; $\delta_e = \delta_a = \delta_r = 0^\circ$.



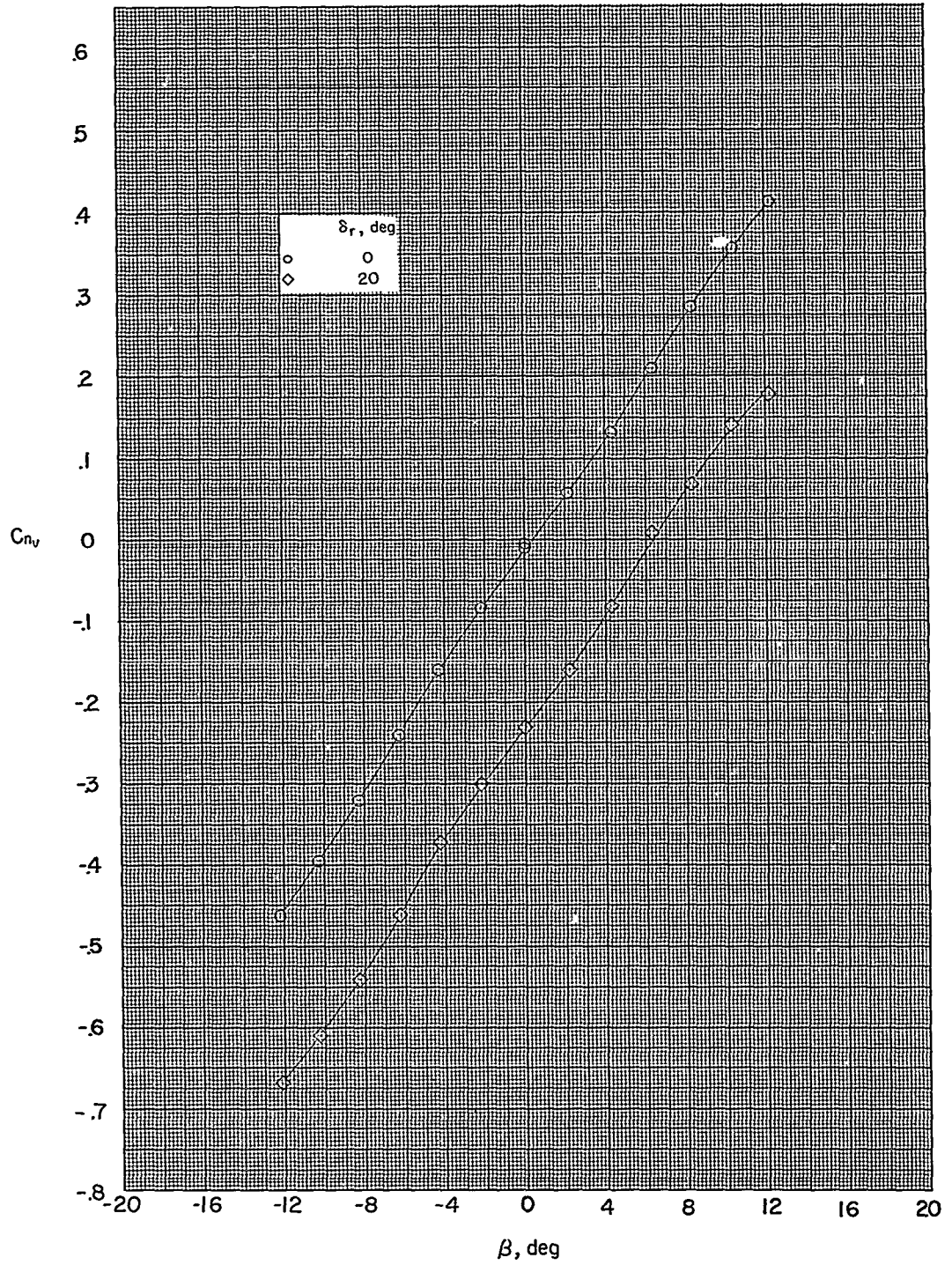
(a) $\alpha \approx 0^\circ$.

Figure 21.- Effect of rudder deflection on variation of yawing-moment coefficient of vertical tail with angle of sideslip for various angles of attack.



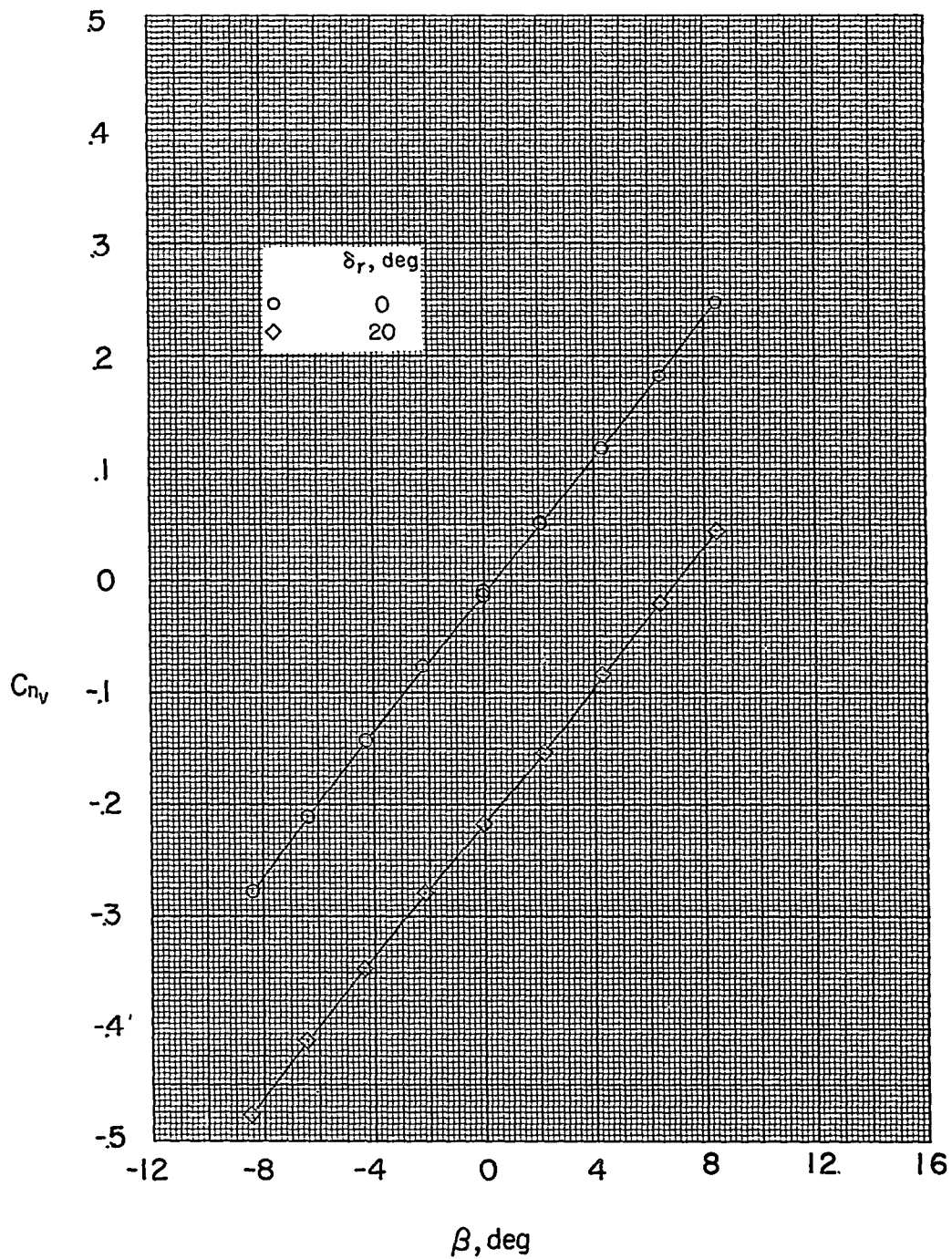
(b) $\alpha \approx 4.3^\circ$.

Figure 21.- Continued.



(c) $\alpha \approx 8.7^\circ$.

Figure 21.- Continued.



(d) $\alpha \approx 13^\circ$.

Figure 21.- Concluded.

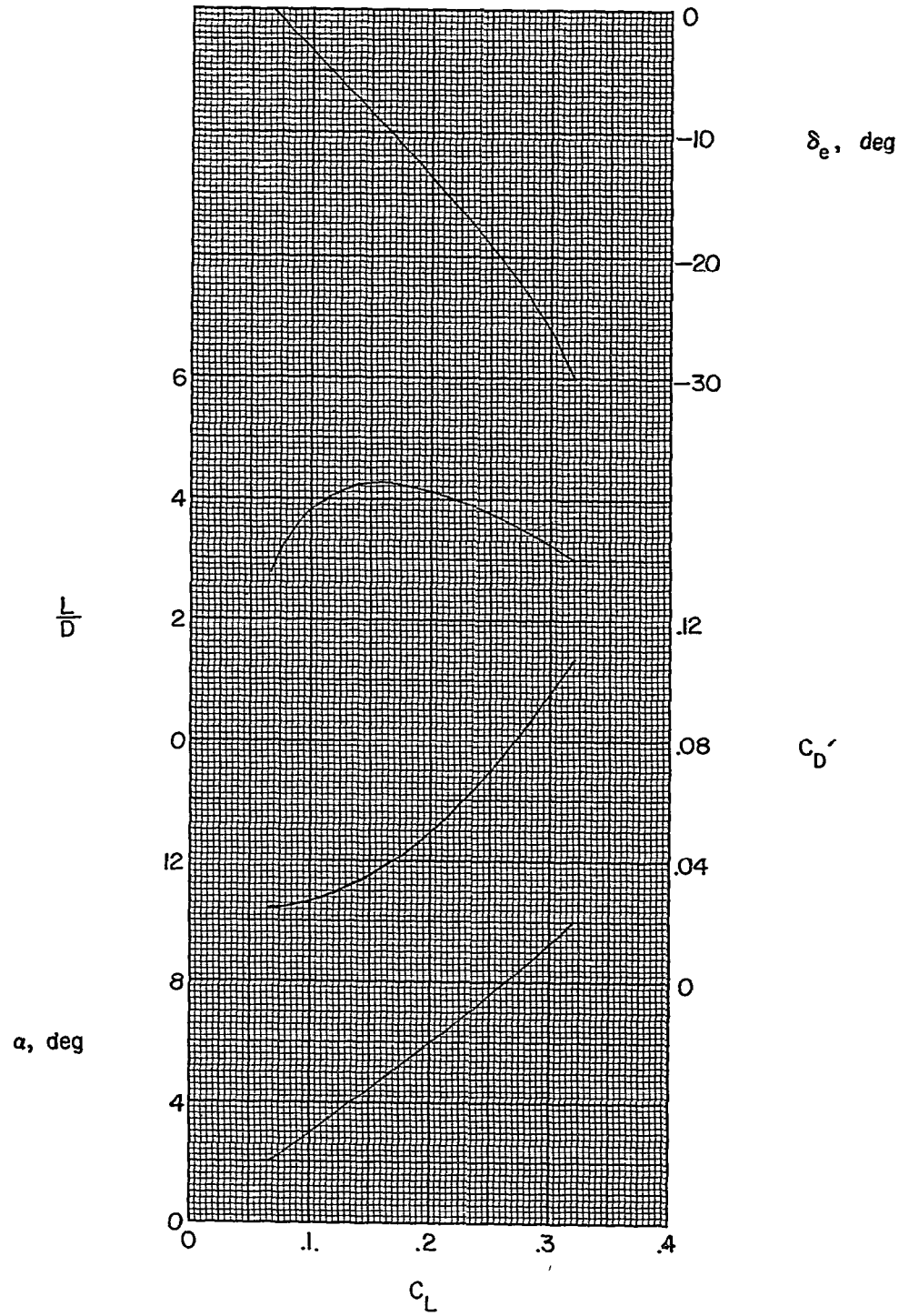


Figure 22.- Trim longitudinal characteristics; complete model, open inlets (uncorrected drag).

...

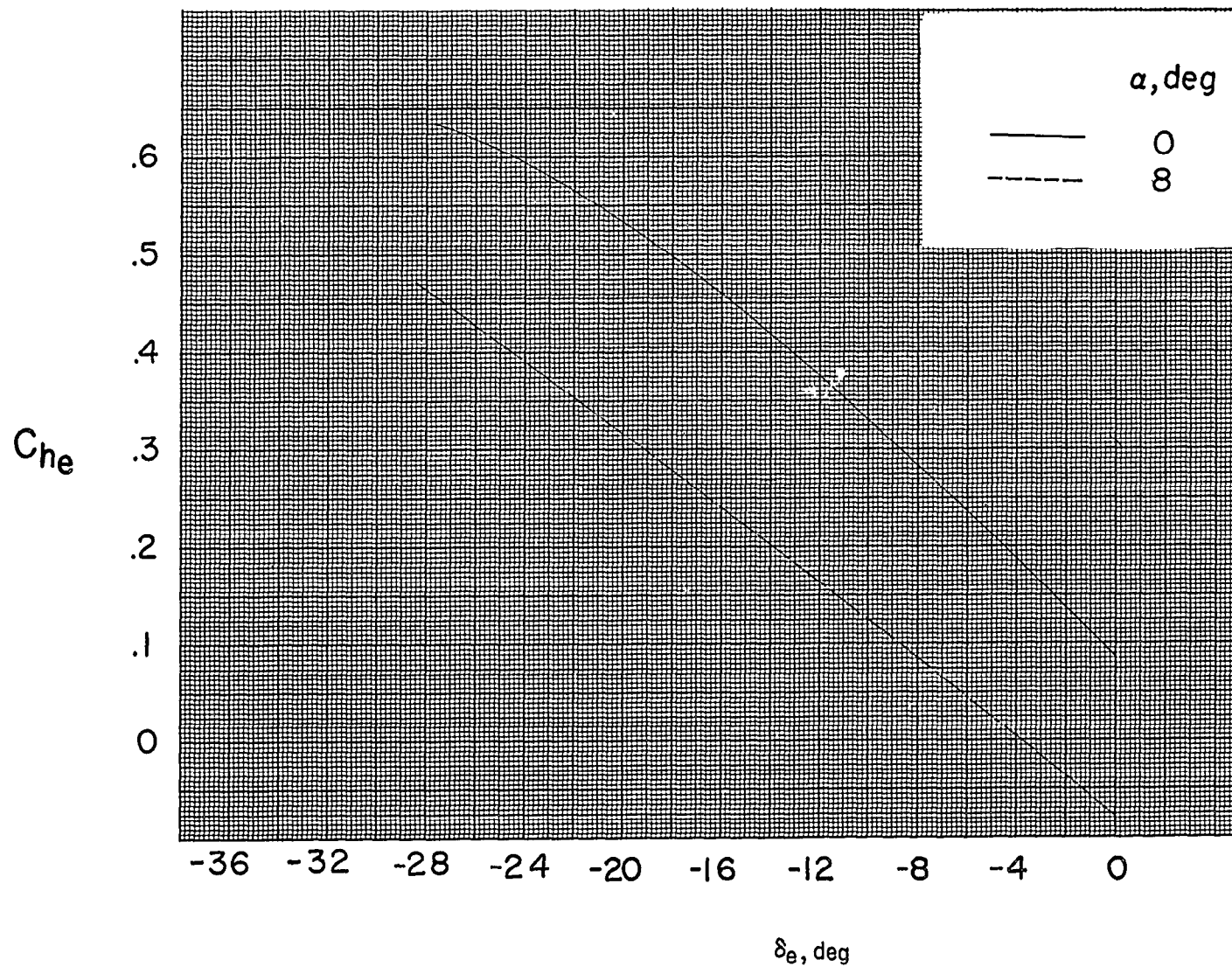


Figure 23.- Variation of elevator hinge-moment coefficient with elevator deflection; $\beta = 0^\circ$.

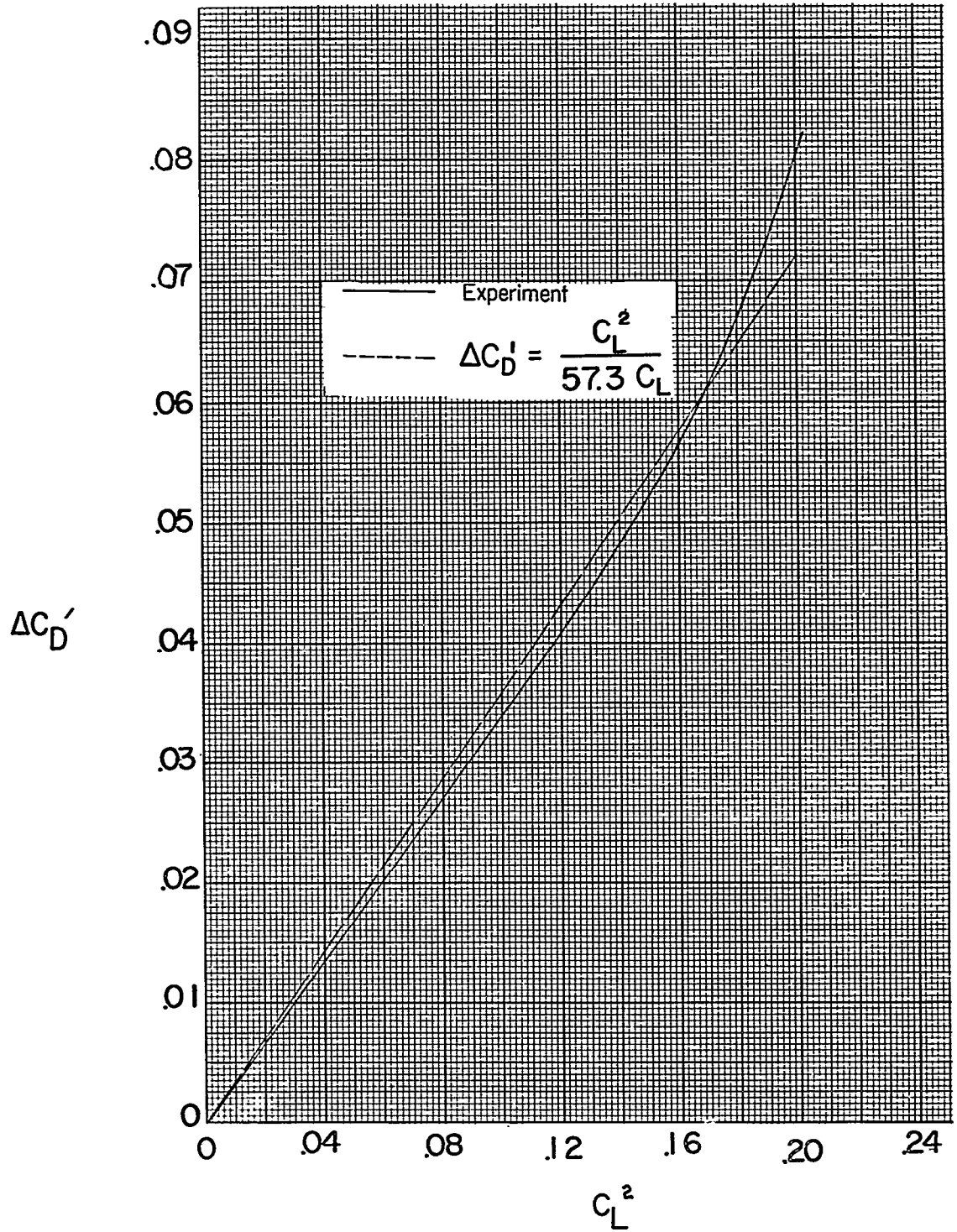


Figure 24.- Characteristics of drag due to lift; complete model, open inlets, $\delta_e = \delta_a = \delta_r = 0^\circ$ (uncorrected drag).

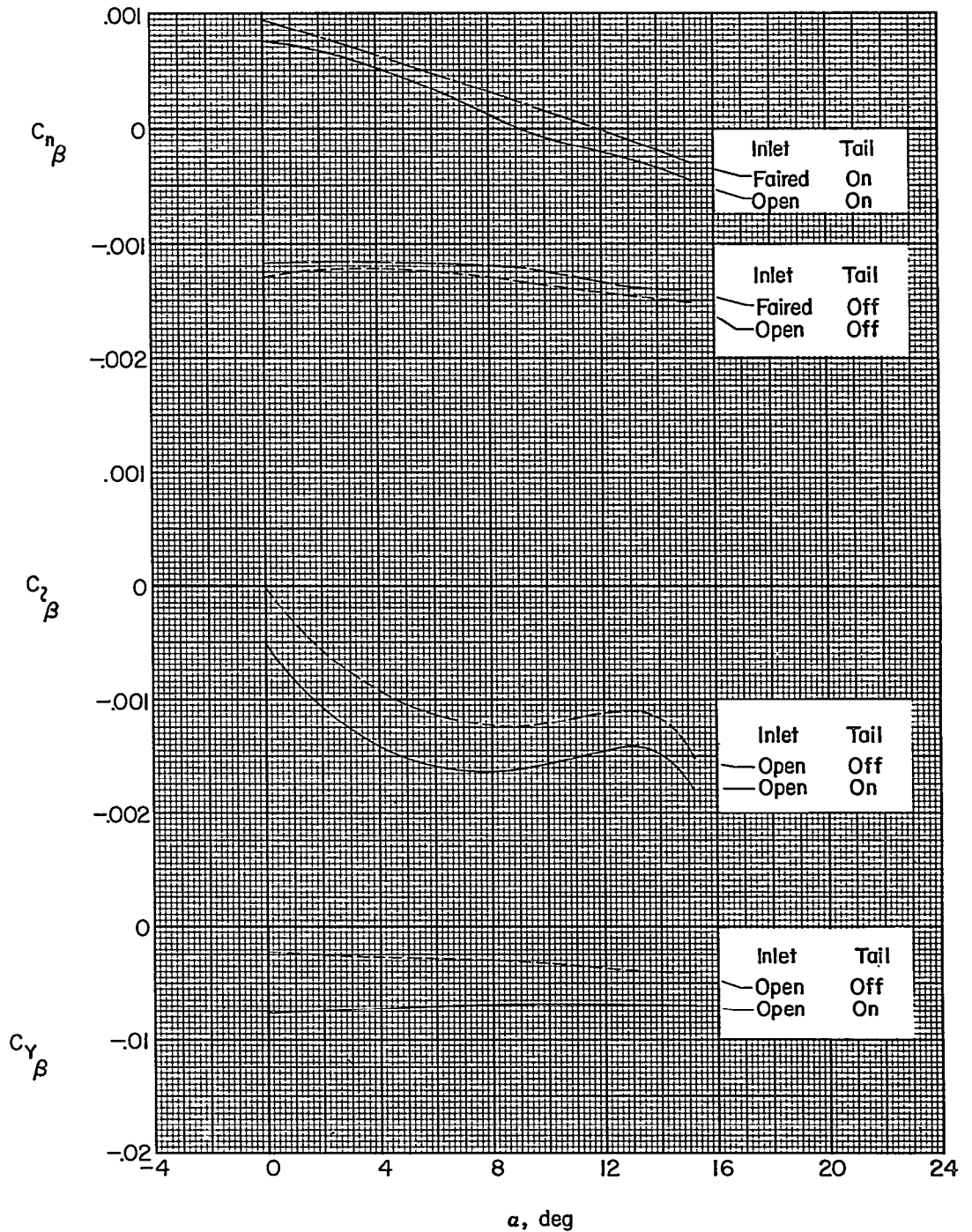


Figure 25.- Variation of lateral and directional stability characteristics for open and faired inlets for complete model and wing-fuselage combination; $\delta_a = \delta_e = \delta_r = 0^\circ$.

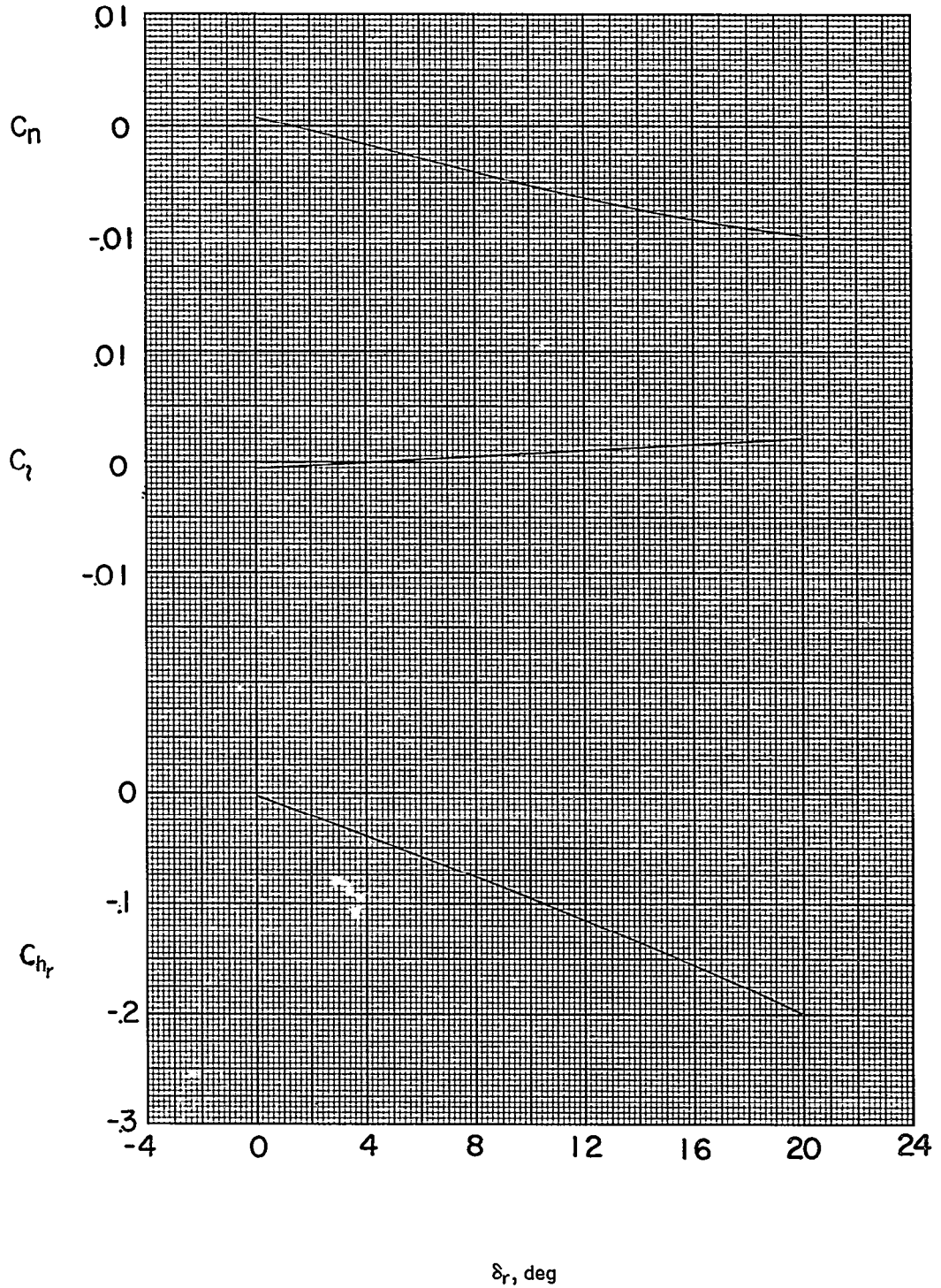
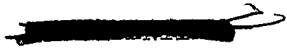


Figure 26.- Variation of rudder control characteristics with rudder deflection; $\alpha = 0^\circ$.



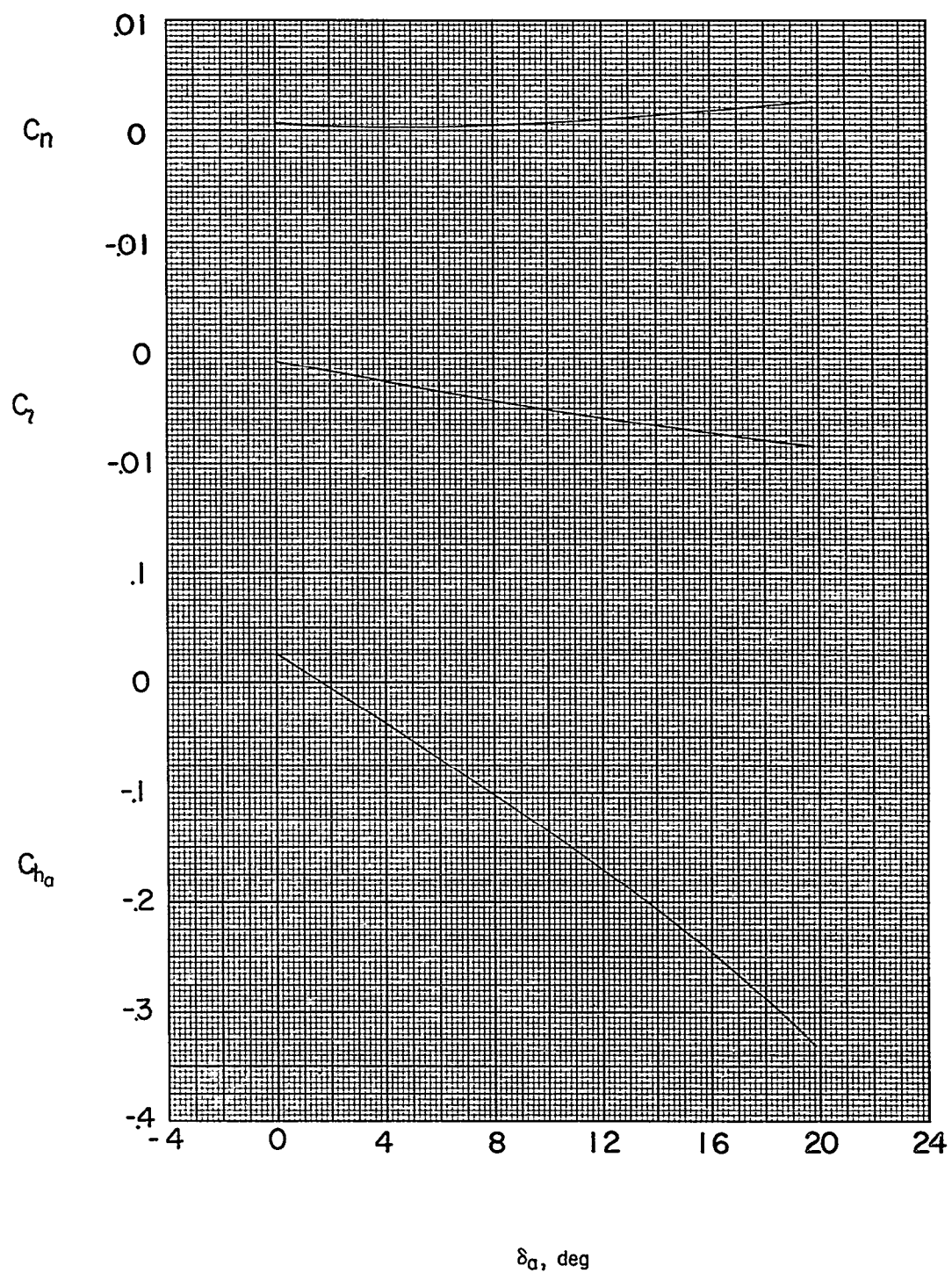


Figure 27.- Variation of aileron control characteristics with aileron deflection; $\alpha = 0^\circ$.

~~CONFIDENTIAL~~

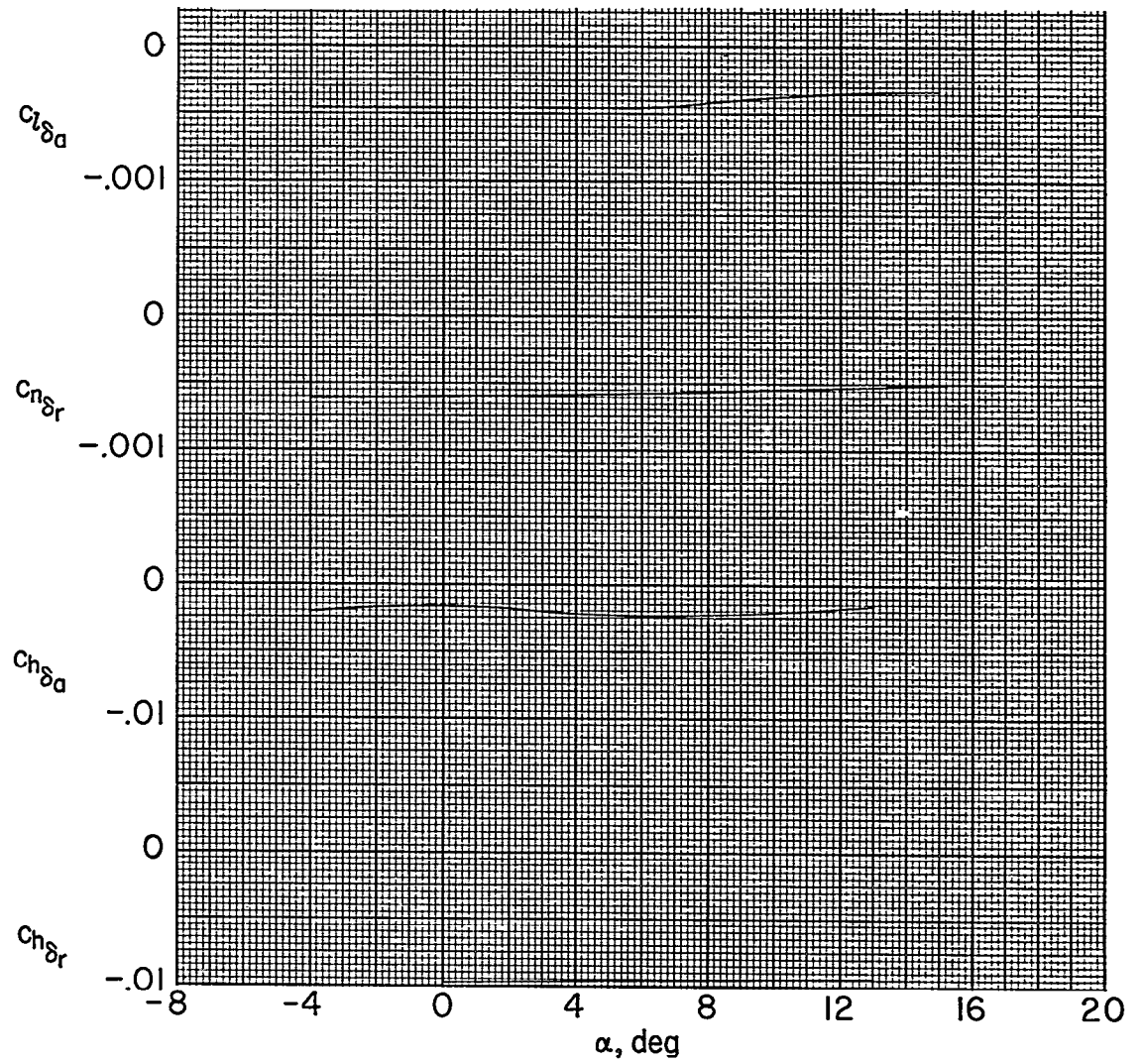


Figure 28.- Effects of angle of attack on aileron and rudder control characteristics; $\beta = 0^\circ$.

~~CONFIDENTIAL~~

INDEX

<u>Subject</u>	<u>Number</u>
Stability, Longitudinal - Static	1.8.1.1.1
Stability, Lateral - Static	1.8.1.1.2
Stability, Directional - Static	1.8.1.1.3
Control, Longitudinal	1.8.2.1
Control, Lateral	1.8.2.2
Control, Directional	1.8.2.3
Control, Hinge Moments	1.8.2.5
Loads, Steady - Tail	4.1.1.2.1

ABSTRACT

An investigation was made in the Langley 4- by 4-foot supersonic pressure tunnel at a Mach number of 1.41 to determine the aerodynamic characteristics of an 0.03-scale model of the Avro CF-105 airplane. The model had a 3.5-percent-thick modified delta wing with a leading-edge sweep of 61.4° , an aspect ratio of 2.04, and a taper ratio of 0.089. Results were obtained through an angle-of-attack range of about -4° to 15° and through a $\pm 12^\circ$ sideslip range at angles of attack of 0° , 4.3° , 8.7° , 13° , and 15.2° . Six-component results for the model with and without the vertical tail, three-component measurements for the vertical tail, and control and hinge-moment measurements for various deflections of the elevator, rudder, and aileron were obtained.

NASA Technical Library



3 1176 01438 5034

~~CONFIDENTIAL~~